SSC-241

THERMOELASTIC MODEL STUDIES OF CRYOGENIC TANKER STRUCTURES

This document has been approved
for public release and sale; its
distribution is unlimited.

SHIP STRUCTURE COMMITTEE

1973

SHIP STRUCTURE COMMITTEE

AN INTERAGENCY ADVISORY
COMMITTEE DEDICATED TO IMPROVING
THE STRUCTURE OF SHIPS

MEMBER AGENCIES:

UNITED STATES COAST GUARD
NAVAL SHIP SYSTEMS COMMAND
MILITARY SEALIFT COMMAND
MARITIME ADMINISTRATION
AMERICAN BUREAU OF SHIPPING

ADDRESS CORRESPONDENCE TO:

SECRETARY
SHIP STRUCTURE COMMITTEE
U.S. COAST GUARD HEADQUARTERS
WASHINGTON, D.C. ~~20591~~ 20590

SR-191
1973

Anticipating one of the problems which could arise in the design of LNG tankers, the Ship Structure Committee undertook studies to investigate the thermal stresses that would result if a sudden rupture occurred in the primary LNG tank.

One project consisted of experimental and theoretical efforts to develop a simplified thermal stress analysis of LNG tankers under the emergency, rupture condition, and to evaluate the importance of the parameters involved.

The enclosed report contains the results of this work. Comments on this report will be welcome.

W. F. REA, III
Rear Admiral, U. S. Coast Guard
Chairman, Ship Structure Committee

SSC-241

FINAL REPORT

on

Project SR-191, "Thermal Study

to the

Ship Structure Committee

THERMOELASTIC MODEL STUDIES OF CRYOGENIC TANKER STRUCTURES

by

H. Becker and A. Colao

Sanders Associates, Inc.

under

Department of the Navy
Naval Ship Engineering Center
Contract No. N00024-70-C-5119

This document has been approved for public release and sale; its distribution is unlimited.

U. S. Coast Guard Headquarters
Washington, D.C.
1973

ABSTRACT

Theoretical calculations and experimental model studies were conducted on the problem of temperature and stress determination in a cryogenic tanker when a hold is suddenly exposed to the chilling action of the cold fluid. The initiation of the action is presumed to be the sudden and complete rupture of the fluid tank.

Model studies of temperatures and stresses were performed on instrumented steel versions of a ship with center holds and wing tanks. Supplementary studies also were conducted on plastic models using photo-thermoelasticity (PTE) to reveal the stresses. Temperatures and stresses were computed using conventional procedures for comparison with the experimentally determined data. Simple calculation procedures were developed for temperature prediction and for stress determination.

The highly simplified theoretical predictions of temperature were in fair agreement with the experimental data in the transient stage and after long intervals. The temperatures and stresses reached peak values in every case tested and maintained the peaks for several minutes during which time the behavior was quasistatic. The experimental temperatures were in good agreement with predictions for the thin models representative of ship construction.

Evidence was found for the importance of convective heat transfer in establishing the temperatures in a ship. In some cases this may be the primary process by which a thermal shock would be attenuated in a cryogenic tanker. It also would influence thermal model scaling.

An important result of the project was the good agreement of the maximum experimental stresses with theoretical predictions which were made from the simple calculations. This agreement indicates the possibility of developing a general design procedure which could involve only a few minutes of calculation time to obtain the peak stress values.

CONTENTS

LIST OF TABLES

LIST OF FIGURES

LIST OF FIGURES (Cont'd)

NOMENCLATURE

Symbols

A	area of cross section, in^2
a,b	radii in cold-spot problem, in.
B	Biot number, hL/k
C	$\sigma/\alpha ET$
c	specific heat - BTU/°F-lb.
D	thermal diffusivity, $k/c\rho$, ft^2/hr
E	Young's modulus, msi
e	radiation constant, $BTU/hr\text{-}ft^2\text{-}°F^4$
F	factor in radiation Eq. (13)
f	material fringe value, psi-in/fringe
G	shear modulus, msi
g	coefficient, $g^2 = (1 + q_r/q_h)(h_L+h_R)/kt$, ft^{-2}
H_w	depth of ship bottom, ft.
h	surface heat transfer coefficient, $BTU/hr\text{-}ft^2\text{-}°F$
J	temperature ratio, see. Eq. (63)
k	thermal conductivity, BTU/hr-ft-°F
L	general length, in. or ft. depending upon use
n	fringe order
p	pressure, psi
Q	heat flow, BTU/hr.
q	heat flux, $BTU/hr\text{-}ft^2$
R_1, R_2	parameters defined by Eqs. (31) and (32)
r	radius in cold-spot problem
S	constant, see Eq. (28)
s	distance, ft.
T	temperature, °C or °F

$\overline{T}$	weighted temperature, see Eq. (34)
t	thickness, in. or ft.
u, v, w	dimensionless lengths in Eq. (6)
x, y	athwartship and vertical coordinates, ft.
α	thermal expansion, 1/°F
β	temperature coefficient of volume expansion, 1/°F
Δ	increment
δ	Stefan-Boltzmann constant, 0.1713×10^{-8} BTU/sq. ft.-hr-°F^4
ε	normal strain
ζ	acceleration of gravity, ft/sec^2
$\Theta, \overline{\Theta}$	time, hr., also dimensionless time in Eq. (6)
μ	absolute viscosity, lb/ft. sec.
ν	Poisson's ratio
ρ	specific weight, lb/cuft
σ	normal stress, psi
τ	shear stress, psi
ℓ	angle of principal stress, deg.

Subscripts

A	Air
e	Emissivity
F	Fluid
H, V	Horizontal, Vertical
h, k, r	Convection, conduction, radiation
i	Initial temperature of plate
L, R	Left, right
m, p	Model, prototype
o, u	Total available, ultimate attainable (stresses, temperatures)

s	View
T	Temperature
W	Water
w	Wall
x, y	Coordinate directions
1, 2	Inner and outer (ship sections) (Radiative surface)
45	Rosette strain gage at 45 degrees to the orthogonal arms

SHIP STRUCTURE COMMITTEE

The SHIP STRUCTURE COMMITTEE is constituted to prosecute a research program to improve the hull structure of ships by an extension of knowledge pertaining to design, materials and methods of fabrication.

RADM W. F. Rea, III, USCG, Chairman
Chief, Office of Merchant Marine Safety
U.S. Coast Guard Headquarters

CAPT J. E. Rasmussen, USN
Head, Ship Systems Engineering and Design Department
Naval Ship Engineering Center
Naval Ship Systems Command

Mr. E. S. Dillon
Deputy Asst. Administrator for Operations
Maritime Administration

Mr. K. Morland
Vice President
American Bureau of Shipping

CAPT L. L. Jackson, USN
Maintenance and Repair Officer
Military Sealift Command

SHIP STRUCTURE SUBCOMMITTEE

The SHIP STRUCTURE SUBCOMMITTEE acts for the Ship Structure Committee on technical matters by providing technical coordination for the determination of goals and objectives of the program, and by evaluating and interpreting the results in terms of ship structural design, construction and operation.

NAVAL SHIP ENGINEERING CENTER

Mr. P. M. Palermo - Chairman
Mr. J. B. O'Brien - Contract Administrator
Mr. G. Sorkin - Member
Mr. C. H. Pohler - Member

U. S. COAST GUARD

CDR C. S. Loosmore - Secretary
CAPT H. H. Bell - Member
CDR E. L. Jones - Member
CDR W. M. Devlin - Member

MARITIME ADMINISTRATION

Mr. J. J. Nachtsheim - Member
Mr. F. Dashnaw - Member
Mr. A. Maillar - Member
Mr. F. Seibold - Member

MILITARY SEALIFT COMMAND

Mr. R. R. Askren - Member
Mr. T. W. Chapman - Member
CDR A. McPherson, USN - Member
Mr. A. B. Stavovy - Member

AMERICAN BUREAU OF SHIPPING

Mr. S. Stiansen - Member
Mr. I. L. Stern - Member

NATIONAL ACADEMY OF SCIENCES
Ship Research Committee

Mr. R. W. Rumke - Liaison
Prof. J. E. Goldberg - Liaison

SOCIETY OF NAVAL ARCHITECTS & MARINE ENGINEERS

Mr. T. M. Buermann - Liaison

BRITISH NAVY STAFF

Dr. V. Flint - Liaison

WELDING RESEARCH COUNCIL

Mr. K. H. Koopman - Liaison

INTERNATIONAL SHIP STRUCTURE CONGRESS

Mr. J. Vasta - Liaison

INTRODUCTION

Purpose of Project

This project was directed toward development of theoretical procedures for the calculation of temperatures and stresses in a cryogenic tanker when a tank ruptures and the liquid natural gas contacts the metal of the hold. The theoretical procedures were to be substantiated through model studies.

It has been one aim of the project to reduce heat transfer and stress analyses to simple procedures. For this reason initial efforts have been devoted to application of simple engineering computation procedures although they may be lacking in fine detail and rigor. This has been done in order to assess the usefulness and limitations of the methods.

Approach to Project

The heat transfer investigations were performed on model configurations which varied from a reasonably well scaled version of a ship to a model in which the walls were much thicker proportionately. Large variations in wing tank width were included. Both non-boiling and boiling chilling fluid experiments were conducted. Relatively simple heat transfer calculation procedures were developed and were used to compare theory and experiment.

The problems relevant to convective heat transfer analysis are identified and discussed, and the relative magnitudes of convective, radiative and conductive heat transfers are identified. The prevalence of convection in a ship is pointed out and substantiated.

An important aspect of the LNG tank failure is the probability of generation of high pressure in a hold that is not vented properly. This would result from the vigorous boiling of the fluid as it comes in contact with the metal of the hold. A discussion is included on the character of this behavior and on the potential danger which it presents.

The literature on thermoelasticity and photothermoelasticity (PTE) contain sufficient data to allow the following two generalizations, which were used to design the approach to this project:

1. Accurate information on temperature distributions will permit theoretical calculations of thermal stresses which will be of comparable accuracy and any loss of accuracy in a thermoelastic problem will stem from inaccuracies in the computation of temperatures from heat transfer calculations.

2. Peak thermal stresses almost invariably can be found, to engineering accuracy, from simple theoretical relations.

These two observations were considered axioms for the present investigation, which concentrated on determining how simple the computation procedure could be and still yield good correlation with the experimental stress data obtained during this project.

The focus of the experimental stress phase was the steel model on which strain gages and thermocouples were placed to provide the required data. Effective data acquisition from that model depended upon placement of the strain and temperature sensors to provide peak values and to establish the distributions reliably. This involved some prior knowledge of the character of the stresses to be anticipated, for which photothermoelasticity was used because of the total picture of the stresses which it provides. In addition, PTE experiments provided further checks with the simple calculation procedure for peak stress determination to supplement the experience with the steel model.

HEAT TRANSFER THEORY

Introduction

The theoretical bases for the temperature calculations of this project are presented in the following paragraphs. The various degrees of approximation for the heat transfer analysis are presented, from which calculations are made subsequently for correlation with the experimental data.

The three elementary equations of heat transfer per unit area are (Ref. 1),

conduction: $$q = k(T_1 - T_2)/L \qquad (1)$$

convection: $$q = h(T_1 - T_2) \qquad (2)$$

radiation: $$q = e(T_1^4 - T_2^4) \qquad (3)$$

They were used to develop calculation methods for temperature as a function of time and position for comparison with measured test data.

Conductive Heat Transfer

The transfer of heat by conduction is usually considered to occur by diffusion of energy through the conducting material. The material thermal conductivity depends primarily upon temperature. In metals, it is essentially independent of strains. The general expression may be written in the form

$$Q_k = kA(T_1 - T_2)/L \tag{4}$$

The numerical analysis of transient temperatures in the plane of a thin plate with insulated faces is often accomplished mathematically by writing Eq. (1) in difference form equivalent to the differential equation for heat conduction,

$$(c\rho/k)\ \partial T/\partial\theta = \partial^2 T/\partial x^2 + \partial^2 T/\partial y^2 \tag{5}$$

This relation is usable for general analysis and also for thermal scaling in heat conduction problems. It can be used to relate times in a model and prototype at which the shape of the temperature distribution in each would be the same provided convection is not a major consideration. This is done by nondimensionalizing Eq. (5) through the use of an arbitrary reference length, L, and an arbitrary reference, time, $\overline{\theta}$,

$$u = x/L, \quad v = y/L, \quad w = \theta/\overline{\theta}$$

By substitution in Eq. (5)

$$(c\rho L^2/k\overline{\theta})\ \partial T/\partial w = \partial^2 T/\partial u^2 + \partial^2 T/\partial v^2 \tag{6}$$

The temperature fields will have the same shape when all the partial derivatives are in the same proportion, or when

$$(c\rho L^2/k\overline{\theta}) = (\partial^2 T/\partial u^2 + \partial^2 T/\partial v^2)\ (\partial\ T/\partial w\ ) \tag{7}$$

both for the model and the prototype. Then the temperature scaling law becomes (using $D = k/c\rho$)

$$(L_m/L_p)^2 = (D_m/D_p)\ (\overline{\theta}_m/\overline{\theta}_p) \tag{8}$$

The choice of scaling length is arbitrary, as indicated above.

Representative values of diffusivity are shown in the following tabulation.

Table 1 - Diffusivities for Metals and Plastics

	Material					
Diffusivity	Alum.	Mag.	Steel	Titan	Nickel	Plastic
$D=k/c\rho$ ft^2/hr	1.97	1.60	0.45	0.24	0.24	0.005 (Approx.)

Consequently, the comparison of steel and plastic would involve times and lengths in the following relation

$$\bar{\theta}_{steel}/\bar{\theta}_{plastic} = 0.011\ (L_{steel}/L_{plastic})^2 \qquad (9)$$

If a steel ship with a 60 foot beam is compared to a plastic model with a 3.33 inch beam (which was used in the PTE experiments described below), then similar temperature distributions would be expected when the prototype time is 520 times as long as the model time.

Convective Heat Transfer

In contrast to conductive heat transfer the apparently simple relation of Eq. (2) actually involves some of the most complex phenomena in engineering behavior. They are all embodied in the convective heat transfer coefficient, h. Values for h have been determined by a combination of dimensional analysis and curve fitting to large quantities of data. Table 1 (from Ref. 1) contains the dimensionless groups which appear in this report.

While k for a given metal may vary by percentages as a function of temperature, h for a fluid may range over 3 or more orders of magnitude as a function of temperature, pressure, velocity, viscosity, pathlength and several other factors including the state of the fluid and whether it is quiescent or boiling. In the case of boiling, surface contamination is an important factor which can affect seriously the reproducibility of data.

The convective heat transfer relation is expressible as

$$Q_h = h_u A(T_1 - T_2) \qquad (10)$$

TABLE I - Dimensionless Groups Used in this Report

Group	Symbol	Name
hL/k	N_{Bi}	Biot number
$D\theta/t^2$	N_{Fo}	Fourier number
$(L^3 \rho^2 \zeta/\mu^2)(\beta\Delta t)$	N_{Gr}	Grashof number

The overall heat transfer coefficient, h_u, is given in Figure 1. It pertains to transfer between two parallel plates enclosed around the edges with a nonconducting material to form a box. The Grashof number is based on the distance between the plates. The overall heat transfer coefficient for this system is defined as

$$\frac{1}{h_u} = \frac{1}{h_1} + \frac{L}{k_A} + \frac{1}{h_2} \qquad (11)$$

where h_1 and h_2 are the unit surface coefficients for free convection on the inner surfaces of the plates and L/k_A represents the conduction through the air between the plates.

The cell behavior (or convective flow path) for the vertical plates consists of one major cell which forms with flow down the chilled wall and up the warm wall. There may be small corner eddies but the action is primarily uni-cellular.

Flow for the horizontal plate arrangements is quite different. For laminar motion the cellular behavior looks hexagonal as depicted in Figure 2. This cell action can be biased by fin behavior induced by stiffeners. It will be affected strongly by the stiffeners as the motion becomes turbulent.

The heat transfer per unit area as given in Figure 1 would be independent of size until the plate separation is large with respect to the wall height (approximatley 2-1/2 to 1). The equation using this heat transfer coefficient would then be used with the exterior surface heat transfer equations to complete the total heat flow analysis.

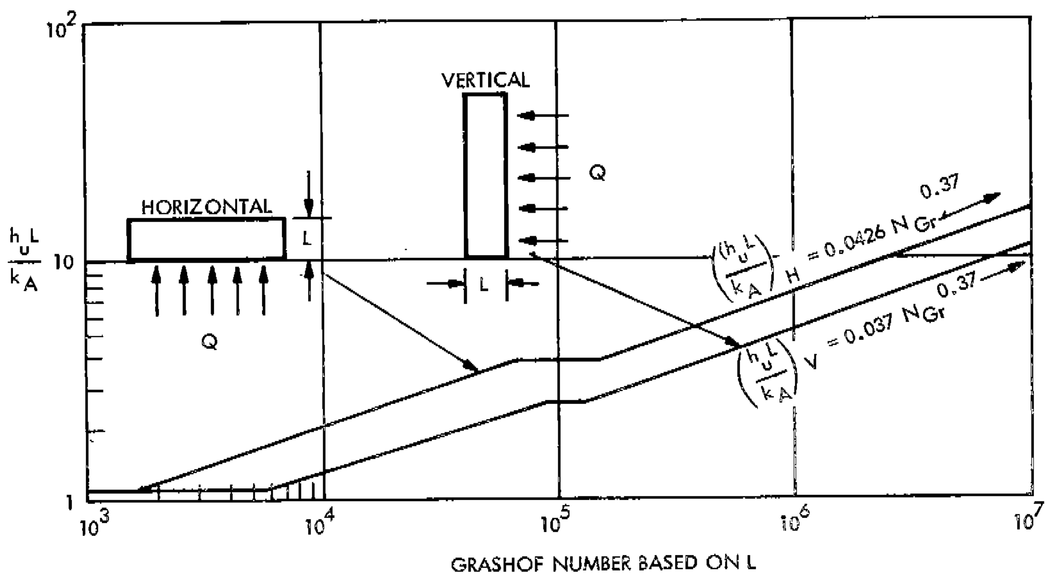

FIGURE 1 - Overall Convective Heat Transfer Coefficient Between Two Walls of an Enclosed Space. (Ref. 1)

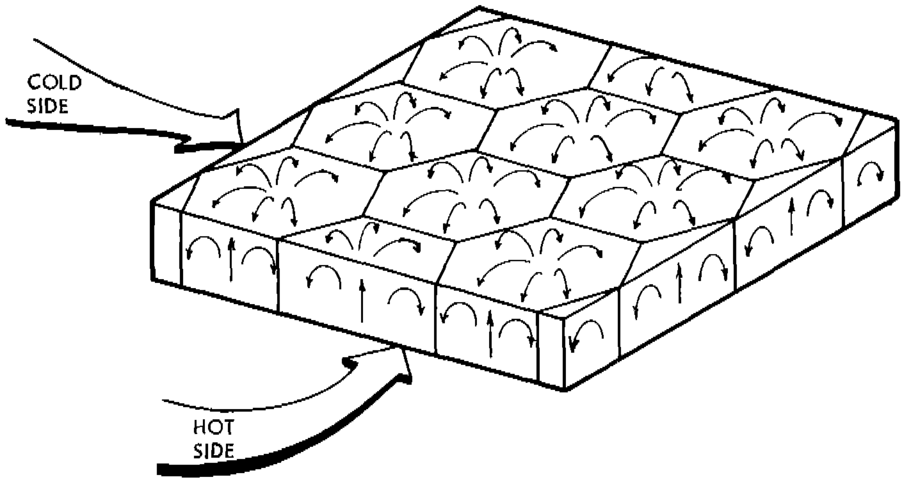

FIGURE 2 - Cellular (Steady/State) Behavior in Horizontally Enclosed Space Heated from Below.

Radiant Heat Transfer (Ref. 1)

Radiant heat transfer between any two surfaces of an enclosure involves the view the surfaces have of each other together with the emitting and absorbing characteristics. This study treated the longitudinal girder and the side shell as the absorber and emitter. The connecting plating was considered to be non-conducting but reradiating. This is consistent with the convection analysis and adequately represents the radiation effects at the mid-plane of the hold and wing tanks away from the end bulkheads.

The radiation equation can be written in the form

$$Q_r = h_r A (T_1 - T_2) \qquad (12)$$

for direct comparison with convective and conductive heat transfer rates. The heat transfer coefficient may be defined

$$h_r = F_s F_e F_T \qquad (13)$$

contains the temperature factors for view, emissivity and radiation. The radiation temperature factor is

$$F_T = 0.172 \times 10^{-8} (T_1 + T_2)(T_1^2 + T_2^2) \qquad (14)$$

where T_1 and T_2 are in degrees Rankine. The emissivity factor is

$$F_e = \frac{1}{1/e_1 + 1/e_2 - 1} \qquad (15)$$

For rough steel plates the emissivity is approximately 0.95. This value drops to 0.80 when there is a coarse oxide layer on the plate. Painting the steel surface does not significantly change that range. In fact, a variety of 16 different colors of the spectrum including white produced an emissivity range on steel of 0.92 to 0.96. Some exceptions were black shiny shellac on tinned steel ($e = 0.82$), black or white lacquer ($e = 0.80$), and the aluminum paints and lacquers ($e = 0.27$ to 0.67). Some red paints were as low as $e = 0.75$.

The view factor, Fs, for this series of experiments ranged from 0.6 to 0.9 as shown in Figure 3. The lower value represents the greatest wall separation.

Relative Magnitudes of Heat Transfer

From Eqs. (4, 10 and 12), it is possible to estimate the relative magnitudes of the three types of heat transfer. For this purpose consider two walls of surface area A_w connected by steel plating with a cross section area A. The relative heat flows between the walls, with one at T_1 and the other at T_2, would be

$$Q_k : Q_h : Q_r = (kA_k/L) : (h_u A_w) : [A_w F_s F_e F_T] \qquad (16)$$

Compared to conduction,

$$Q_h/Q_k = (h_u L/k) A_w/A_k = B\ A_w/A_k \qquad (17)$$

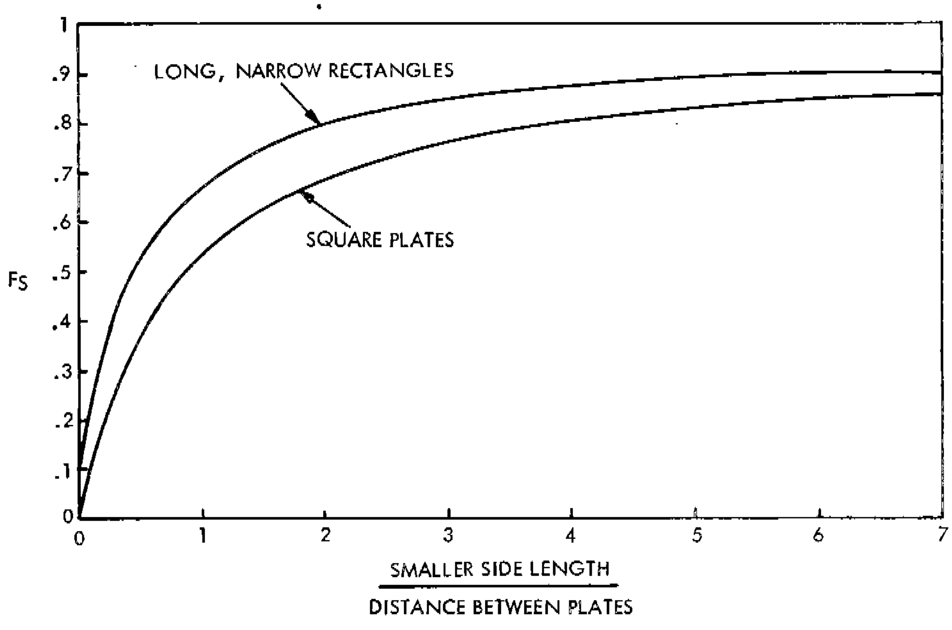

FIGURE 3 - View Factor for Radiation Between Parallel Plates Connected by Non-Conducting but Reradiating Walls. (Ref. 1)

$$Q_r/Q_k = (F_e F_s F_T L/k)(A_w/A_k) \tag{18}$$

$$Q_r/Q_h = (F_e F_s F_T/h_u) \tag{19}$$

In order to obtain an estimate of the heat transfer ratios for a ship assume the wing tank dimensions to be 40 feet high, 60 feet long and 10 feet wide. Assume a constant plate thickness of 1/20ft. which could account for stiffeners and ribbing. Further assume that the hold wall and the side shell are the two heat transfer surfaces for convection and radiation. The plates that connect these two walls constitute the conduction path. The upper and lower plates (decks) are used at full material thickness for conduction. However, the side plates, (fore and aft bulkhead) are used at 1/2 the material thickness for conduction heat transfer to the wing tank. This 1/2 thickness assumption allows 1/2 the conduction heat transfer to go to the wing tanks adjacent to the compartment under consideration. This is not done with the lower plate (deck) of the compartment because it is assumed that all the heat conducted along that path comes almost directly from the water at the connection to the outer hull. Assume a hull plating thickness of 1/20 ft. The conduction expression of Eq. (4) is written

$$Q_k = (kA_k/L)\ \Delta T \tag{20}$$

where $k = 25$ BTU /hr.-ft^2-°F

$L = 10$ feet

$$A_k = (1/20)(2x60)+(1/2)(1/20)(2x40) = 8 \text{ sq. ft.}$$

This yields a conduction heat transfer of

$$Q_k = 20\ \Delta T \ \text{BTU/hr-ft-°F} \tag{21}$$

The convection relation of Eq. (10) can involve the establishment of a temperature difference to determine the heat transfer coefficient from Figure 1. Therefore, assume the hold wall temperature at -259°F (methane boiling point) and (for convenience) an outer hull wall temperature of 41°F for a total temperature difference of 300°F. The above temperature difference and the assumed constants

$k_A = 0.013$ BTU /ft^2-hr-F

$L = 10$ feet

yield $h_u = 1.2$ BTU/ft^2-hr°F

The convection heat transfer becomes

$$Q_h = 2880\ \Delta T \ \text{BTU/hr°F} \tag{22}$$

The radiation heat transfer is determined from Eqs.(12) through (14)

$$Q_r = A_w F_e F_s F_T \Delta T \tag{23}$$

The constants are chosen as emissivity equal to 0.9, F_e = 0.82, F_T = 0.35 and F_s = 0.85 in this wing tank for the assumed temperature gradient. When combined above the radiation heat transfer equation is

$$Q_r = 580 \ \Delta T \quad \text{BTU/hr°F} \tag{24}$$

A comparison of the ship heat transfer magnitudes may be made with the aid of Eqs. (17), (18), (19), (21), (22) and (24).

$$Q_h/Q_r/Q_k = 144/29/1$$

$$Qh/Q_k = 144$$

$$Q_r/Q_k = 29$$

$$Q_h/Q_r = 5$$

$$(Q_h + Q_r)/Q_k = 173$$

The ratios that would be obtained in the models used in this program for overall temperature changes of 40°F and 300°F are given in Tables 2 and 3 which are based on models to be described subsequently.

General Equation for Thin Plates

A representation of a section of thin plate is shown in Figure 4. It is assumed to have unit depth perpendicular to the plane of the paper. The stiffener web is shown at the midheight of the side. It is likely that little error would accrue if the stiffener total heat flow is assumed to be distributed over the length instead of concentrated locally provided the areas are taken into account properly.

The heat balance is obtained by relating the heat flows to the rate of temperature rise in the element, $\Delta T/\Delta\theta$,

$$(q_L+q_r)\Delta s - (q_2 - q_1)t = c\rho t\Delta s(\Delta T/\Delta\theta) \tag{25}$$

The fluid end stiffener components are assumed to be constant in time and also over the length Δs. In general they may vary with respect to both.

If $q_2 - q_1$ is represented by Δq then the change in heat flow rate along the element

$$q_L + q_R - t\Delta q/\Delta s = c\rho t(\Delta T/\Delta\theta) \tag{26}$$

Now employ Eqs. (1) through (3) and utilize the partial derivative notation for the differential limits of time and length. Then if T is the only dependent variable, the one-dimensional equation becomes (recalling the sign of $\partial T/\partial s$)

$$[(F_s F_e F_T)_L (T_L - T) + (F_s F_e F_T)_R (T_R - T) + h_L (T_L - T) + h_R (T_R - T)]/t + k(\partial^2 T/\partial s^2) = c\rho\,(\partial T/\partial \Theta) \quad (27)$$

The analysis is easily extendable to two dimensional heat transfer by adding $k(\partial^2 T/\partial v^2)$ to the left side of Eq. (27).

TABLE II - Relative Heat Transfers, $\Delta T = 40^{\circ}F$

Quantity	Model						TF (Long Path)	TF (Short Path)
	2T8	2T4	2T2	3T12	3T6	3T3		
b(ft)	2/3	1/3	1/6	1	1/2	1/4	2/3	0.208
b^3	0.296	0.0370	0.00463	1	0.125	0.015625	0.296	0.0090
k(BTU/hr-ft-°F)	26	26	26	26	26	26	26	26
A_h (ft^2)	0.39	0.39	0.39	1	1	1	0.856	0.856
A_k (ft^2)	0.0139	0.0139	0.0139	0.0075	0.0075	0.0075	0.0345	0.0345
b/k	0.0255	0.0128	0.00642	0.0385	0.0192	0.00962	0.0255	0.0080
A_h/A_k	28.1	28.1	28.1	133.3	133.3	133.3	24.8	24.8
$(b/k)\ (A_h\ A_k)$	0.715	0.359	0.181	5.13	2.56	1.28	0.633	0.198
h_u	0.43	0.395	0.36	0.44	0.405	0.379	0.43	0.371
Q_h/Q_k	0.307	0.142	0.065	2.26	1.04	0.485	0.272	0.0735
F_T	0.92	0.92	0.92	0.92	0.92	0.92	0.92	0.92
h_r	0.736	0.736	0.736	0.736	0.736	0.736	0.736	0.736
Q_h/Q_r	0.585	0.538	0.490	0.60	0.55	0.516	0.584	0.504
Q_r/Q_k	0.525	0.263	0.133	3.77	1.89	0.94	0.464	0.146
$(Q_h + Q_r)/Q_k$	0.832	0.405	0.198	6.03	2.93	1.43	0.736	0.220

TABLE III - Relative Heat Transfers, $\Delta T = 300^oF$

Quantity	Model						TF (Long Path)	TF (Short Path)
	2T8	2T4	2T2	3T12	3T6	3T3		
b (ft)	2/3	1/3	1/6	1	1/2	1/4	2/3	0.208
b^3	0.296	0.0370	0.00463	1	0.125	0.015625	0.296	0.0090
k (BTU/hr-ft-°F)	26	26	26	26	26	26	26	26
A_h (ft^2)	0.39	0.39	0.39	1	1	1	0.856	0.856
A_k (ft^2)	0.0139	0.0139	0.0139	0.0075	0.0075	0.0075	0.0345	0.0345
b/k	0.0255	0.0128	0.00642	0.0385	0.0192	0.00962	0.0255	0.0080
A_h/A_k	28.1	28.1	28.1	133.3	133.3	133.3	24.8	24.8
$(b/k)(A_h/A_k)$	0.715	0.359	0.181	5.13	2.56	1.28	0.633	0.198
h_u	0.913	0.861	0.784	0.955	0.888	0.825	0.913	0.800
Q_h/Q_k	0.654	0.309	0.142	4.90	2.25	1.055	0.578	0.158
F_T	0.35	0.35	0.35	0.35	0.35	0.35	0.35	0.35
h_r	0.28	0.28	0.28	0.28	0.28	0.28	0.28	0.28
Q_h/Q_r	3.26	3.08	2.90	3.41	3.17	2.95	3.26	2.86
Q_r/Q_k	0.200	0.100	0.049	1.43	0.71	0.36	0.178	0.0554
$(Q_h + Q_r)/Q_k$	0.854	0.409	0.191	6.33	2.96	1.41	0.756	0.213

In a transient the temperature often is observed to peak at which time the term on the right will vanish. Then Eq. (27) will have the character of a steady state relation from which some useful calculation simplifications are possible. This situation is relevant to the present investigation since both temperatures and stresses were observed to reach extreme values at approximately the same time.

Linearized Method

From the standpoint of a designer, there would be considerable value in a reasonably reliable design temperature determination scheme that would require virtually no computation. A straight line temperature gradient might be possible if heat conduction predominates and if a metal temperature would be close to the temperatures of a liquid wherever the two are in contact. This may be inaccurate depending upon the amount of convection and radiation which is present.

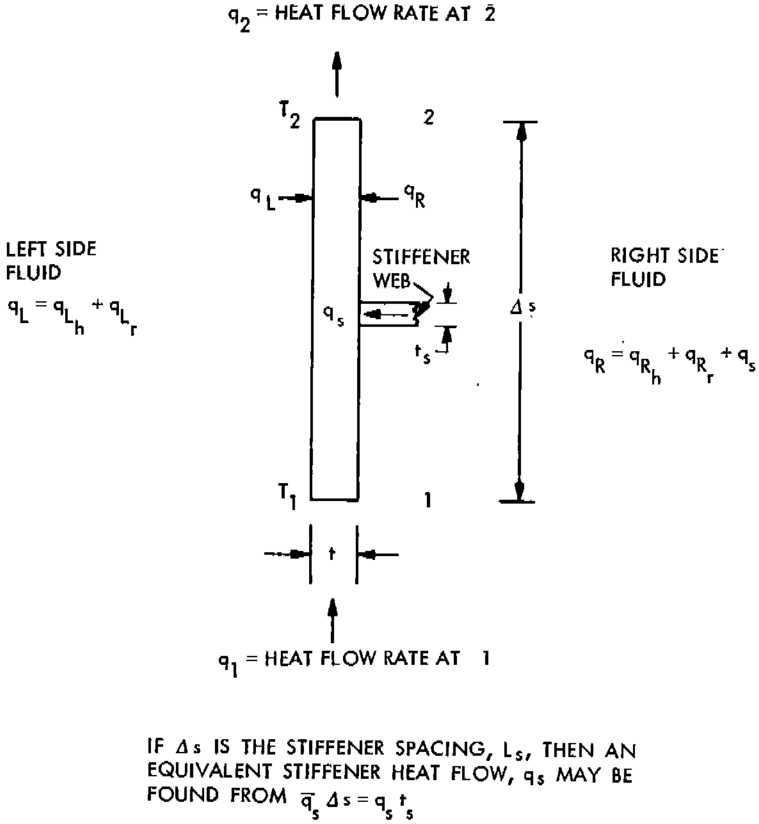

FIGURE 4 - Plate Strip Element for Heat Transfer Analysis.

This linearized method is probably the simplest method. It was found to agree reasonably well with some of the experimental data of this investigation.

Quasistatic Method

An improved method of temperature determination (relative to the linear approximation) may be achieved through use of the quasistatic approximation, $\partial T/\partial\theta = 0$. This condition was observed in the late stages of all the experimental transients of this project. The following is confined to a simple strip which relates to two dimensional heat transfer, vertical and athwartship.

From Eq. (27) with $\partial T/\partial\theta = 0$,

$$d^2T/ds^2 = 2eT^4/kt + (h_L+h_R)T/kt - S \tag{28}$$

where $S = [(F_sF_eF_T)_L + (F_sF_eF_T)_R]/kt + (h_LT_L+h_RT_R)T/kt$ (29)

If the radiation term is assumed to be a constant fraction of the convective term, then

$$S = (1 + q_r/q_h)(h_L T_L + h_R T_R)/kt \quad (30)$$

If all the coefficients in Eq. (28) are assumed constant, then

$$T = (T_1 + T_2)/2 + R_1(T_2 - T_1)/2 + R_2\overline{T} \quad (31)$$

where

$$R_1 = [\sinh gs - \sinh g\,(L-s)]/\sinh gL \quad (32)$$

$$R_2 = 1 - [\sinh gs + \sinh g\,(L-s)]/\sinh gL \quad (33)$$

$$g^2 = (1 + q_r/q_h)(h_L + h_R)/kt \quad (34)$$

$$\overline{T} = (1 + q_r/q_h)(h_L T_L + h_R T_R)/(h_L + h_R) - (T_L + T_R)/2 \quad (35)$$

The graphs of R_1 and R_2 appear in Figure 5 in terms of s/L and gL. They show that R_1 becomes linear and R_2 becomes zero at very small gL which corresponds to prevalence of conductive heat transfer. For that case (Figure 6a)

$$T = T_1 + (T_2 - T_1)(s/L) \quad (36)$$

For large gL (which would be the case in a ship with a strong wind blowing across the deck) R_1 and R_2 approach step functions, convection controls, and T approaches the form of Figure 6c.

Eq. (31) was compared with experimental data at long times for all temperature model tests conducted during this project. For those comparisons it was necessary to determine the temperature of the air outside and inside the wing tank. This was done by assuming that the temperature T_L was that of the outside air, T_A, and that T_R (for the air inside the tank) was the weighted average of the temperature of the metal surrounding the tank. It was also assumed that $h_L = h_R = h$ with h determined as shown in the section on experimental data.

As for the weighted average of the metal temperature, this was estimated for each test on the assumption of a linear variation of temperature from that of the chilling fluid to that of the water. This estimate certainly is open to question. However, it is consistent with the desire for simplicity in calculation.

Finite Difference Procedures

Eq. (27) may be written

$$\partial^2 T/\partial s^2 = (1+q_r/q_h)(h_L+h_R)T/kt - (1+q_r/q_h)(h_L T_L + h_R T_R)/kt + (1/D)(\partial T/\partial \theta) \quad (37)$$

The finite difference form is

$$\frac{T_{s+1,t} - 2T_{s,t} + T_{s-1,t}}{\Delta s^2} = g^2 T_{s,t} - S + \frac{T_{x,t+1} - T_{x,t}}{D\Delta\theta}$$

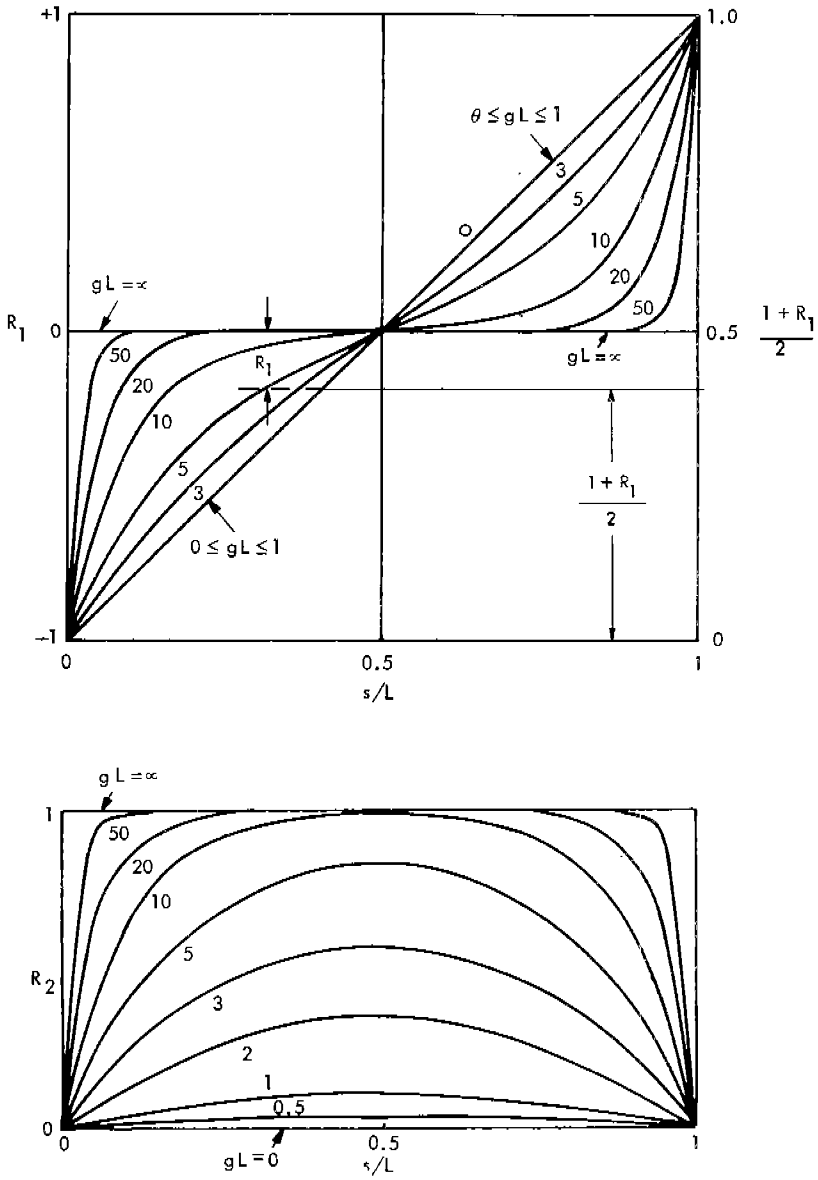

FIGURE 5 - Curves for R_1 and R_2.

As in Dusinberre (Ref. 2) assume $(\Delta s)^2 = 2D\Delta\theta$. Then

$$T_{x,t+1} = (1/2)(T_{x+1,t} + T_{x-1,t}) + (S - g^2 T_{x,t})(\Delta s)^2/2 \qquad (38)$$

This is the strip transient equation. When $S = q_r/q_h = 0$ it becomes the Schmidt plot relation (Ref. 2). Eq. (38) was used to predict transient temperatures for comparison with test data at several locations on one of the thermal models and at one point on the thermoelastic model. These calculations employed a typical value of $D = 1/2$ sq·ft/hr.

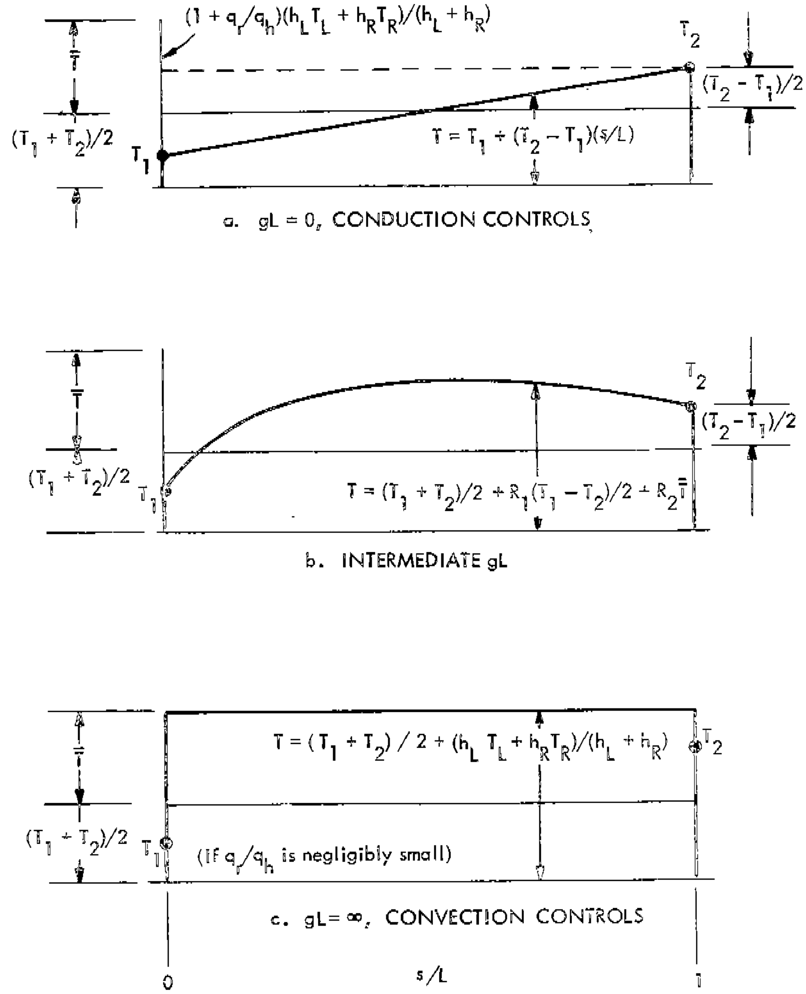

FIGURE 6 - Range of Quasistatic Temperature Distributions Along a Strip, Shown Schematically.

THERMAL STRESS THEORY

Nature of Thermal Stresses

Thermal stresses are mechanical stresses that arise from restraint of free thermal expansion. This is the generic term for dimensional changes due to either increasing or decreasing temperatures. The interaction between the thermally induced expansions and the restraint-induced stresses is thermoelasticity. The restraints may be external, or they may be purely internal because of the inability of adjacent structural elements at different temperatures to deform freely because they are attached. The general nature of thermoelasticity has been delineated by Melan and Parkus (Ref. 3).

The emphasis of this project is upon the development of a theoretical procedure which can be used for reliable prediction of the thermal stresses in a structure which essentially is comprised of numerous intersecting plates. The thermal field is to be assumed to originate from the sudden introduction of a mass of cold fluid into a relatively warmer region of that structure. That type of behavior commonly is termed "thermal shock". It is a loosely used term, as is discussed in Ref. 4. Furthermore, the theories for predicting temperatures under thermal shock necessarily have had to assume specific forms of the initiating temperature transient in order to achieve a tractable closed form solution which is often mathematically desirable.

In this report, as was indicated in the Introduction, thermoelastic theories are advanced which are of the utmost simplicity since experience has shown that relatively simple theories may be employed to predict stresses in a complex structural problem with reasonable accuracy.

Some Aspects of Thermal Stresses

It is possible to approximate the solutions to a thermal stress problem in various manners. A hypothetical maximum can be computed which would be independent of all the shape and thermoelastic parameters of the problem except for α, E and T_o. The quantity αET_o may be used as an upper limit which may be approached rather closely under certain conditions but would never be attained. (In a thermal stress field with $\sigma x = \delta y$ the quantity would be increased by the multiplying factor $1/(1 - \nu)$). It would be the most conservative estimated solution to the edge-heated plane problem.

A closer approximation may be made through use of the Biot number, hL/k, as will be explained later in this report. The magnitude of B depends upon properties of the two media which come into contact to initiate the thermoelastic field in one of the media, such as liquid methane and steel. A relation has been developed which delineates the ultimate fraction of αET_o which can be attained no matter what the problem geometry may be. This value would involve a lesser degree of conservatism than the first. (See Eq. (43) and ff below).

Finally, the precise value of the thermal stress can be calculated from a knowledge of all the geometric and thermoelastic aspects of the problem. This would involve no conservatism, of course.

One of the directions of this investigation has been to explore all three of these situations and ascertain how they are related for the cases investigated during this project. The results of that comparison form an important part of the report and are discussed in the Conclusions.

Discussions of Related References

Investigations of thermal stresses in ships have been reported in the open literature (Refs. 5 through 8). These studies relate to the generation of thermal stresses induced in a ship by the external environment. They involved radiation from the sun, convection from the air, and primarily conduction from the sea. The model studies have involved air convection and simulated sea conduction.

In all these studies, the ship structure was tacitly assumed to be a series of connected plates. No results were reported on the distributions of temperatures and stresses through the plating or across the stiffening systems in planes perpendicular to the stiffened plates. As a result, none of the theoretical procedures discussed in the references would be completely satisfactory in their present form for use in the analysis of ship thermoelastic problems since the latter type of heat transfer (and the resulting thermal stresses) could be important for stiffened plate stresses. However, present theories could be modified and adapted to that purpose.

In general, the agreement of theory and experiment by Lyman and Meriam (Ref. 8) was found to be good with deviations mostly in the order of a few percent for the ship measurements. However, it is surprising to observe that several experimental data differed by more than 10 percent from theoretical computerized predictions of thermal stress in the model studies conducted by Lyman and Meriam.

The most significant aspect of the cited references was the confinement of the problem to direct measurements of temperatures and of thermal stresses. Heat transfer calculations were not performed, nor were measurements made, to determine temperatures from heat inputs.

In summary, therefore, it appears that the result of Ref. 5 through 8 can serve only as a preliminary indication of the general nature of the stresses in a ship resulting from thermal shock.

Basic Thermoelasticity

The basis for almost all thermoelasticity is the axiom that the total strain in a thermally stressed structure is the algebraic sum of the strains arising from unrestrained thermal expansion and from internal stresses,

$$\varepsilon = \sigma/E + \alpha T \qquad (39)$$

Eq. (39) holds for uniaxial stresses because the mechanical stress is uniaxial. Otherwise it would be necessary to employ the three-dimensional stress field relations, of which the total strain in one direction is expressed

$$\epsilon_x = \sigma_x/E - \nu\sigma_y/E - \nu\sigma_z/E + \alpha T \qquad (40)$$

If we return to Eq. (39) and consider a situation in which the total strain is zero, then the thermal component balances the mechanical component and if the minus sign is disregarded,

$$\sigma = \alpha E T \qquad (41)$$

Eq. (41) is the simplest possible thermal stress theoretical relation of the induced stress to the average values of thermal expansion, Young's modulus and temperature change. In the case of a length of longitudinally restrained wire which has been chilled through a temperature change, T, it provides the precise solution in the region of the wire removed from the ends.

Suppose, now, that a general three dimensional structure is subjected to action by a fluid mass initially different from the structure temperature by an amount, T_o. If the structural material is homogeneous, and the structure is free in space, then it is possible to write the thermal stress relation for any location at any time after application of the fluid mass

$$\sigma = C_o \alpha E T_o = C_o \sigma_o \quad (\sigma_o = \alpha E T_o) \tag{42}$$

where the coefficient, C_o, contains all the complexity of the structural geometry and the character of the heat transfer between the fluid mass and the structure. In fact, for initial estimates of the magnitude of severity of a thermal stress condition, Eq. (42) is often used with values of C_o dictated by experience. For a large range of problems C_o may be chosen to be 1/2 (a linear gradient across a restrained bar, for example).

Stresses in a structure generally tend to peak at discontinuities. Mechanical stress concentration factors are well documented in the literature (for example, see Peterson's compendium, Ref. (9). The situation with regard to thermal stress concentration factors is radically different, as has been shown by Colao, Bird and Becker in Refs. 4, 10 and 11. One broad generalization relates to the maximum thermal stress in a structure of any shape, with or without discontinuities. The basic study of Ref. 4 showed theoretically and experimentally that there is an upper bound

$$\sigma_{max} = \sigma_o \tag{43}$$

while more recent studies by Emery, Williams and Avery (Ref. 12) have added more substantiation to the prediction, also through both theoretical and PTE analyses.

The simplest calculation of thermal stress can be made by substituting appropriate data in Eq. (43), which also will yield the most conservative estimate of thermal shock stress resulting from tank rupture. If αE is assumed to be 300 psi/°F then

$$\sigma_o = 300 T_o \tag{44}$$

where T_o is the difference in temperature between the cryogenic fluid and the steel of the ship structure before the thermal transient begins. Actually, heat transfer considerations (as reflected in B) dictate the almost certain reduction of the largest usable temperature difference to some value less than the fluid-ship difference. In terms of maximum achievable thermal stresses, Emery, Williams and Avery have shown that for photoelastic plastics the effective difference may be only about 60 to 65 percent of the maximum (Ref. 12). Their results are displayed in Figure 7 which indicates that for the steel model of this investigation C_u would be less than 1/2.

The preceding relate to a rather simple type of structure and for a case in which the fluid temperature remains constant throughout the thermal transient. Actually, the chilling of the steel will be accompanied by warming of the fluid, thereby reducing the available temperature difference still further.

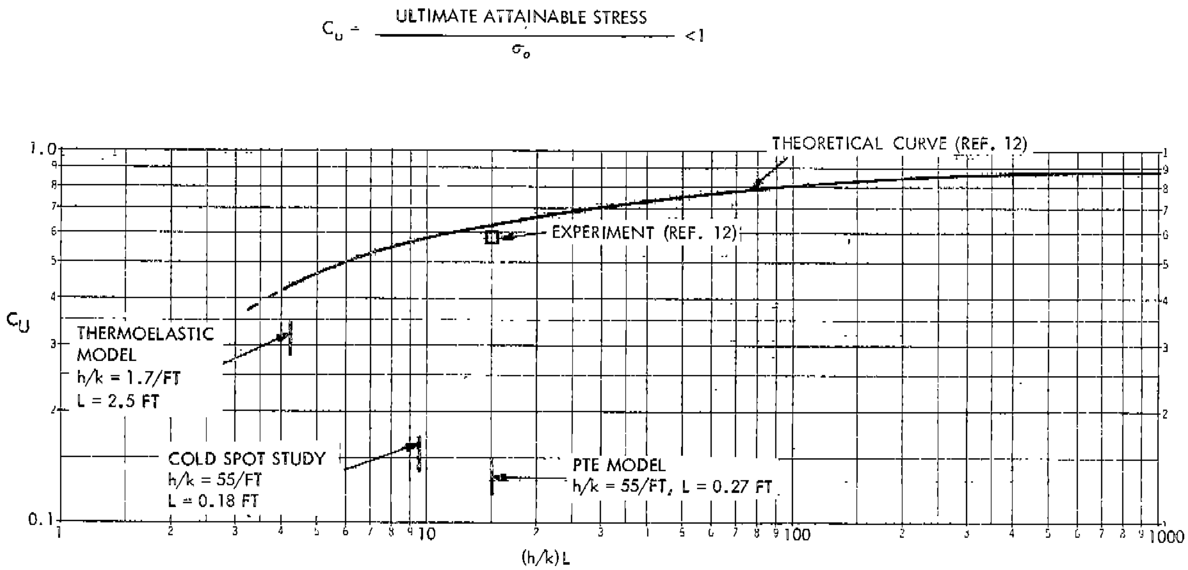

FIGURE 7 - Effect of Biot Number on Thermal Shock Stresses.

The coefficient, C_o, may be invested with the role of reflecting this change.

These simple calculation methods represent steps in the approach toward determination of the precise value of thermal stresses in the steel ship model. One more factor is the relative cross section areas of the cold and warm regions of the ship immediately following chilling of the hold walls and bottom. If the longitudinal forces are balanced and the cross section strain is assumed to remain planar, then (Figure 8) the force and strain relations are:

$$\sigma_1 A_1 + \sigma_2 A_2 = 0 \qquad (45)$$

$$\sigma_1/E + \alpha T_1 = \sigma_2/E + \alpha T_2 \qquad (46)$$

where T_1 is the average temperature of the inner structure when the peak stress is reached, and T_2 is the assumed uniform initial temperature of the ship steel before the transient. That is not the type of initial distribution that would exist at sea. The temperatures from the actual initial and transient conditions would be additive if the superposition principle is operative, which it would be if stresses remain elastic. The combination of inelastic thermal stress fields is a subject for a subsequent project.

It is a simple matter to combine Eqs. (45) and (46) so that either σ_1 or σ_2 may be found. For example, for the model region outside the center tank,

$$\sigma_2 = \sigma_o (T_1/T_o - T_2/T_o)/(A_2/A_1 + 1) \qquad (47)$$

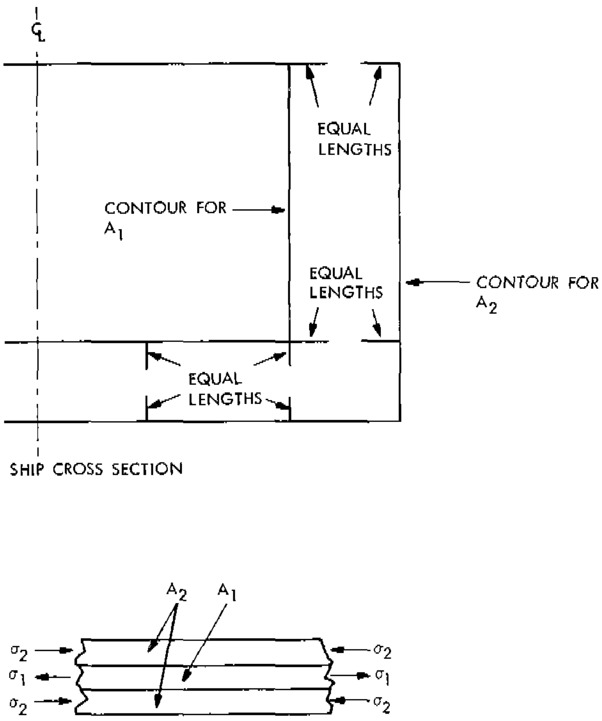

FORCE BALANCE DIAGRAM ASSUMING CENTROIDS OF A_1 AND A_2 ARE COINCIDENT

FIGURE 8 - Schematic Representation of the Ship Cross Section Force Balance and Strain Equilibration.

where T_o (the difference between the initial fluid temperature and the initial model temperature) is introduced as a normalizing factor. If T_2 represents room temperature (the initial temperature of the model) and T_1 is the deviation from room temperature due to chilling in the tank region, then let $T = T_2 - T_1$, and the last terms in parentheses are the area corrections from the force balance relation. Consequently

$$\sigma_1/\sigma_o = (T/T_o)(A_2/A_1)/(1 + A_2/A_1) \tag{48}$$

$$\sigma_2/\sigma_o = (T/T_o)/(1 + A_2/A_1) \tag{49}$$

If A_1 and A_2 are nearly equal, then the above-mentioned factor of 1/2 would apply as long as T is close to T_o.

In any structure the selection of the proper values for A_1 and A_2 normally would involve some judgement based upon experience. In this effort the areas were chosen arbitrarily by first selecting the approximate location of the anticipated mean temperature between the cold and warm regions. Errors are to be expected since the temperatures actually vary throughout a structure and are not so simply divided.

Cold Spot Problem

As a means of evaluating the general nature of the stress field in the ship, a relatively simple problem was chosen for an initial PTE investigation as shown in Figure 9. In order to compare the result with a classical closed form theoretical solution, it was assumed that the problem could be approximated by a cold spot in the center of a circular disk.

The general expression for the tangential stress is (Ref. 13)

$$\sigma/\sigma_o = \{1/2 - (a/b)^2[1 + (b/r)^2]/4 - (1/2)\ln(b/r)\}/\ln(b/a) \qquad (50)$$

where σ_o relates to the difference in temperature between the inner cold spot and the disk exterior. For the PTE study, one area of interest is the outer boundary of the disk. Since $r = b$ at that location, then Eq. (50) becomes

$$\sigma/\sigma_o = (1/2)[1 - (a/b)^2]/\ln(b/a) \qquad (51)$$

Out-of-Plane Behavior

The thermoelastic problem in a ship has been approached in this investigation mainly as the study of multiple-plate plane stress. However, the presence of stiffeners on one side of a plate would induce heat flow normal to the plane of the plate. The consequence would be out-of-plane stresses and deformations. If the stiffener flanges were symmetric about the web, then the deformations and stresses might be confined to bending. Angle stiffeners, however, might tend to bend and twist, and any tendency to buckle could be aggravated in certain cases. The buckling process would tend to relieve the thermoelastic field. However, it could lead to instability strength loss against the pressure-induced forces from the sea.

Angle-shaped longitudinal stiffeners were used on the steel model to accentuate this effect in order to assess the importance to ship design. In the current study, numerical values of stiffener stresses were obtained on the steel model. However, only a relative assessment was made of the stress levels compared to the maximum values in the model. A more detailed evaluation of stiffener behavior was deferred to possible subsequent investigations in which the possible significance to structural stability may be considered.

Thermal Stress Scaling

If two structures are identical in shape but differ in size and material, it is necessary to utilize a theoretical relation to determine the nature of the stresses in one structure when the stresses in the other are known in a given set of circumstances. For mechanical loads the shapes of the stress distributions in the two structures would be essentially identical. Small differences may exist at discontinuities if Poisson's ratio is not the same for the two materials, but this is usually a negligible consideration.

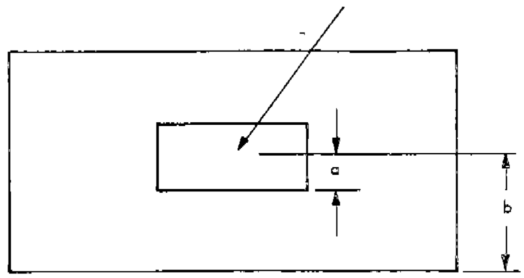

EXPERIMENTAL MODEL CONFIGURATION

FIGURE 9 - Cold-Spot Problem.

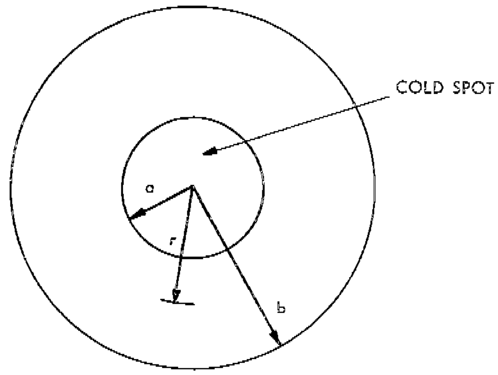

EQUIVALENT COLD-SPOT CONFIGURATION

The best means of relating the stress fields is to develop a non-dimensional ratio of stresses which would have the same value for both structures. For example, it is well known that an appropriate scaling law for pressure vessels would be

$$(\sigma/p)_{model} = (\sigma/p)_{prototype} \tag{52}$$

This means that the stress at a given point and in a given direction on a model would be exactly the same on the prototype if the pressures applied to each are the same and that the prototype stress would be further increased beyond that value as the pressure is increased.

The relation in Eq. (52) applies to static pressures. For transients a time factor must be considered. This is also the case for temperature transients. However, when the time factors are accounted for as described for thermal scaling, then an appropriate scaling law for thermoelastic problems would be

$$(\sigma/\alpha E T_o)_{model} = (\sigma/\alpha E T_o)_{prototype} \tag{53}$$

or, in the form of Eq. (42) and abbreviating the subscripts,

$$(C_o)_m = (C_o)_p \tag{54}$$

MODELS AND EXPERIMENTS

General Descriptions

Seven steel ship configuration models and two plastic models (Table 4) were designed and fabricated to acquire experimental data in this project. Three two-dimensional steel models and three three-dimensional steel models were employed solely for temperature studies while the last steel model was used for both temperature and stress determinations. The two photoelastic models were tested to obtain supplementary thermal stress data.

The characteristics of all models appear in Figures 10 through 21 which depict the dimensional and material data as well as the locations and types of instrumentation. Discussions of the models and test procedures appear in subsequent portions of this section.

A flat plate was employed to measure the surface heat transfer coefficients for the various fluids employed in these investigations. These tests are discussed below also.

Temperature Models

Two models were designed and fabricated to represent a range of ship proportions and heat transfer characteristics. The cross-sections appear in Figure 10. A view of both ship models and the general experimental arrangement appear in Figure 11.

Each temperature model consisted of one half of a ship region. It was rendered thermally symmetric about the vertical centerplane by 1 inch thick styrofoam plate cemented to the steel with RTV silicone rubber. In addition, styrofoam was cemented to the ends of each temperature model. As a result the 2D models were constrained to essentially vertical and athwartship heat transfer whereas the 3D model was free to transfer heat longitudinally for one bay on each side of that into which the chilling fluid was introduced.

As is shown in Figure 10, each model was modified twice by halving the wing tank width so that three widths were available for study in 2D and in 3D. Since two non-boiling and two boiling runs were performed on each configuration, twelve pairs of tests were conducted to obtain experimental data for comparison with theory. Each experiment was performed by rapidly filling the center hold of the model with chilling fluid. Thermocouple data were recorded for 1/2 hour after the start of the pour which required from 6 to 15 seconds depending on the model and the fluid.

Model for h

Part of the temperature investigation was assigned to measurement of surface heat transfer coefficients for the fluids which were used. The experiments involved rapid pouring of enough fluid into the square cavity above a plate (Figure 12) to fill the cavity almost completely. Temperatures were recorded from the beginning of the pour which required only a second to accomplish.

TABLE IV - Model Descriptions

Model	Figures	Use
2T, Three Widths	10	Two-dimensional temperature distribution. Large proportion of conductive heat flow compared to convection and radiation. Thick steel plates unreinforced.
3T, Three Widths	10	Three-dimensional temperature distribution. Small proportion of conductive heat flow compared to convection and radiation. Thin steel plates reinforced against buckling.
3TE	18	Thermoelasticity in simulated ship. Conduction comparable to convection or radiation. Thick steel plates reinforced.
2PTE	13	PTE local cold spot, two-dimensional problem. Single plastic plate.
3PTE	15	PTE ship simulation, three-dimensional behavior. Thick plastic plates.
Flat Plate	12	Experimental determination of heat transfer coefficients for non-boiling and boiling fluids.

Photothermoelastic Models

PTE investigations were conducted on a rectangular flat plate with a central chilled spot and on a plastic simulation of the steel model. One purpose was to determine how closely Eqs. (48) and (49) would agree with experimental data for these cases to provide a base for evaluating the steel model results. Another was to obtain a preliminary indication of the usefulness of simple theoretical prediction procedures for temperatures and stresses in the steel model. The PTE simulated ship experiment also provided data to aid strain gage placement on the steel model.

Cold-Spot Model

The cold-spot model is a simplified delineation of the bottom plane of the ship. The region within the dam represents the hold floor and the external rectangular annulus corresponds to the remainder of the ship structure at that level, except that the vertical walls of the ship introduce the equivalent of additional cross section areas to the tank bottom and the external regions.

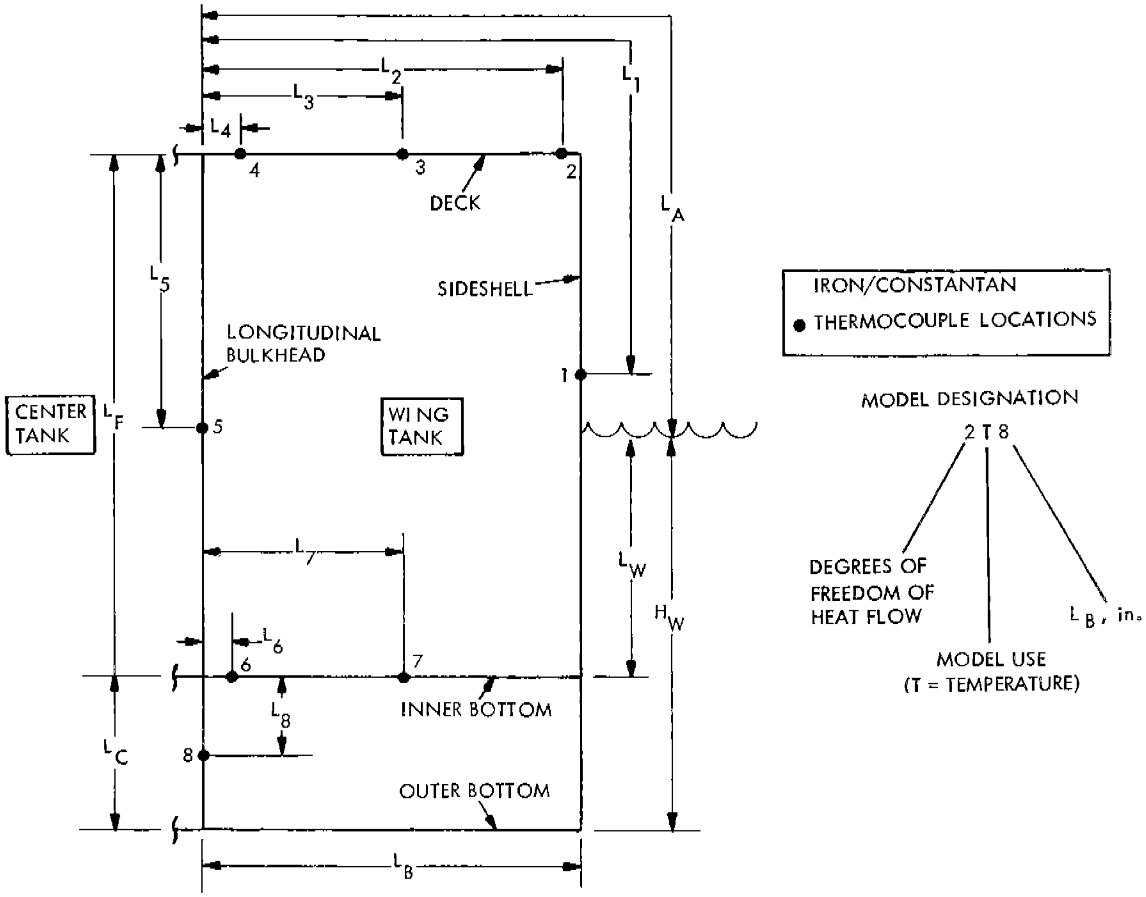

OVERALL HEIGHT, ALSO BAY LENGTH
2T MODELS, 8 IN. 3TMODELS, 12 IN.

MATERIALS: 2T MODELS, 1/8 IN. CARBON STEEL
3T MODELS, 0.032 IN. CARBON STEEL

ALL DIMENSIONS IN INCHES

MODEL	L_F	L_A	L_W	L_C	H_W	L_1	L_2	L_3	L_4	L_5	L_6	L_7	L_8
2 T 8	7	12	3	1	4	11.5	8.0	4.0	0	3.4	0	4	0.5
2 T 4	7	8	3	1	4	74	40	2.0	0	3.4	0	1.8	0.5
2 T 2	7	6	3	1	4	5 5	2.0	1 0	0	3.4	0	1.0	0.5
3 T 12	10	18	4	2	6	173	12.2	6.3	0	5.1	0	6.1	1.0
3 T 6	10	12	4	2	6	11.1	5.8	3.1	0	5.1	0	3.1	10
3 T 3	10	9	4	2	6	8.1	3.1	1 5	0	5.1	0	1.5	1.0

FIGURE 10 - Thermal Model Data.

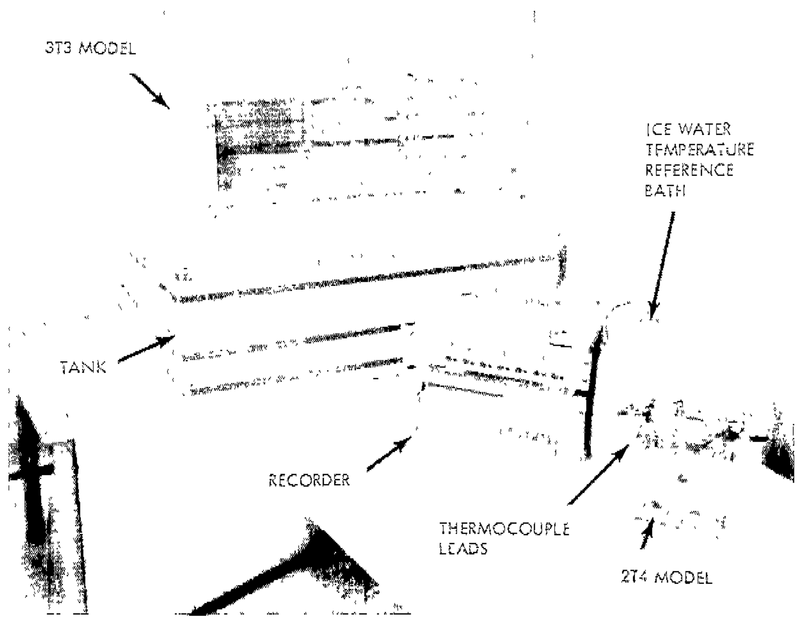

FIGURE 11 - Ship Temperature Models and Experimental Equipment.

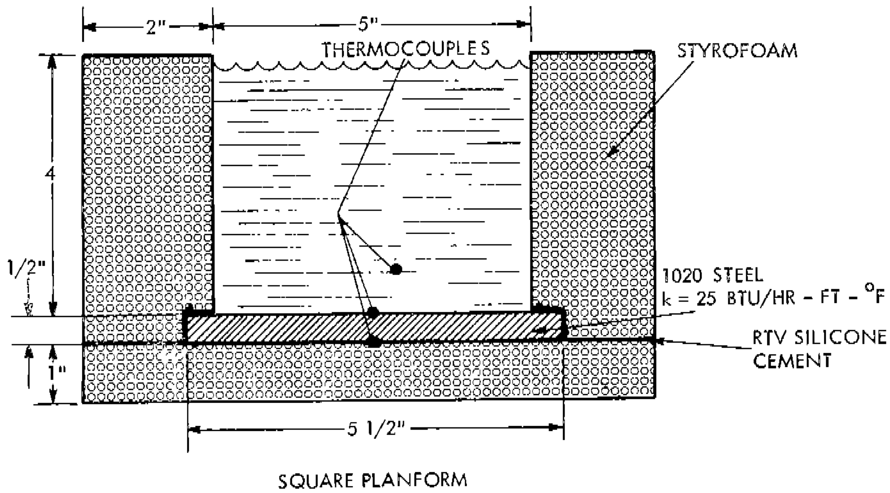

FIGURE 12 - Model for Heat Transfer Coefficient Tests.

The model is shown in Figures 13 and 14 together with the PTE material properties. It was important, in designing the experiment, to select a dam wall material and joint which would not resist the deformations in the plate. Furthermore, the joint had to prevent leakage of the ethylene glycol under the walls. Some experimentation showed that these conditions would be satisfied with a fiberglas wall 0.064 in. thick and a silicone RTV rubber joint, as shown in Figure 13.

The experiment was initiated by sudden introduction of the chilled ethylene glycol. Temperatures and fringe patterns were recorded at selected intervals.

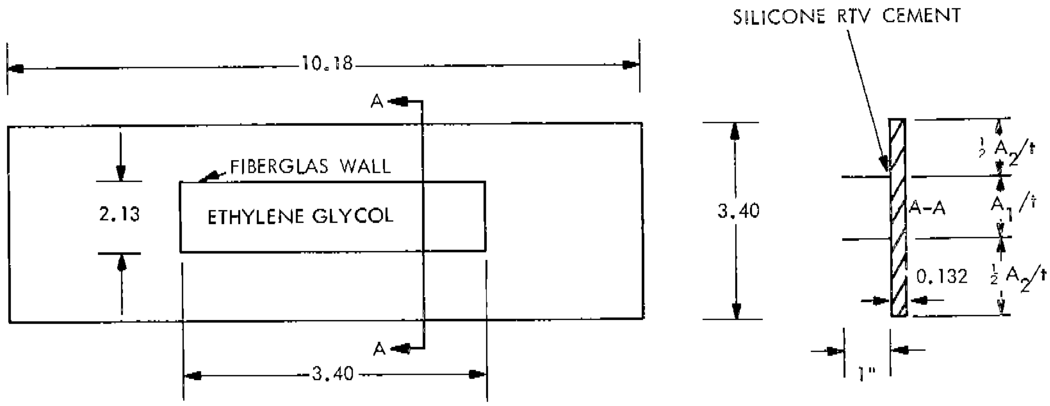

MODEL MATERIAL,

α, $37 \times 10^{-6}/^{\circ}F$
E, 0.36 MSI
f, 40 PSI-IN/FRINGE
$k/c\rho = 0.005$
(COMPARED TO 0.45 FOR STEEL)
$\alpha E = 13.32$ PSI/ °F
$A_2/A_1 = 0.60$

FIGURE 13 - Cold-Spot Model.

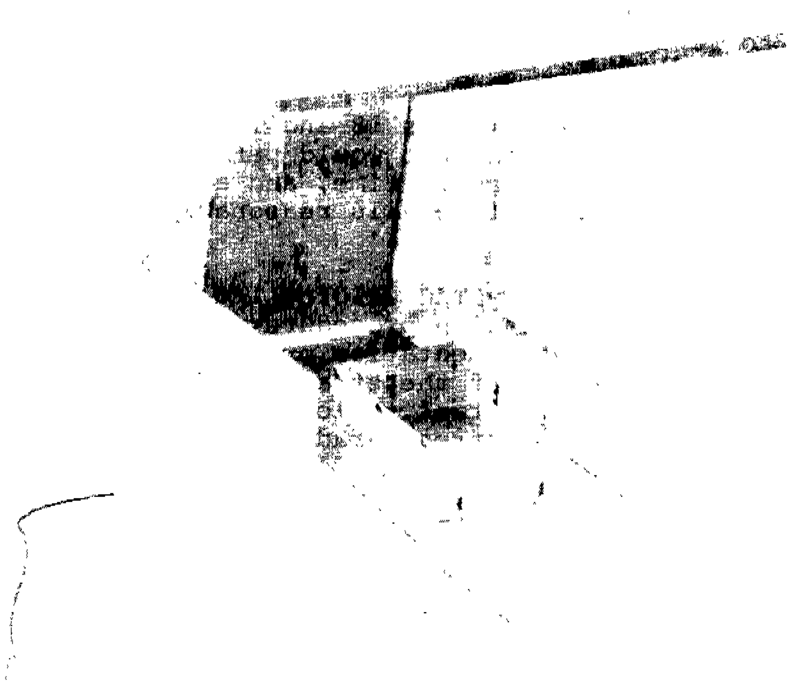

FIGURE 14 - Photograph of Cold-Spot Model Test.

PTE Simulated Ship Experiment

Before this project began a small photoelastic model was built to reveal the general character of thermal stresses in a ship with sudden chill applied to the center hold. The model details appear in Figure 15. During this current project the experiment was repeated for the reasons discussed previously.

The model was fabricated from flat plates of PSM-1, which was used for the cold-spot study also. They were cemented to the configuration shown in Figures 15 and 16. The polariscope sheets were built into the model so as to reveal the stress field in every plate, although polarizing sheets were located only at one quarter of the model plates because of the model and experiment symmetries. It was desirable to view all polariscopes simultaneously. This was accomplished with the experimental arrangement shown in Figure 17 which enabled the camera film to contain all the fringe pattern images.

Thermoelastic Model

Thermoelastic studies were conducted on a welded steel model fabricated to represent three bays of a cryogenic tanker in general configuration.

The model is depicted in Figures 18 and 19. The size was a compromise between a small model that would permit complete filling of the central hold in a short time, and a large enough model to enable the duplication of details reasonably representative of an actual ship.

The model was fabricated by TIG welding 1/8 inch thick plates of T-1 steel. The fabrication procedure required coordination of the welding and instrumentation processes in order to permit internal installations of the strain gages and thermocouples. Also, since it was important to locate strain gages close to the plate intersections where stress gradients are greatest, it was necessary to establish the minimum distances from the final welds at which strain gages could be located without damage by the heat of the welding process. These necessitated tests to establish the smallest size weld which would provide a sound joint, and experiments on gage survivability as a function of proximity to those welds. (In spite of all these precautions, a few gages were lost during fabrication)

Welding studies were conducted to design the details of the model welding procedure so as to maintain plate flatness and accurate alignment of adjacent plates.

These tests and the model fabrication schedule consumed a large portion of the project. However, the efforts resulted in a well-built model, optimized the gage proximity to intersections, and minimized the number of gages.

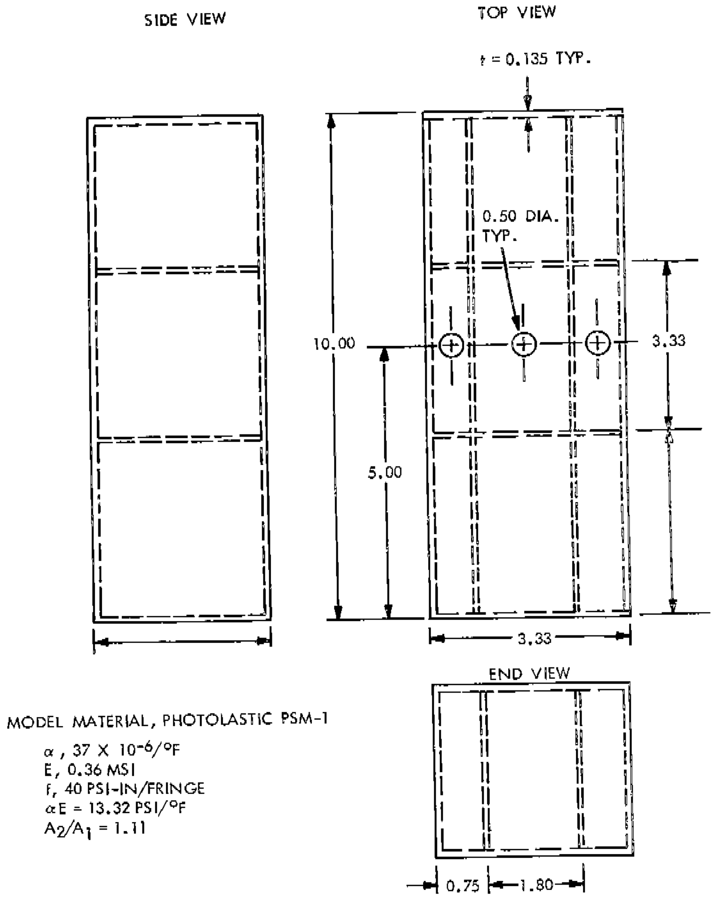

FIGURE 15 - PTE Ship Model.

FIGURE 16 - PTE Ship Model Photograph Showing General Experimental Arrangement.

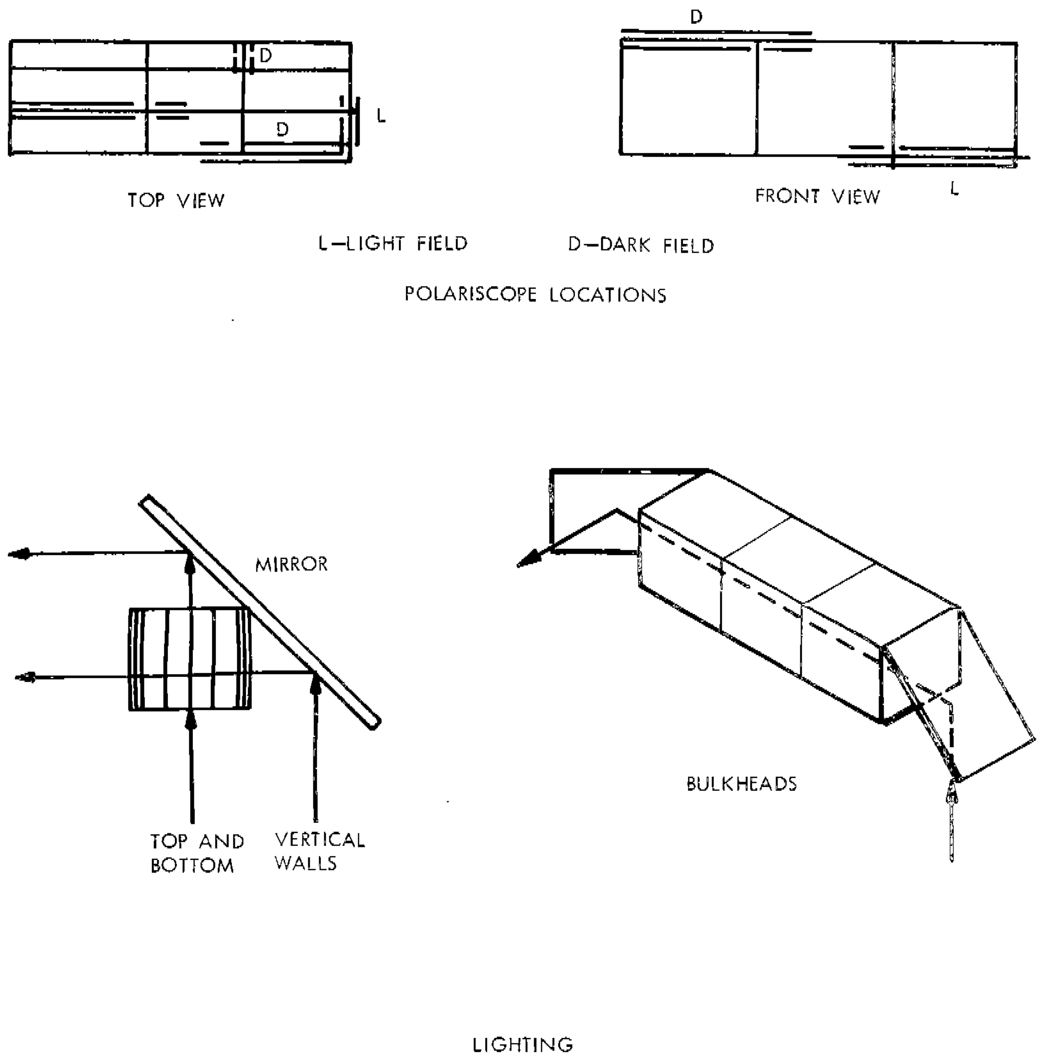

FIGURE 17 - Ship PTE Model Experimental Arrangement.

Instrumentation

The temperature sensors were fashioned from 24 gage iron-constantan thermocouple wire, beaded and wound into a 3-turn spiral. The bead and the spiral were held in close contact with the steel while the epoxy cement bonding agent dried and hardened. The strain gages (Table 5) were adhered to the steel with BLH SR-4 EPY-550 cement. Data were obtained on a Visecorder. The applications of the uniaxial gages are depicted in Figure 20 while the arrangements of the others are shown in Figure 21.

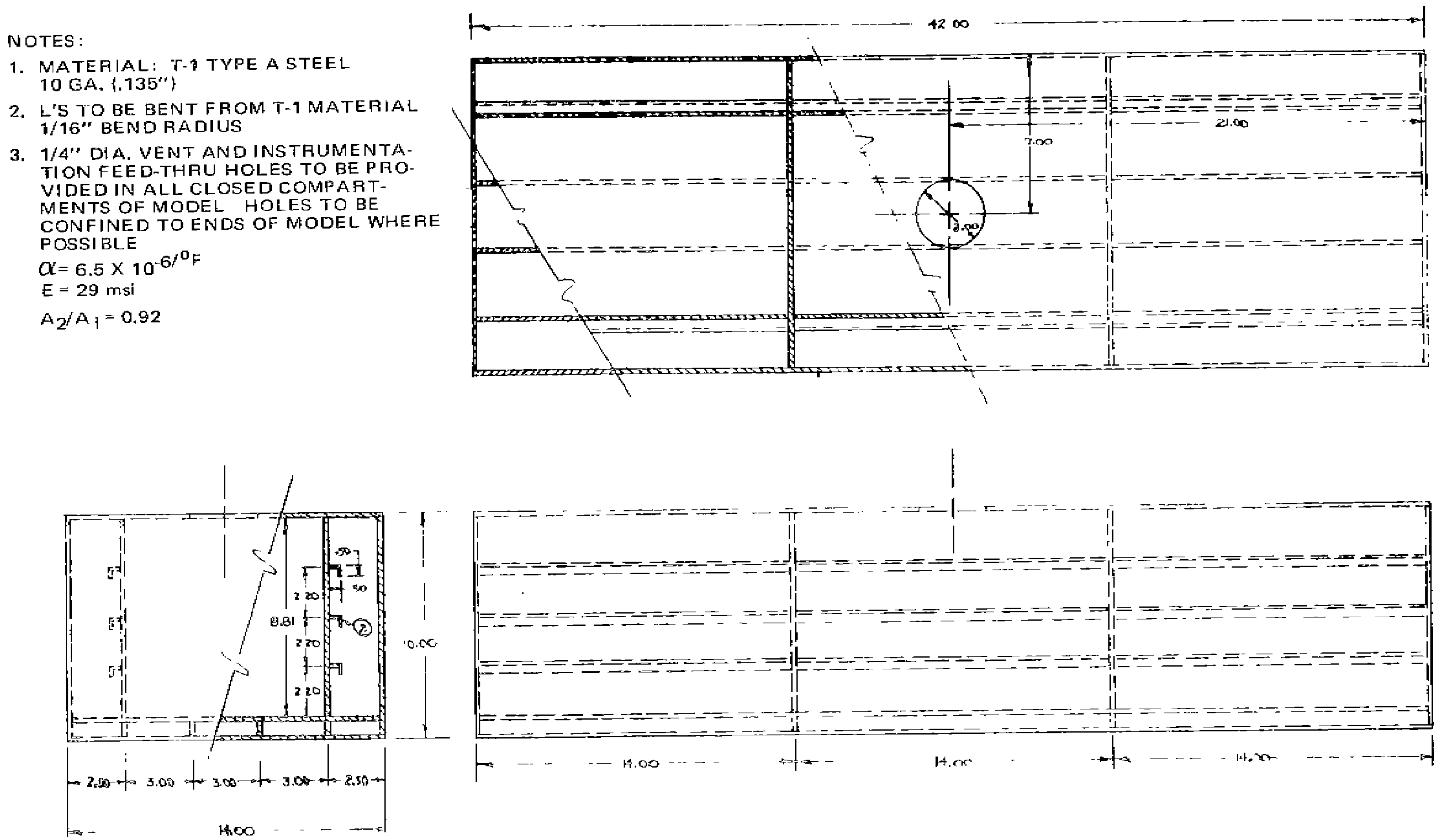

FIGURE 18 - Steel Ship Model Dimensions.

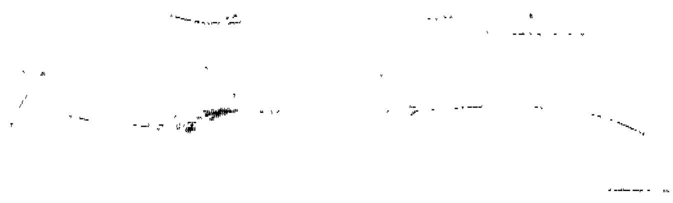

Thermocouples Attached to Plates Before Welding

Completed Interior Structure

FIGURE 19 - Photos of Model at Different Stages of Construction.

TABLE V - Strain Gage Characteristics and Locations

Type	Shape	Locations
BLH FAE-12-12S6 120 ohms, gage length = 1/8 in.	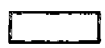	9, 10, 11 Figure 20
Vishay Micro-Measurements WK-06-250WT-120 120 ohms, gage length = 1/4 in.	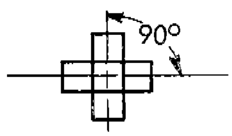	1, 6, 7, 8 Figure 21
Vishay Micro-Measurements WK-06-250WR-120 120 ohms, gage length = 1/4 in.	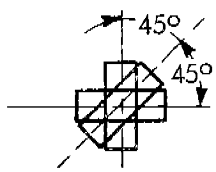	2, 3, 4, 5 Figure 21

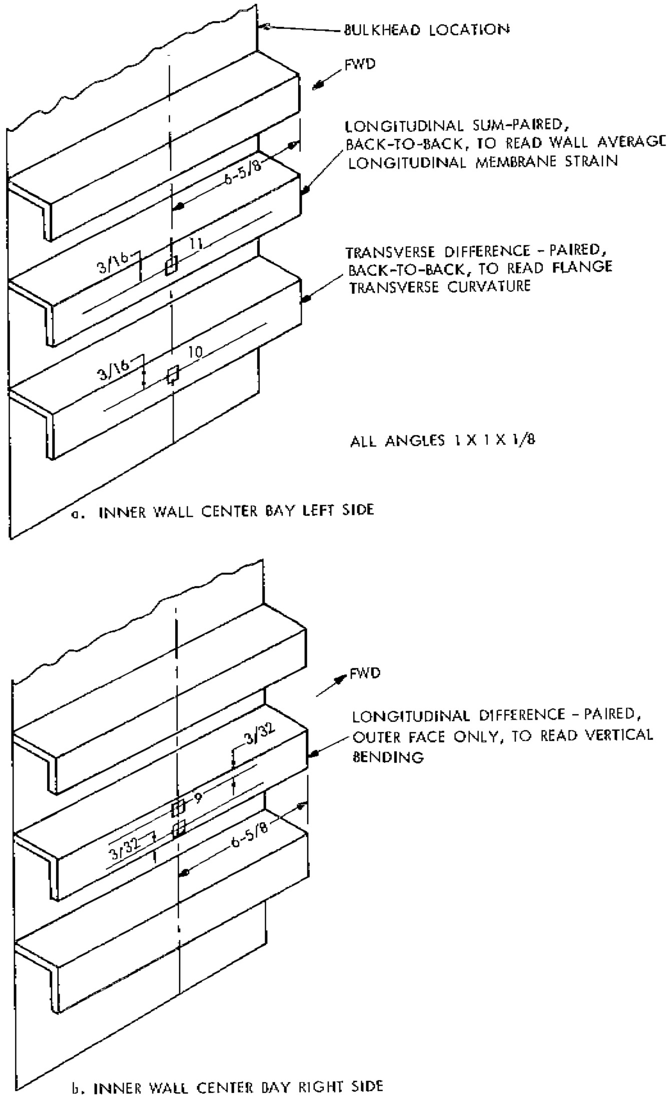

FIGURE 20 - Thermocouple and Uniaxial Strain Gage Locations.

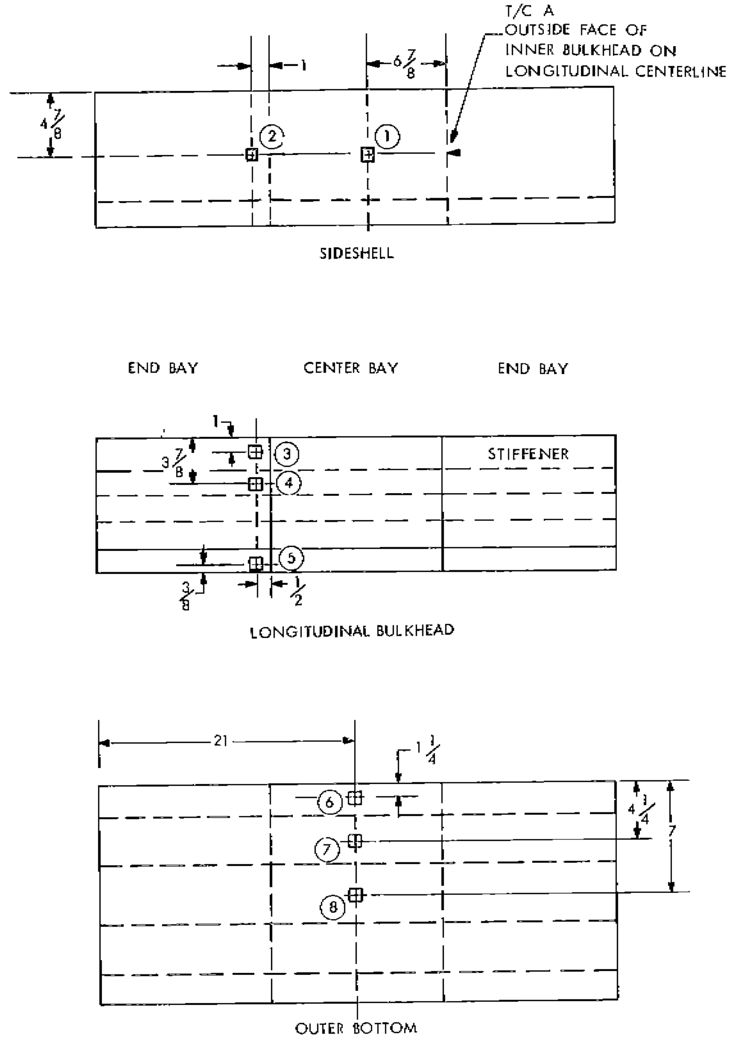

FIGURE 21 - Biaxial and Rosette Strain Gage Locations and Thermocouple Locations.

Experimental Procedure for Thermoelastic Model

The center bay was chosen to receive the sudden introduction of chilled fluid. A special pumping system was designed and constructed for rapid injection of the chilled denatured alcohol into the center bay. A Minneapolis-Honeywell light beam oscillograph was used to record the data throughout each run, which was typically of 6 to 7 minutes duration.

Each experimental run was begun by cooling the denatured alcohol by immersing the tank in chopped dry ice until a temperature of about -30°C had been reached. The recorder was activated and then the pump was started to inject 5 gallons of chilled denatured alcohol into the center hold. Injection was accomplished within 8 to 10 seconds, with a final fluid level of from 1 to 2 inches below the undersurface of the hold top. Appendices I and II contain temperatures and stresses obtained during all the runs.

At the completion of the tests the thermocouple signals were converted to temperatures and the strain gage data were converted to stresses. The culmination of the project was the comparison of the experimental data with the predictions of the theoretical procedures.

Five runs were required to acquire all the necessary strain and temperature data. T_o varied from run to run. However, all the principal stresses were normalized to σ_o.

EXPERIMENTAL MECHANICS

Introduction

Thermocouples were applied to the steel temperature models while strain gages were used on the steel thermoelastic model together with thermocouples. Photothermoelasticity was employed to obtain pertinent data from two supplementary experiments, one of which was conducted on a plastic simulation of the steel model. The three experiment types together with the theoretical analyses, were planned to provide the data on which to base the prediction procedures sought as the goal of this project.

The properties of the steel model instrumentation are described in the sections relating to those experiments. They are in broad use and are familiar to most naval architects and engineers. However, PTE is not in universal employment. Therefore, a brief sketch of the technique is presented.

PTE

When transparent structures are loaded in polarized light, interference fringes are observed, the nature of which may be related to stress through a calibration procedure. The basic character of the process is more than 150 years old. Detailed descriptions are available in numerous textbooks and journal articles. Two of the best known references are the treatises by Coker and Filon (Ref. 14) and by Frocht (Ref. 15). The basic relation between stress level and fringe order is shown to be

$$n = (\sigma_1 - \sigma_2)L/f \tag{55}$$

where 1 and 2 refer to the principal stresses and L is usually the thickness of the model. For a free edge, $\sigma_2 = 0$.

In all the work in photoelastic analysis of structural behavior the loading was a mechanical force system until about 15 years ago. At that time a series of investigations was initiated (Refs. 16 through 19 contain many of the results) in which the models were loaded by temperature fields, most of which were initiated by application of dry ice directly to the model surfaces. The resultant transient temperature fields induced fringe patterns which are related to stress in exactly the same manner as for mechanical loads. Although the stress distributions generally are different for the two types of loads, the usual calibration process and fringe interpretation of mechanical photoelasticity apply without modification to thermally loaded structures. It is only necessary to measure the relevant model material parameters as functions of temperature to obtain reliable data.

After a series of relatively simple investigations, experimentalists found that the achievable precision of a PTE investigation was as good as, or better than, that of a mechanical investigation. Correlation with theory was found to better than 1 percent in almost every case. This success led to the use of PTE to evaluate the precision of thermoelastic theories, as was done by Becker and Colao on rectangular strips (Ref. 10). It also was used to establish broad generalizations of thermoelastic behavior such as the lemma advanced in Ref. 4 relative to the maximum attainable thermal stress in a structure, and the generalization that thermal stress concentration factors are not the same as mechanical stress concentration factors except possibly in a few special cases. This latter generalization was established by Becker and Bird (Ref. 11) in a study of holes in a plate.

Perhaps one of the most important aspects of the PTE investigations to date is the observation that a relatively simple theory may be found to predict the observed stress maxima. In some cases it also was possible to predict the stress distributions reliably (ref. 4). The experience with PTE has provided a part of the basis for the approach to this project which was focused on initially simple methods for calculation of thermal stresses and temperatures.

As was stated in the introduction, there are numerous instances in the photothermoelastic literature to demonstrate that excellent agreement of theory and experiment is achievable when the stress predictions proceed from the known temperature fields (Refs. 16 through 19). All the observed discrepancies are directly traceable to the heat transfer aspects of the problem. These lie either in the errors of measurement of surface heat transfer coefficient or in the errors resulting from unwarranted simplifications in heat transfer analysis methods. These latter often involve one dimensionalization of truly two dimensional problems, and the assumption of temperature-independent properties when the properties really are temperature sensitive. The Biot number is in this category. Tramposch and Gerard (Ref. 17) showed the importance of these factors when analyzing a plate-type structure which is typical of aircraft wings and ship structures.

Strain Gage Data Reduction

In terms of mechanical strains alone, the relations between plane stresses and strains are (Ref. 20, for example)

$$\sigma_x = E(\epsilon_x + \nu\epsilon_y)/(1 - \nu^2) \tag{56}$$

$$\sigma_y = E(\epsilon_y + \nu\epsilon_x)/(1 - \nu^2) \tag{57}$$

$$\tau = G(\epsilon_x + \epsilon_y - 2\epsilon_{45}) \tag{58}$$

and the principal normal stresses and maximum shear stresses are obtainable from

$$\sigma_1 = (\sigma_x + \sigma_y)/2 + [(\sigma_x - \sigma_y)^2/4 + \tau^2]^{1/2} \tag{59}$$

$$\sigma_2 = (\sigma_x + \sigma_y)/2 - [(\sigma_x - \sigma_y)^2/4 + \tau^2]^{1/2} \tag{60}$$

$$\tau_{max} = [(\sigma_x - \sigma_y)^2/4 + \tau^2]^{1/2} \tag{61}$$

The principal normal stress direction may be found from

$$\tan 2\phi = 2\tau/(\sigma_x - \sigma_y) \tag{62}$$

In this investigation Eqs. (53) through (59) were utilized to yield the magnitudes of σ_x, σ_y, and τ, and the magnitudes and directions of the principal normal stresses and the maximum shear stresses.

Experimental Errors

The experimental data consisted of temperature and strain measurements. Generally, both of these measurements may be made to an accuracy of better than 1 percent. Another view of accuracies achievable with these types of instrumentation is through identification of the magnitude of the smallest measureable quantity. For strain gages read through a bridge balance this can be as little as 5 microinches per inch under the conditions which existed in our laboratory during the testing phase. For the thermocouples the minimum measurable quantity would be 1/4°F. However, both these types of data were recorded on an oscillograph and then were deduced from the recorder traces. As a result the accuracy of reproducibility would control the accuracy of the data. For the Minneapolis-Honeywell recorder used in this project the strain scale was 940 microinch/inch for 1 scale inch with a direct reading precision of 1/100 inch which indicates a maximum precision of 9.4 microinch/inch. The temperature correction chart was of comparable precision. For the thermocouples used on the thermoelastic model the scale was 7.05 millivolts/inch directly readable to 1/100 inch which corresponds to a precision of 1.4°C or 2.5°F. On the temperature models the scale was 0.67 millivolts/inch. The net precision was better than 0.5°F.

TEMPERATURE INVESTIGATIONS

Thermal Models

The six thermal model configurations, each tested twice boiling and twice non-boiling, provided 24 runs with which to evaluate the theories proposed for determination of ship structure temperatures under cryogenic shock. The ensuing discussions have been designed to explore the correlation of theory and experiment. This was done by first examining the temperatures on the deck and upper sidewall. After that the interior plate temperatures were examined.

Attention is directed to the discussion of experimental errors which has been presented previously. The range of temperature error should be borne in mind when exploring the figures to be presented during this discussion.

Normalized Temperatures and Distances

The initial model, air and water temperatures were close to 70°F in every model test. However, the initial temperatures of the chilling fluid varied from +40°F to -100°F. In addition, the most severe test of the usefulness of the calculation methods is the reliability with which they may be used to determine the distribution of temperature from one location to another along a plate. The absolute temperatures are of little importance in this type of evaluation. Only the change between locations is important.

For these reasons the portrayal of the temperatures on graphs was accomplished by normalizing them with respect to $T_W - T_F$. Furthermore, the lowest temperatures were reached when the quasistatic behavior was observed. This occurred at approximately 1/2 hour in every test on the thermal models. Consequently, the graphs display the 1800 second values of

$$J = (T - T_F)/(T_W - T_F) = (1+R_1)/2 + R_2\overline{T}/(T_W - T_F) \qquad (63)$$

as a percentage of the distance from the deck/girder joint to the total length between the waterline and the top of the longitudinal girder. This completely nondimensionalizes the data. In a few cases other lengths were employed as references. They are described subsequently.

Tables A1 through A4 display the theoretical and experimental temperatures. Table A4 contains the normalized experimental temperatures. The theoretical curves were plots from Eq. (31) using Figure 5 to construct the highest and lowest curves only.

Presentation of Data

The theoretical and experimental information appear in Figures 22 through 32. After preliminary examination of the experimental data, it was apparent that there was enough scatter to invalidate a test-by-test comparison of theory with experiment. It appeared more reasonable to present all the information for one model on one graph and to compare scatter bands in the manner shown on the graphs. This manner of presentation is consistent with the scatter. It also permits a visualization of the range of theoretical curves for each model. Finally, the clustering of the data permit a clearer observation of the trends in the data.

Discussion of Results

The scatter of the experimental data and the general agreement with theory are somewhat better for the 3D models than for the 2D models. However, there does not appear to be a great deal of difference between them.

In most cases the temperatures were higher at the girder/deck corner and lower at the waterline than the theory predicted based upon the use of T_F and T_W as the reference temperatures. This was probably the result of the details of the convective heat transfer process in these regions. The direct test of the predictive power of the quasistatic 2D theory may be seen in Figures 23, 26, 28 and 30 in which the plate was analyzed between thermocouples 1 and 4 instead of between the water and the girder. The agreement with theory is considerably improved but there are still some unexplained large deviations for these cases. The reference length was changed to the distance between these thermocouples and the reference temperature difference was $T_1 - T_4$ so that J became $(T - T_4)/(T_1-T_4)$. The temperatures were taken from Table A3 and the lengths were taken from Figure 10.

The quasistatic theory was derived on the basis of a model in which the plate length is the distance between the longitudinal girder (assumed to be at T_F) and the point of contact with the wetted surface (assumed to be at T_W). In the cases of the 2D models however, conduction controls and therefore these reference surfaces would not be expected to be isothermal. Gradients would be expected along them, as is verified by comparison of the temperatures at thermocouples 4, 5 and 6 at the top, center and inner bottom of the bulkhead, respectively. (Table A3) The path length was increased 3.5 inches in front of thermocouple 4 and 2 inches beyond thermocouple 1 for model 2T8 (Figure 24). The revised plots of measured and calculated temperatures display a better matching of scatter bands than in Figure 22. It is apparent that the fine details of radiation and convection should be considered if better agreement of theory and experiment is required.

Bottom Structure

There is one thermocouple at the middle of the inner bottom (No. 7) and another at the middle of the girder between the inner and outer bottoms (No. 8). The temperatures at these locations appear to deviate radically from the average of the water and chilling fluid (Table A3). However, they do not depart

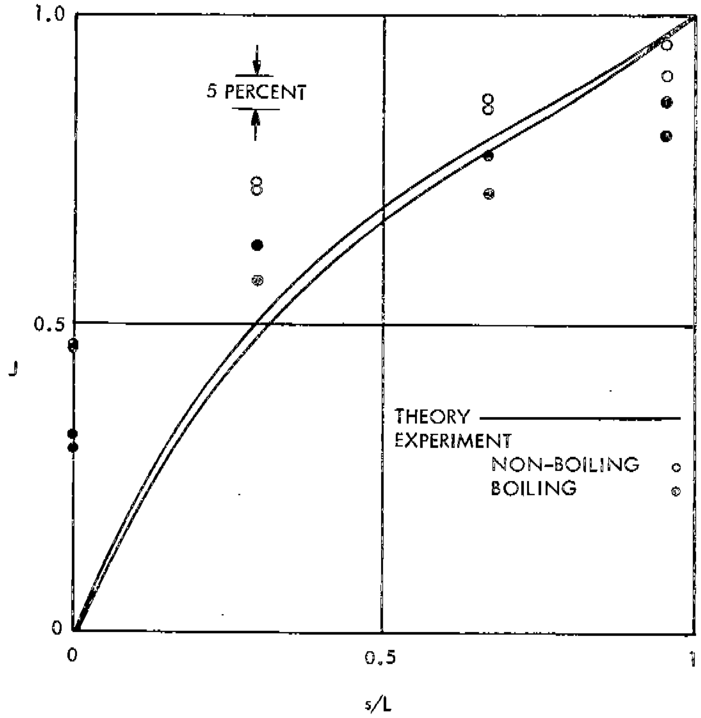

FIGURE 22 - Comparison of Theory with Experiment, 2T8, Between $T = T_F$ at s/L = 0 and $T = T_W$ at s/L = 1. Path Length from Bulkhead to Waterline.

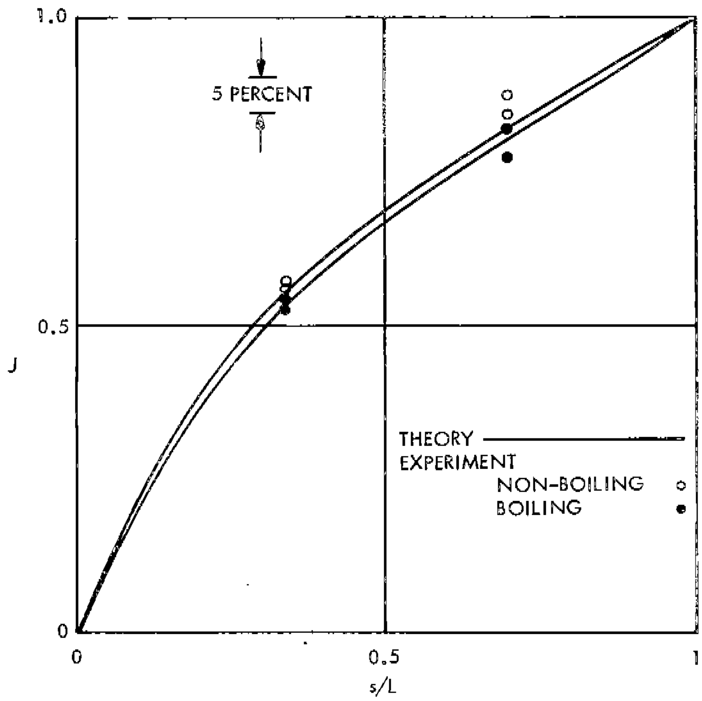

FIGURE 23 - Comparison of Theory with Experiment, 2T8, Between Thermocouples 1 and 4 Using Measured Temperatures at Those Locations.

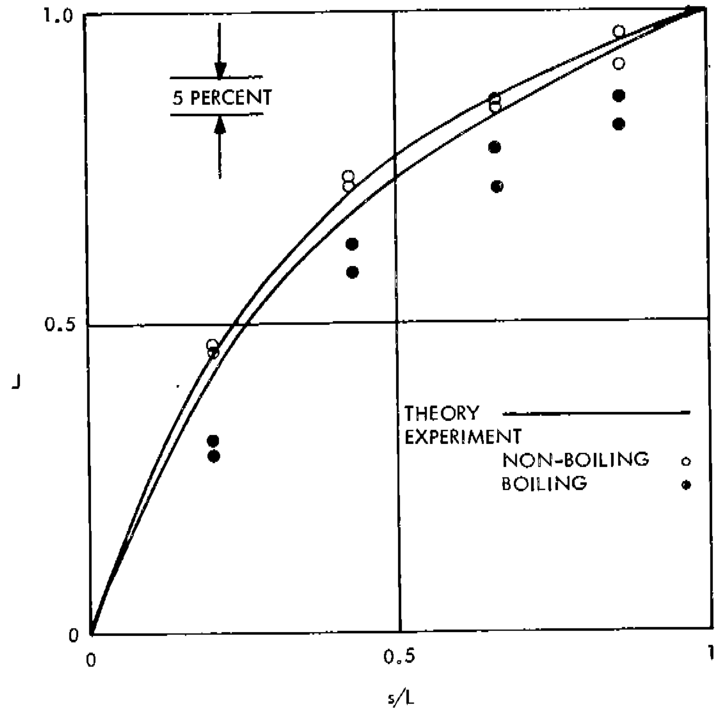

FIGURE 24 - Comparison of Theory with Experiment, 2T8, Using Expanded Path Length and $T = T_F$ at $s/L = 0$, $T = T_W$ at $s/L = 1$.

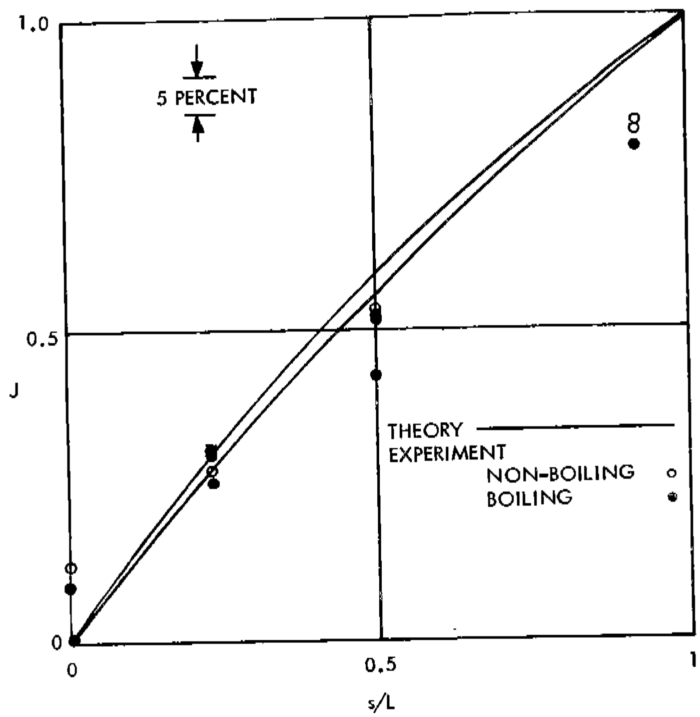

FIGURE 25 - Comparison of Theory with Experiment, 2T4, Between $T = T_F$ at $s/L = 0$ and $T = T_W$ at $s/L = 1$. Path Length from Bulkhead to Waterline.

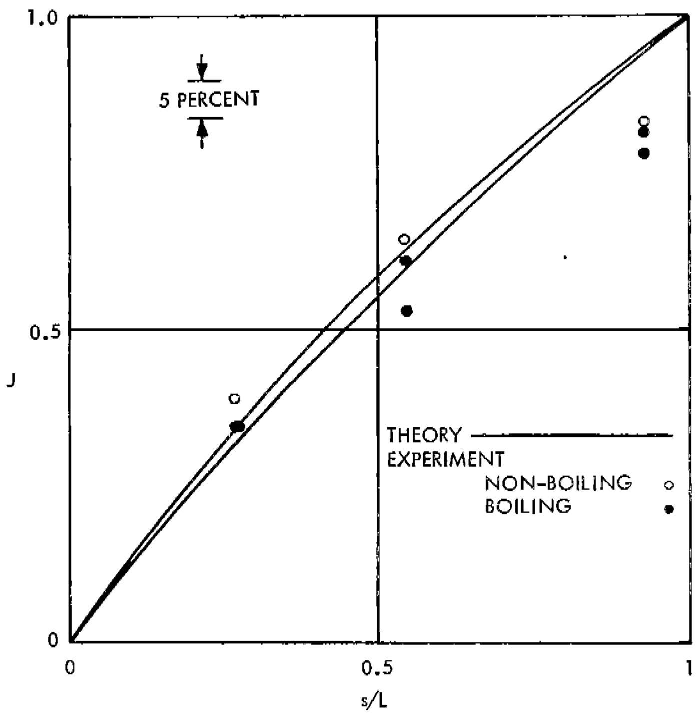

FIGURE 26 - Comparison of Theory with Experiment, 2T4, Between Thermocouples 1 and 4 Using Measured Temperatures at Those Locations.

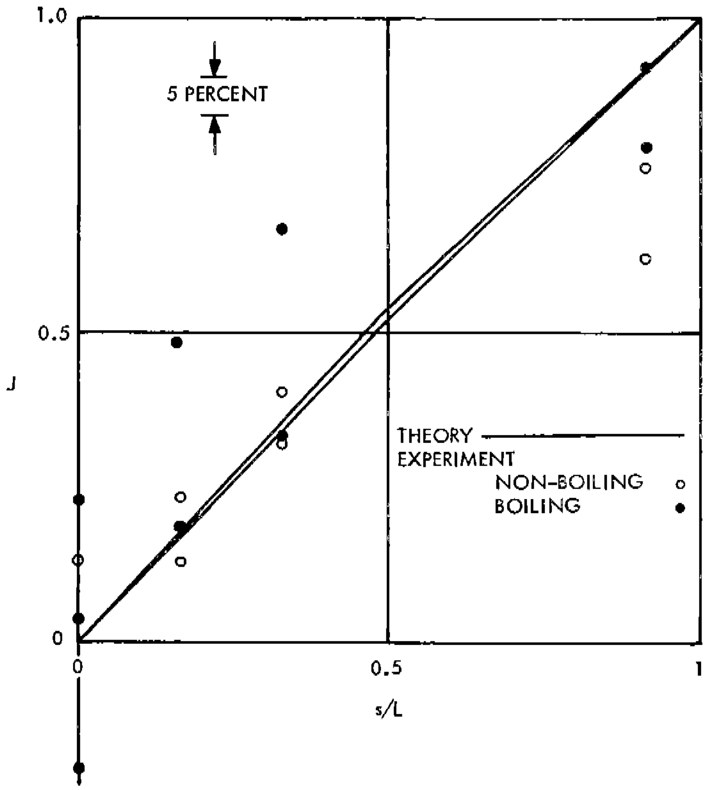

FIGURE 27 - Comparison of Theory with Experiment, 2T2, Between $T = T_F$ at $s/L = 0$ and $T = T_W$ at $s/L = 1$. Path Length from Bulkhead to Waterline.

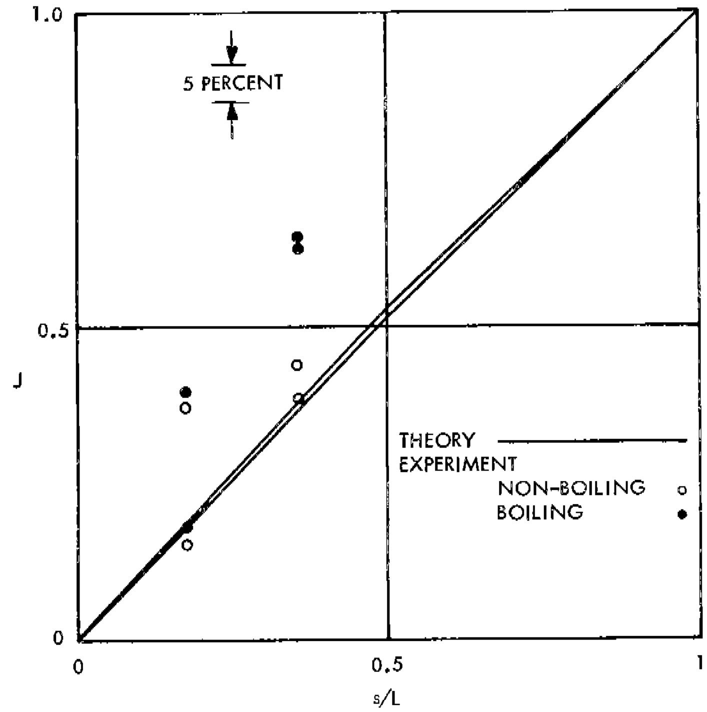

FIGURE 28 - Comparison of Theory with Experiment, 2T2, Between Thermocouples 1 and 4 Using Measured Temperatures at Those Locations.

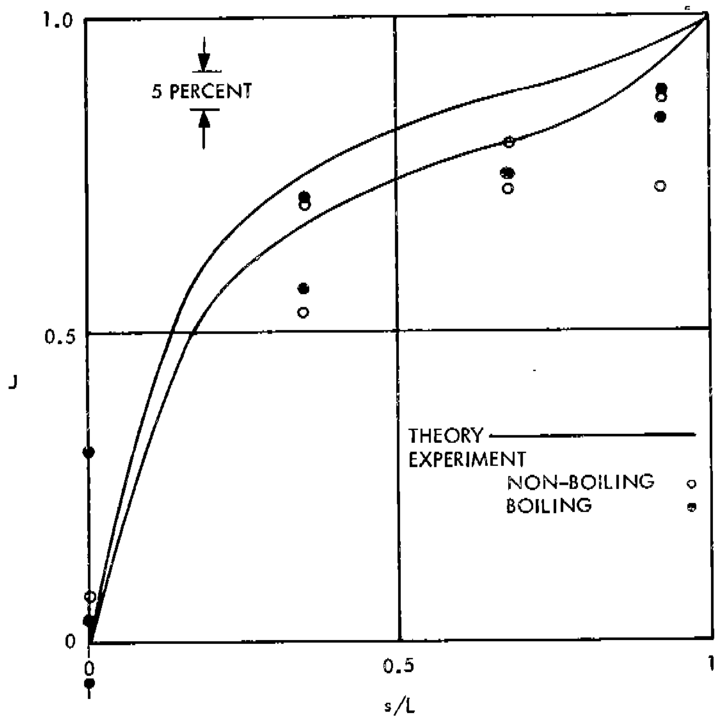

FIGURE 29 - Comparison of Theory with Experiment, 3T12 Between $T = T_F$ at $s/L = 0$ and $T = T_W$ at $s/L = 1$. Path Length from Bulkhead to Waterline.

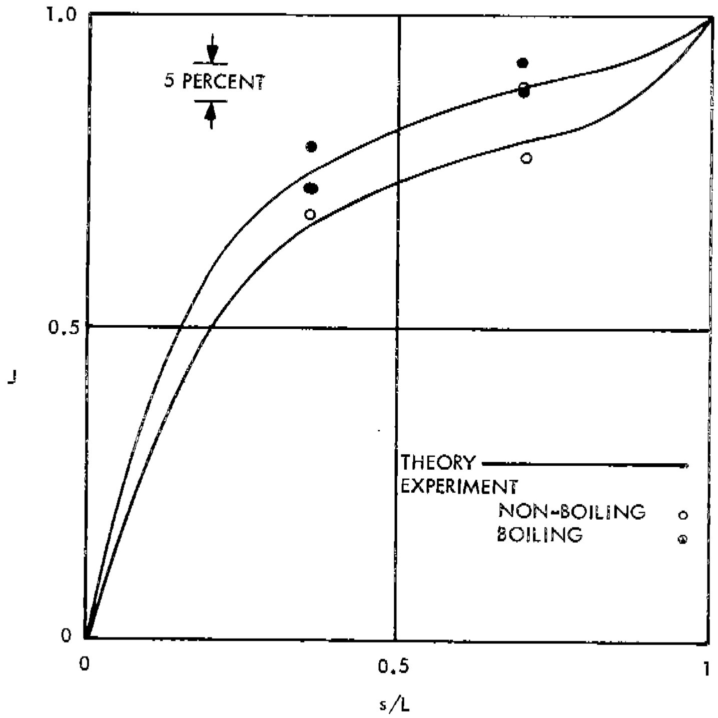

FIGURE 30 - Comparison of Theory with Experiment, 3T12, Between Thermocouples 1 and 4 Using Measured Temperatures at Those Locations.

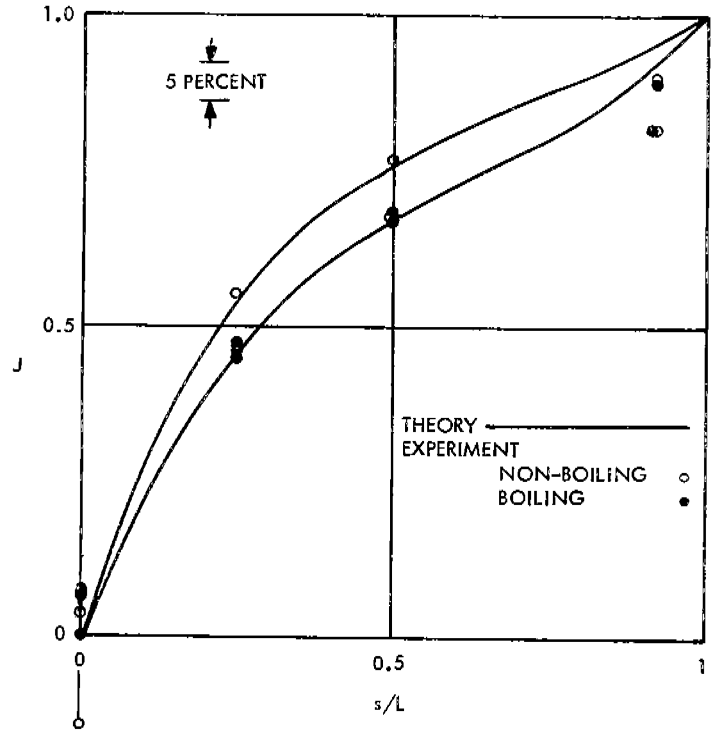

FIGURE 31 - Comparison of Theory with Experiment, 3T6, Between $T = T_F$ at $s/L = 0$ and $T = T_W$ at $s/L = 1$. Path Length from Bulkhead to Waterline.

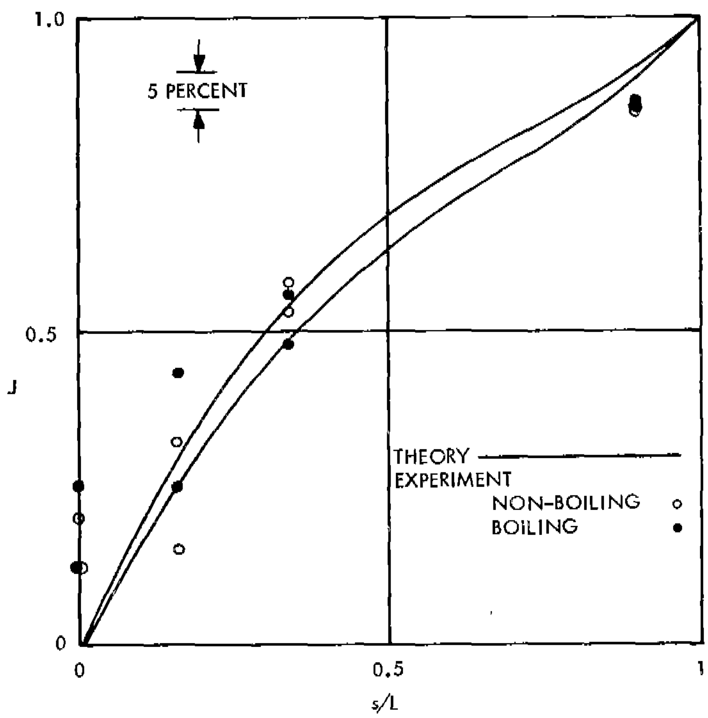

FIGURE 32 - Comparison of Theory with Experiment, 3T3, Between $T = T_F$ at s/L = 0 and $T = T_W$ at s/L = 1. Path Length from Bulkhead to Waterline.

as greatly from the average of the water temperature and the temperature at thermocouple No. 6 as shown in Table 6. In these regions, then, the thermal gradient apparently is predictable reasonably well by linear theory between the fluid temperatures at the ends of the strip. The problem (as in the corresponding case of the deck and upper sideshell) lies in being able to predict the temperature at thermocouple No. 6.

Transient

Transient temperatures were computed theoretically from Eq. (38) for the first 180 seconds of run 3T6B-1. The choice of 70°F as the starting temperature was made since that was the initial temperature of thermocouple No. 4 which was the boundary value controller for the analysis.

The results are compared to the experimental data in Figure 33 which shows a reasonably good match. The early-time difference between theory and experiment appeared to wash out quickly for thermocouple No. 3, but it seems to have been retained at thermocouples 1 and 2.

The general agreement is good but it is clear that the fine details of the character of the convective heat transfer affected the correlation at thermocouples 1 and 2.

TABLE VI - Temperatures in Bottom Structure, ^{0}F

Run	T_W	T_6	T_{av}	T_7	T_8
2T8-1	70.5	-4	33	34	40
2T8-2	71	1	36	39	46
2T8B-1	73	-16	29	27	43
2T8B-2	71.5	-10	30	30	42
2T4-1	67	52	60	57	57
2T4-2	75	53	64	60	67
2T4B-1	68	-5	32	37	-
2T4B-2	67	48	58	55	54
2T2-1	74	52	63	57	57
2T2-2	72	53	63	59	60
2T2B-1	74	43	59	54	53
2T2B-2	72	44	58	53	55
3T12-1	75	45	60	61	58
3T12-2	72	48	60	61	57
3T12B-1	70	42	56	56	56
3T12B-2	70	44	57	57	58
3T6-1	73.5	47	60	59	60
3T6-2	71	47	59	57	57
3T6-3	69	46	58	56	56
3T6B-1	68.5	42	55	54	57
3T6B-2	68	41	55	52	52
3T3-1	78	49	64	60	61
3T3-2	75	49	62	59	60
3T3B-1	71.5	45	59	55	57
3T3B-2	72	44	58	55	56

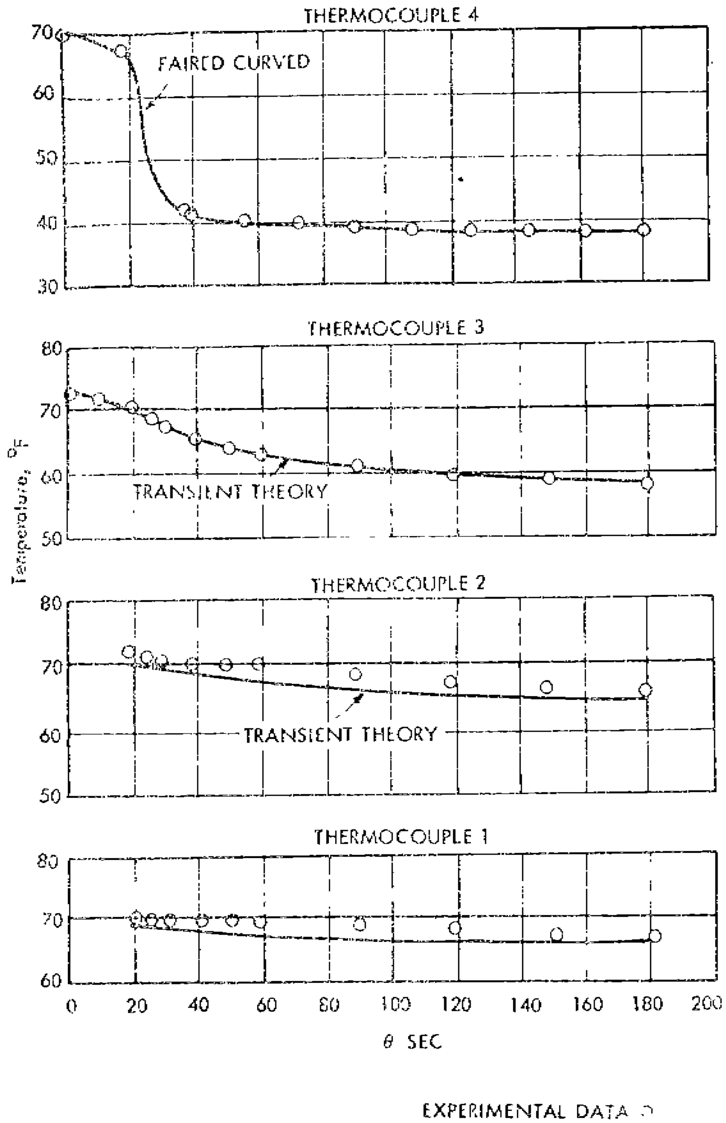

FIGURE 33 - Thermal Transient on 3T6B4.

Effects of Wind and Sun

A short run was made after 1800 seconds on model 2T2B-1 to assess the influence of wind and sun on the temperature in a ship. This involved the use of a 4-inch-diameter fan and a 150 watt lamp in a reflector. The lamp was 7 inches above the deck, 6 inches outboard and 11 inches forward of the fore-and-aft centerplane, tilted to illuminate the model directly. The fan was 6 inches above the deck and 18 inches abeam. It was aimed to blow directly on the model.

At 1800 seconds the Freon 114 in the model was topped off (about one inch) and the lamp was turned on. The fluid temperature was 39°F and that of the water was 73°F at the start of this sequence. The rest of the test sequence is shown in Table 7. Thermocouples 1 and 2 were at locations closest to the lamp and fan while thermocouples 3 and 4 were successively farther away.

During the test little heating or cooling penetrated to the interior of the model. Only the deck and sideshell appear to have responded. The largest change occurred at thermocouple 2 where the temperature rose 14°F under radiant heating alone and another 8 degrees while the fan was on. The total change of 22°F was 65 percent of $T_W - T_F$.

This result cannot be related quantitatively to the corresponding behavior of a ship at sea. Qualitatively, however, it indicates that the effect would be large. Consider the convection alone. Assume again, a wing tank 40 feet high, 60 feet long and 10 feet wide with 1/20 feet thick plate all over. If a 20 kt. wind at -80°F is assumed to blow across the deck, so that a value of h = 4 might be realistic, then g^2 would be (4+1)/(25 x 1/20) = 4 if h = 1 for the air in the wing tank and Eq. (34) is used to determine g^2. Assume T_W = 30°F and assume, also, that the steel girder is at 50°F while the wing tank air is at 0°F. If radiative effects are neglected, then $\overline{T}$ = (-80x4)/5 - (50 + 30)/2 = -104°F using Eq. (35). The path length would be 10 ft. plus the height of the deck above the water. If this is 20 ft. then gL = 2 x 30 = 60. The temperature would approach a step function and according to Eq. (31) the steel temperature would be close to T = (50 + 30)/2 - 104 = -64°F.

TABLE VII - Simulated Wind and Sun Study, Model 2T2B-1

	Time Sec.	Thermocouples 1	2	3	4	5	6	7	8
Heat Lamp On	1800	67	51	46	40	39	43	54	55
	1870	70	57	50	42	39	43	55	54
	2100	73	64	56	46	39	43	55	55
	2220	74	65	56	47	39	43	55	55
Fan & Lamp On	2400	75	65	56	48	39	43	55	54
	2420	75	65	56	48	39	43	54	54
	2430	76	65	57	49	39	43	54	54
	2460	76	66	58	49	39	43	54	54
Fan On, Lamp Off	2700	76	73	63	49	39	43	54	53
	2730	76	70	61	48	39	43	54	53
	2760	75	70	59	47	39	43	54	52
	3200	71	62	56	47	39	43	54	53

Convective Heat Transfer Coefficients

The surface heat transfer coefficient between the fluid in the hold and the hold wall is of prime importance for the determination of the temperature as a function of position and time in the ship structure. It also is the factor which identifies the energy transfer to the fluid to obtain the boil-off rate.

Experiments were performed during this investigation to determine surface heat transfer coefficients for the various fluids used. The determination employed the experimental model depicted in Figure 12 together with the theoretical solution for the temperature response of a plate with an insulated back face when there is a step function change in the fluid in contact with the front face. The solutions were obtained from the curves provided by Schneider (Ref. 21). Three thermocouples were used for the test as shown in Figure 12. One was welded to each side of the plate while the third was suspended in the fluid cavity just above the plate. The thermocouple on the chilled face was used for qualitative data only because of uncertainties such as the fact that the leads were in the fluid.

The data are shown in Figures 34 through 37. They represent the response at the insulated face which is sufficient to determine the Biot number by interpolation between the theoretical curves. Figures 34 and 35 depict fluids which do not boil and will warm up as the plate cools down depending on the relative masses and specific heats. Therefore, only the initial part of the experimental plot shows h before any appreciable warming of the fluid has occurred.

The Freon fluids boil at constant temperature at room pressure. Figures 36 and 37 present the thermal responses obtained. Figure 37 indicates the effect of the surface-generated gas on the heat transfer coefficient during the early stages of the event. When the fluid was first poured into the cavity it erupted. As time progressed and more fluid met the surface the heat transfer coefficient rose. When the temperature of the metal approached that of the fluid the heat transfer coefficient dropped significantly. This occurred when the metal no longer provided enough energy for phase change over the total surface in contact with the fluid. The boiling action stopped when the metal was at the fluid temperature. The only phase change occurring at this time was at the air interface of the fluid.

An interesting sidelight to these experiments was a reduction below the boiling temperature in metal surface temperature when total fluid evaporation was permitted.

The temperature approached the boiling point temperature coincident with the partial pressure of the Freon in the air. This was equivalent to evaporative cooling. Therefore, if liquid methane were to splash onto any metal the interface temperature could fall well below the boiling point of the liquid methane.

The terminology used on Figures 36 and 37 to describe the boiling action can be defined as:

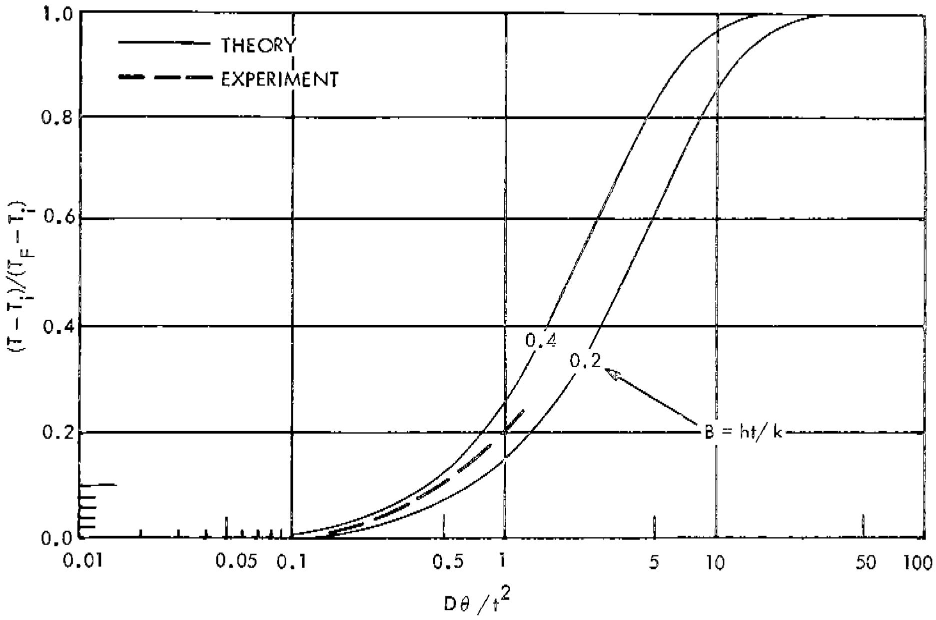

FIGURE 34 - Temperature Response on the Insulated Side of a Plate When Chilled with Alcohol Mixed with Dry Ice. The Experimental Value of h was 220BTU/Hr. Sq. Ft. ^{o}F.

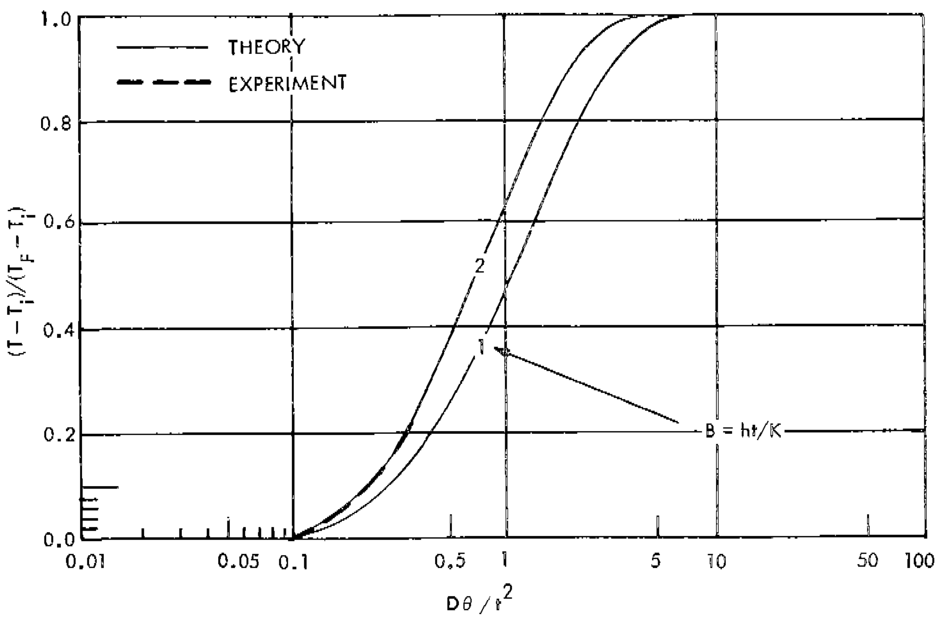

FIGURE 35 - Temperature Response on the Insulated Side of a Plate when Chilled with Water. The Experimental Value of h was 1250BTU/Hr. Sq. Ft. ^{o}F.

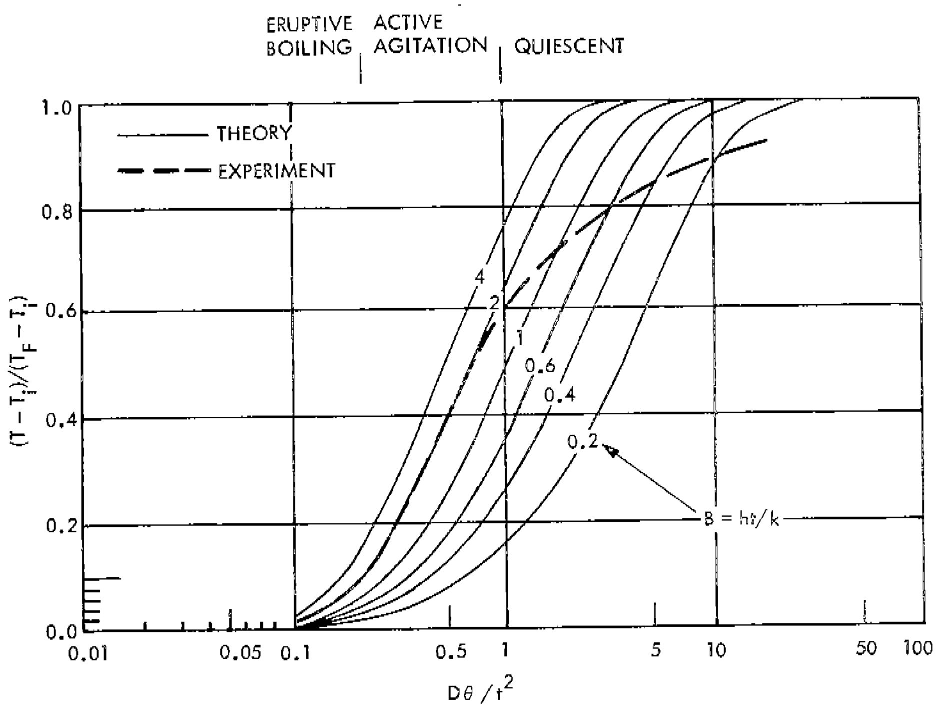

FIGURE 36 - Temperature Response on the Insulated Side of a Plate Chilled with Freon 114. The Experimental Value of h was 1250BTU/Hr. Sq. Ft. ^oF.

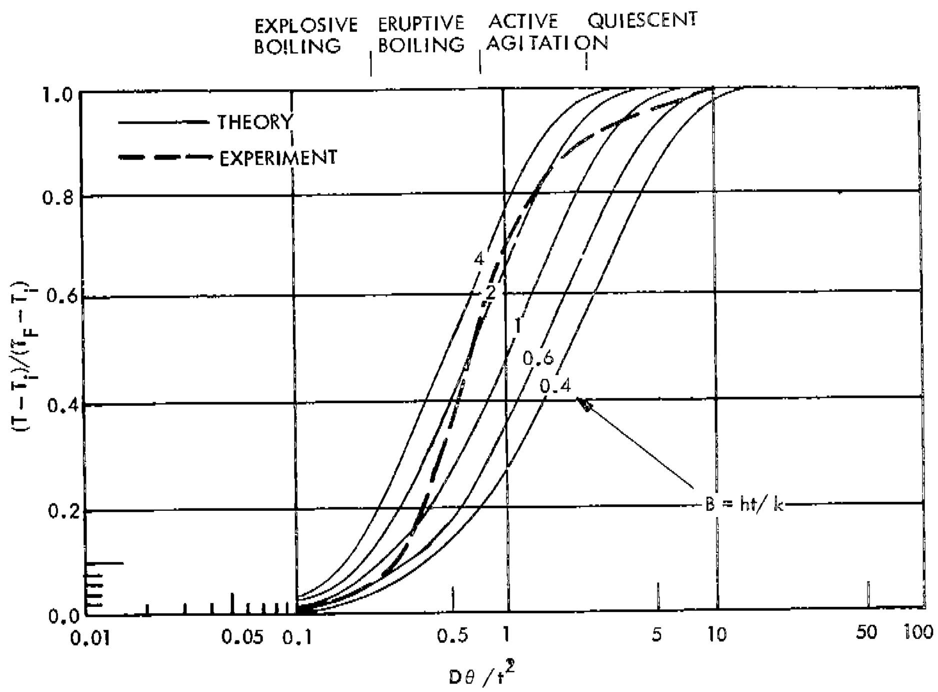

FIGURE 37 - Temperature Response on the Insulated Side of a Flat Plate Chilled with Freon 12. The Maximum Experimental Value of h was 1625BTU/Hr. Sq. Ft. ^oF.

1. Explosive Boiling - Unable to maintain any appreciable fluid in the experimental cavity.

2. Eruptive Boiling - Violent action with excessive splashing.

3. Active Boiling - Can be compared to boiling water.

4. Quiescent - Gentle boiling to none at all.

PTE AND TE

Temperature records were obtained during the PTE and TE tests. The results appear in Figures 38 and 39. No attempt was made to analyze the PTE data. However, the TE results were analyzed for the thermocouple at gage 1 using the transient calculation procedure of Eq. (38) with the result shown in Figure 40. The convective and radiative heat transfers were asssumed to be 1/2 of the conductive, which is the average of the values shown in Tables 2 and 3. The differences are seen to be of the order of a few percent. The experimental temperatures at all the stations of Figure 40 were used to compute stresses as shown in the following section.

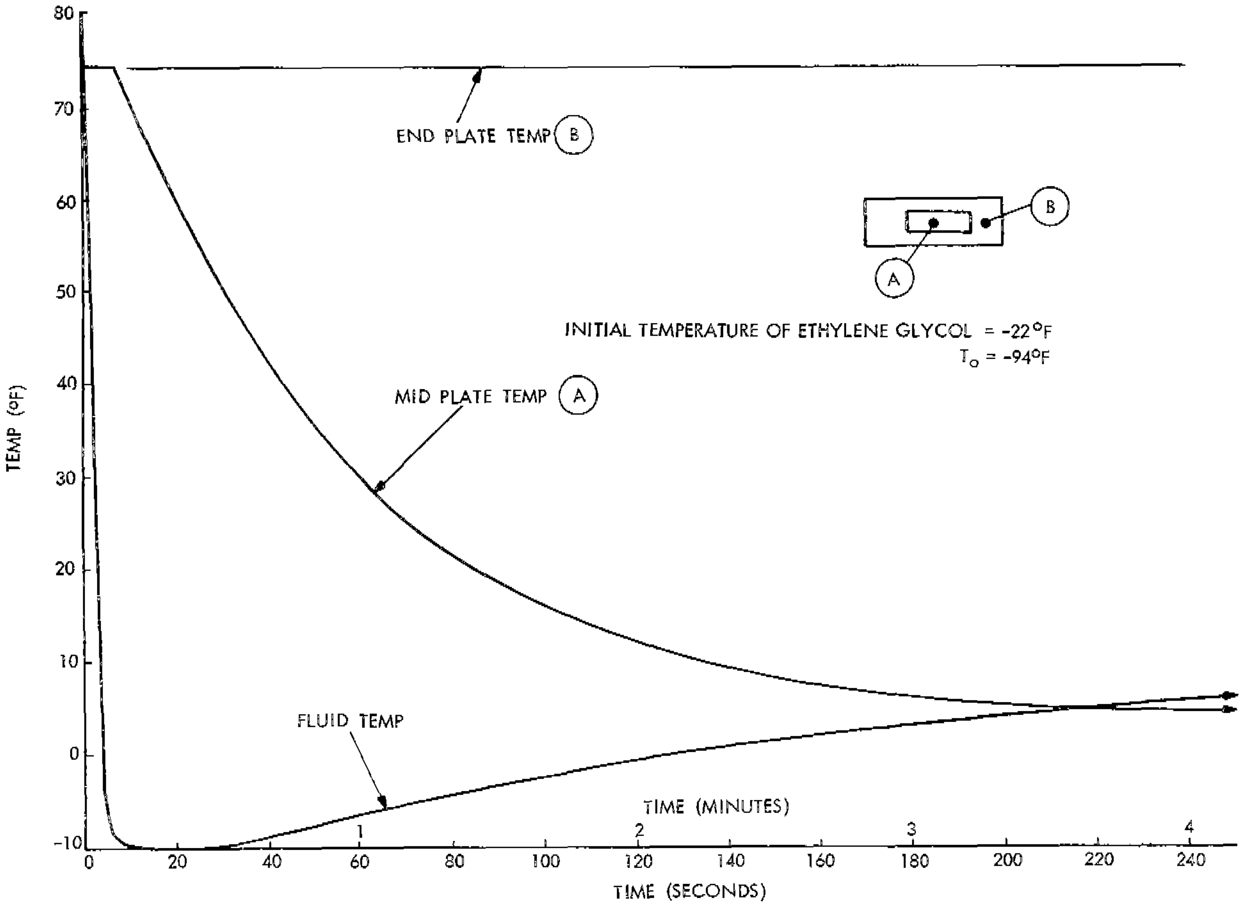

FIGURE 38 - Temperature History in the Cold-Spot Model.

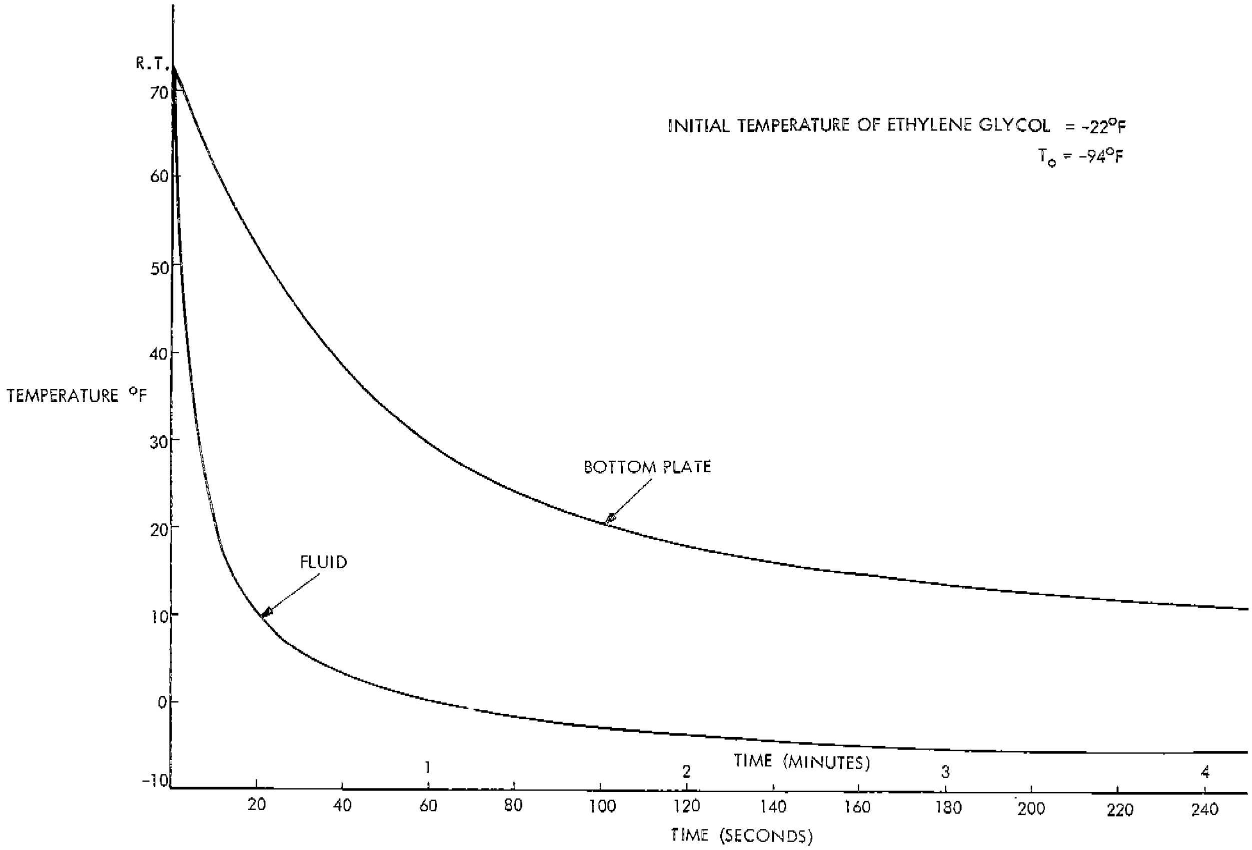

FIGURE 39 - Temperature Measurement History in Ship PTE Model.

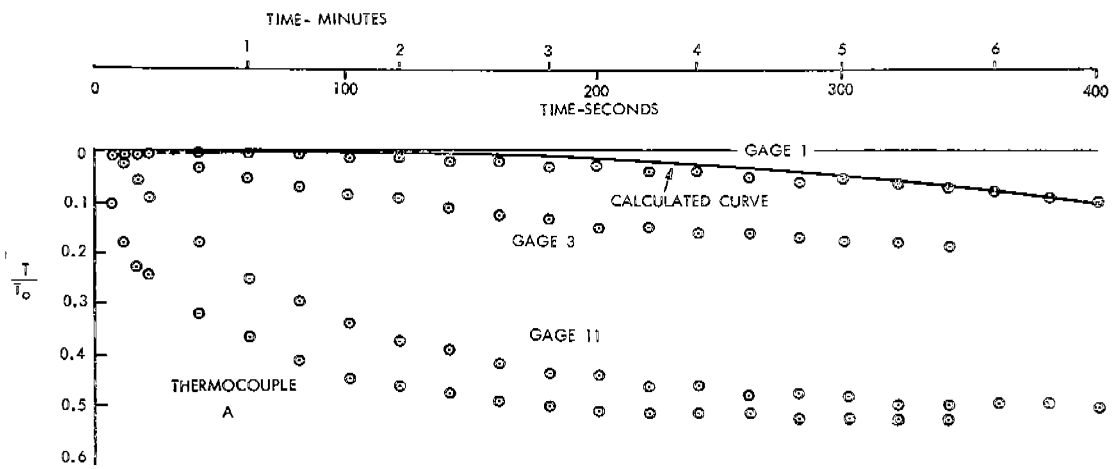

FIGURE 40 - Normalized Temperatures on Steel Thermoelastic Model.

STRESS INVESTIGATIONS

Introduction

PTE investigations were conducted on a rectangular flat plate with a central chilled spot and on a plastic simulation of the steel model. One purpose was to determine how closely Eqs. (48) and (49) would agree with experimental data for these cases to provide a base for evaluating the steel model results. Another was to obtain a preliminary indication of the usefulness of simple theoretical prediction procedures for stresses in the steel model. The PTE simulated ship experiment also provided data to aid in strain gage placement on the steel model.

In the following descriptions each study is discussed separately. Comparisons have been made of the PTE data with the simplified predictions which are discussed in the Theory Section.

Cold Spot Model

The photoelastic fringe patterns are shown in Figure 41. The results are typical of a thermal transient. The peak stress occured at approximately 4 minutes after inception of the test. Actually, there was little variation in the stress field from 3 minutes to almost 7 minutes.

The cold-spot and balanced force theoretical solutions were compared to the experimental results. The magnitude of the difference between the two theories is shown in Figure 42. The nature of the agreement is to be expected since Eq. (48) and (49) are basically the result of a force balance analysis with consideration for the curvature of the disk.

The relevant data for the cold-spot experiment appear in the following summary. The temperature difference, T, is the change from room temperature to the temperature measured at the center of the plate model at the time of peak stress.

Area ratio, $A_2/A_1 = 0.60$
$T_o = -92^oF$
$\sigma_o = 1200$ psi
Maximum model temperature change, $T = 69^o F$
$\alpha E T = 920$ psi
Maximum fringe order, $n = 2.03$ (extrapolated)
Location, centers of long edges
Experimental thermal stress, Eq. 55 , $\sigma = 613$ psi
$C_o = \sigma/\sigma_o = 0.49$
$C = \sigma/\alpha E T = 0.67$
Theoretical thermal stresses,
- Force balance, Eq. (49), $\sigma = 575$ psi
- Cold-spot analysis, Eq. (51), $\sigma = 598$ psi

Percentage errors, theory compared to experiment,
- Force balance, 6.6 percent
- Cold-spot analysis, 2.5 percent

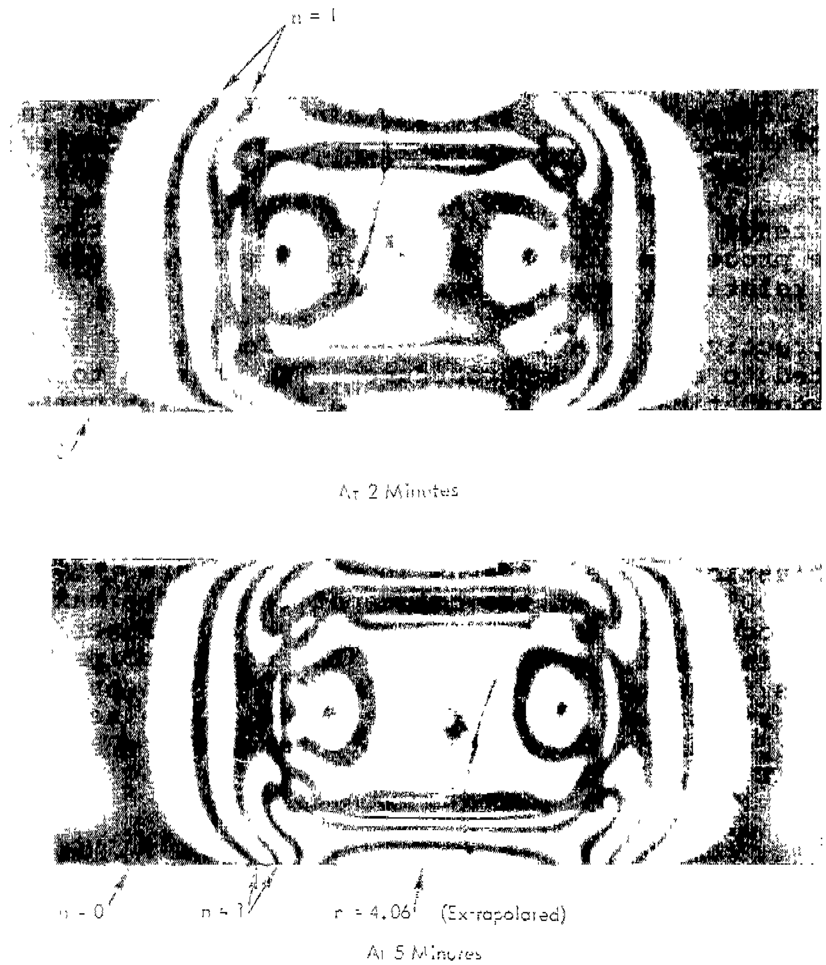

NOTE: These are doubling polariscope photographs. All fringe orders must be halved for stress calculation.

FIGURE 41 - PTE Fringe Patterns in Cold-Spot Model.

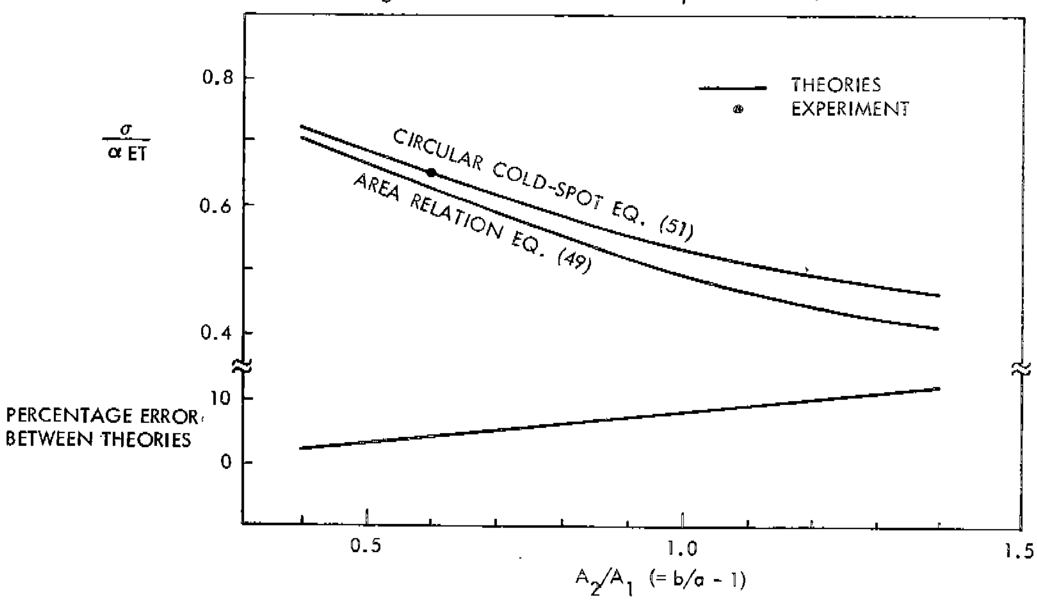

FIGURE 42 - Comparison of Cold-Spot on Area Ratio Solutions.

The correlation is in accordance with numerous PTE investigations in which excellent agreement of theory and experiment have been obtained for problems of equal or greater complexity (Refs. 16 through 18, for example). In the cold-spot problem the error was slightly larger than has been sustained in the past in which accuracies of the order of 1 percent were common. However, some portion of the difference must be identified with the approximate natures of Eqs. (49) and (51) as applied to the experiment. In spite of the size of the error for the balanced force method, the utility of the procedure for LNG tankers has received some support from this relatively simple investigation.

It is instructive to examine the various degrees of conservatism related to estimating procedures. C_o is seen to be 0.49 while the hypothetical upper bound for a finite Biot number, C_u, is seen to be 0.57 according to Figure 7. As a result the use of σ_o would have predicted a theoretical peak stress which would have been more than twice as high as observed while C_u would have been 17 percent too high.

The photoelastic fringe patterns appear in Figure 43. It follows that σ_o = 1200 psi, as in the cold-spot test. The maximum fringe order of 1.4 occurred at the lower corner of the inner wall. If the fringe order is substituted into Eq. (55) the principal stress difference is found to have been 1.4 x 303, or 424 psi, and the principal shear stress was 212 psi. The numerical value of αET (Figure 33) was 813 psi using the bottom plate temperature at 4 minutes (11° F) so that T = 61° F.

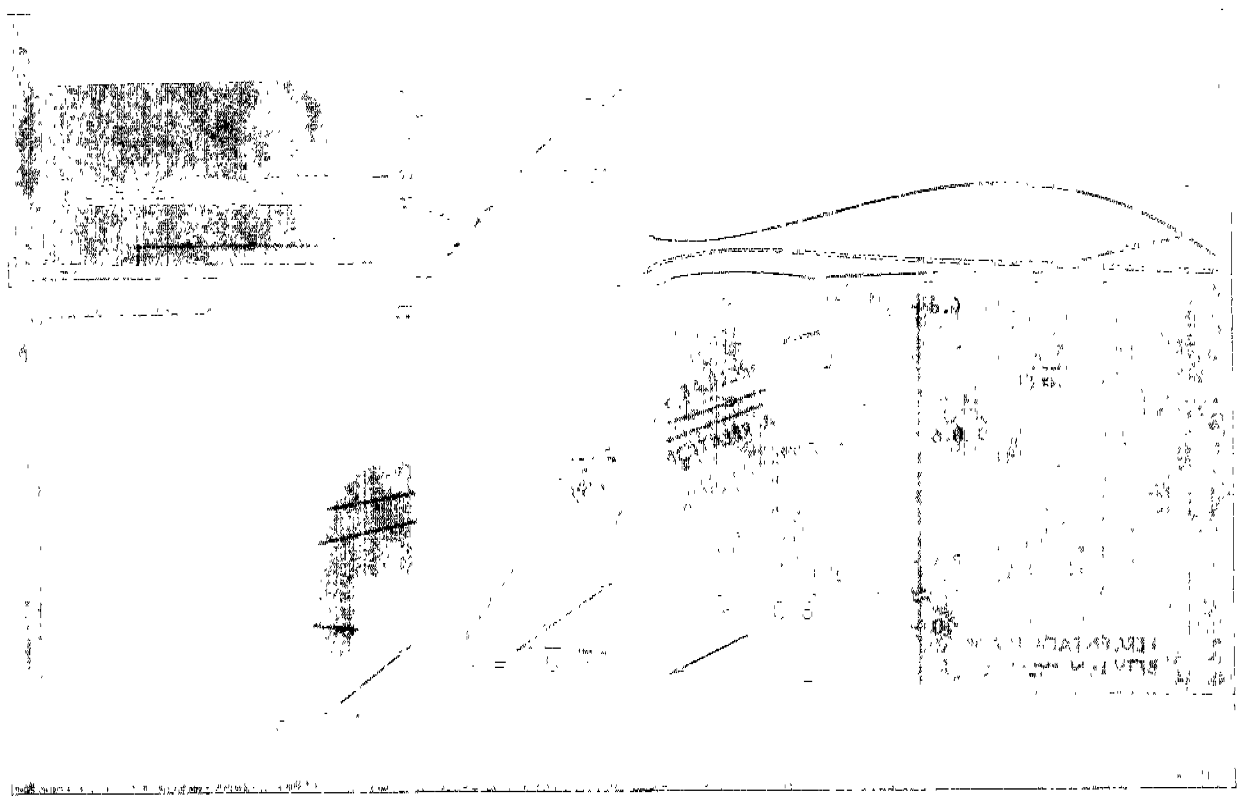

FIGURE 43 - Photoelastic Fringe Patterns in Simulated Ship Model at 5 Minutes.

At the centers of the inner and outer walls the peak fringe orders were 1.0 and 0.8, respectively. These are equivalent to 303 and 244 psi, respectively. If the inner and outer section areas are as shown in Figure 15, then the application of Eqs. (48) and (49) (using the bottom plate temperature as a reference so that T = 61° F) yield predictions of the longitudinal inner and outer thermal stresses of 426 psi and 383 psi at those locations. It was not possible, in the current PTE tests, to separate the principal stresses and obtain the two values experimentally because of the manner in which the polariscopes were built into the model. As a result it was necessary to assume values of σ_y in order to perform the correlation. If σ_y were chosen equal to 1/4 of σ_x, then σ_x would be 404 and 325 psi at the inner and outer walls, respectively. The test data on the steel model indicated that this assumed order of the ratio of vertical-to-horizontal stress might not be improper.

The simulated ship experiment revealed no stress concentration at any location. It did demonstrate the presence of significant shears since the principal shear was 1/2 of the principal normal stress.

The results from this study played an important role in aiding the selection of strain gage locations on the steel model in order to reveal the peak normals and the corner shears. More importantly, however, it indicated the order of accuracy with which the force balance relations of Eqs. (48) and (49) can predict the peak stresses in a shiplike structure subjected to thermal shock in one hold.

Because of the uncertainties in the values of the separated principal stresses, the following summary of the various stress bounds may be somewhat inaccurate. However, the exercise is felt to be important to the aspect of this investigation which deals with approximation procedures. The results above show that C_o = 455/1200 = 0.38. For the ship PTE model, Figure 7 shows that for the pertinent Biot number C_u = 0.64. Therefore, use of σ_o instead of the observed value would have resulted in a prediction of thermal stress that would have been about 3 times as high while the attainable ultimate, C_u, would have been 87 percent too high.

Steel Ship Model Investigations

Thermoelastic studies were conducted on the welded steel model described above. The significant stress data are summarized in this section.

The peak thermal stresses were observed at the centers of the inner and outer walls (gages 1 and 11). As shown in Figure 44, the experimental peaks were in reasonably good agreement with the predictions of Eqs. (48) and (49). The locations of the peaks were in the same places as on the PTE ship model. The peak value of C_o was 5 percent smaller than theoretical on the inner wall and 6 percent smaller on the outer wall. The largest C_o was 0.258 which means that the use of σ_o as an estimate for this case would have been too large by a factor of nearly 4. If the Biot number estimate of 0.43 were to be used (Figure 7) then the prediction would have been 67 percent too high.

The point-by-point comparison shows similarity of the theory and experiment. However, the correlation becomes close only at long times.

Vertical shear was observed in the corners, as in the case of the PTE model. The largest value of the principal shear was half of the peak principal normal stress.

The peak stress on the inner wall was measured on the outstanding leg of the angle stiffener. As can be seen from Figure 44, the stress started as compression and then reversed after about 5 seconds. This may be explained by assuming that the temperature on the wall plate caused shrinkage relative to the stiffener and induced a combination of compression and bending with a net tension on the flange. Then the temperature reached the stiffener after which it began to act in concert with the inner wall. The differentially connected strain gage at location 9 revealed a small amount of vertical curvature which would have induced a rolling action on the stiffener. The relatively small compression in the flange before reversal does not imply that this is a negligible problem in a full size ship. Because of the time scaling law of Eq. (8) the stiffeners may not become chilled for several minutes after the plate is chilled. As a result the compression stresses and rolling action could be much greater than observed in this investigation. This is an area for possible future study.

The minimum principal stress at the center of the wall was approximately 1/4 of the maximum. The minimum was oriented vertically and the maximum was horizontal. This result provided the basis for the assumption made for the PTE ship model to indicate how the photoelastic principal stress difference could be converted into separated stresses.

Some other features of the steel model response may warrant subsequent investigation. For example, the plateau at 10 to 20 seconds may reflect the finite injection time for the chilled alcohol. The reversal in sign at gage location 5 indicates the adjustment of the model to the changing temperature field. It may be important to inquire into the reasons for the time difference in the attainment of the peaks at the inner and outer walls. However, the resolution of that problem would require extensive theoretical analysis in a subsequent investigation.

OTHER SHIP PROBLEMS

Local Temperature Fields

It is apparent from Eq. (48) that a narrow longitudinal cold strip would induce much higher tensile stress than if the entire hold were to be chilled to the same temperature of the strip. This follows from the area ratio term, A_2/A_1, which would become much larger than unity for which case σ_1 would come close to

$$\sigma_1/\sigma_o = \Delta T/T_o \qquad (64)$$

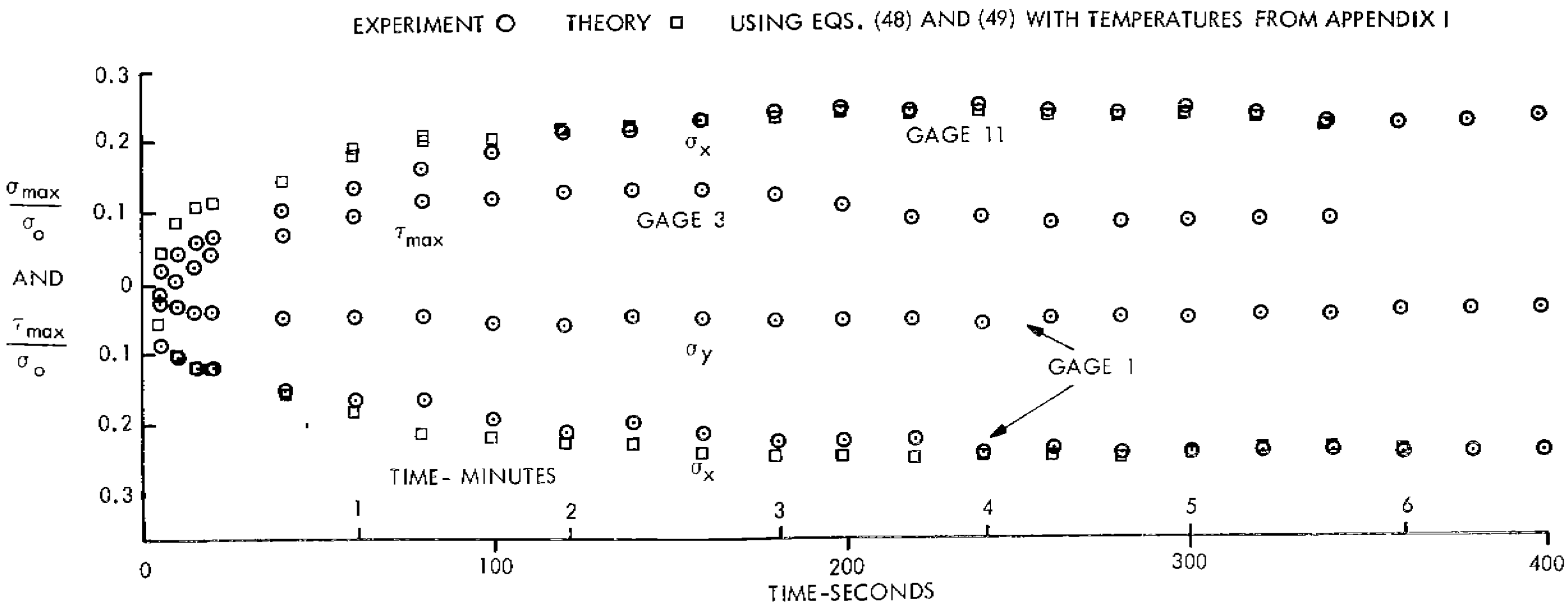

FIGURE 44 - Normalized Stresses on Steel Ship Model. $A_2/A_1 = 0.92$.

in which $\Delta T/T_o$ would be related to Biot number and the heat capacities of the hold and chilling fluid. In the thermoelastic investigations $\Delta T/T_o$ was approximately 1/2. However if the convective heat transfer coefficient is very high, as in a boiling condition, then $\Delta T/T_o$ would approach unity also and therefore σ_1 would approach $\sigma_o = \alpha E T_o$ which is the maximum possible value with no holes, cracks or other forms of stress concentrators.

Pressure Surge

For the past two years the investigators have been concerned about the pressure rise which would be caused by rapid gas generation during the assumed tank failure. If a small amount of cryogenic fluid were to come in contact with any part of the much warmer hold structure enough pressure could be generated to initiate a chain reaction failure of the tank container and, soon after, failure of the hold if inadequate venting is provided.

The experiments which utilized the Freon fluids provided vivid visual evidence of the violent gas generation that would take place during the assumed accident. The Freon 12 (-21°F boiling point) fluid erupted from the container which held the heat transfer coefficient experiment. It also was quite difficult to pour the Freon 12 fluid into the hold of the 2T4B-1 model. The blowback during the beginning of the pour restricted the flow rate until an initial chill was obtained. The Freon 114 (38.8°F boiling point) exhibited the same behavior but at an understandably reduced level.

Some simple calculations were performed to yield an order-of-magnitude pressure rise effect. A hold size of 60 feet square by 40 feet high was assumed for the calculations. An average wall thickness of 1 inch was chosen. However, the event would occur so rapidly that the effect almost would be independent of wall thickness when examining typical ship plate thicknesses and construction.

The heat transfer coefficient was based on the Freon 12 data. The vent size was assumed circular in order to provide simple supersonic nozzle flow calculations.

The initial conditions considered were liquid methane at atmospheric pressure (-258.5°F boiling point) in the tank and a hold metal temperature of 41.5°F for an initial 300°F temperature difference.

The result of the calculations is depicted in Figure 45 which indicates the pressure to be expected during the first 10 seconds. The average wall temperature rise in the assumed 1 inch thick wall is only 22 percent of the total temperature change available.

For more precise calculations the surface heat transfer coefficients obtained for the Freon fluids during the program would have to be obtained for the various cryogenic cargo tanker fluids. The surface heat transfer coefficient would vary by orders of magnitude during the transient and the variation as a function of metal surface condition would be important for further design calculations.

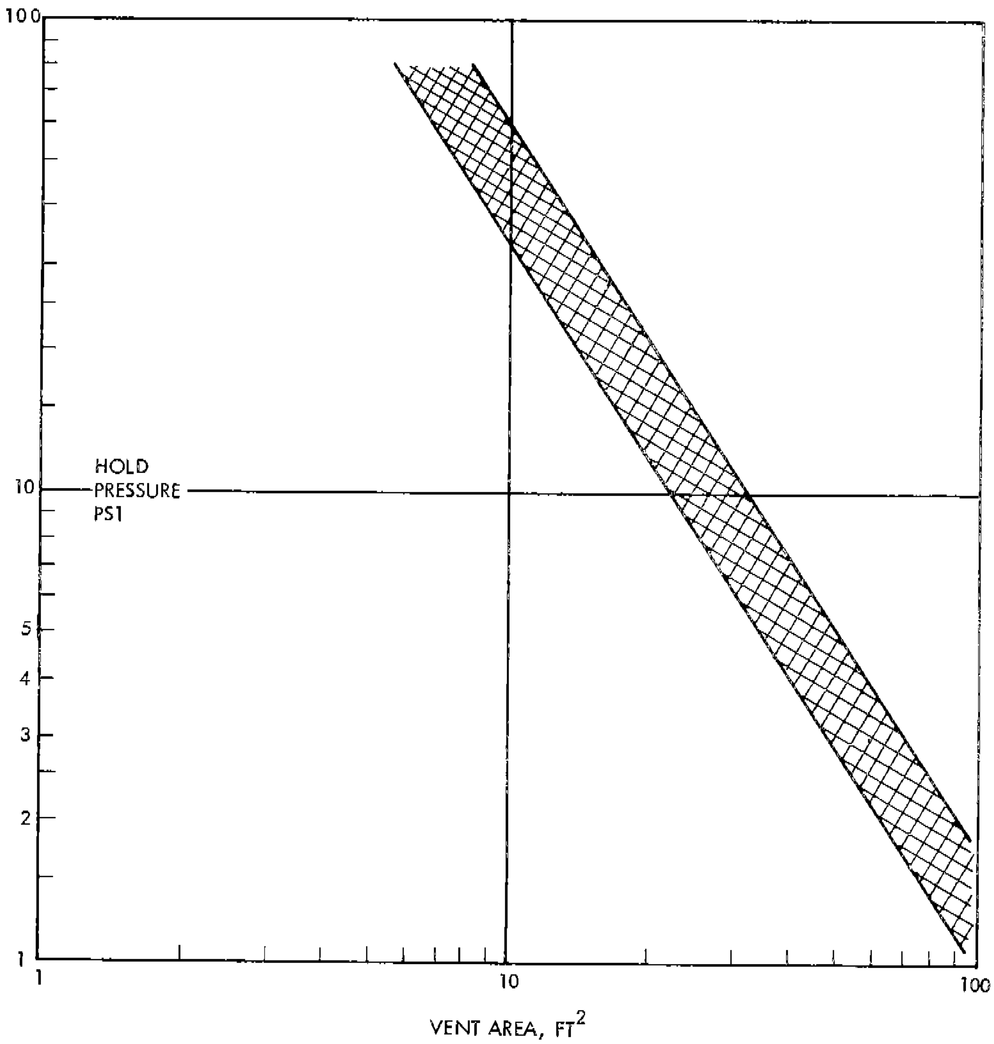

FIGURE 45 - Hold Pressure Versus Accessible Vent Area During the First 10 Seconds of a Liquid Methane Accident for a Ship with the Configuration Described in the Text.

A calculation was made to demonstrate the order of magnitude of the venting area. The hold side plate was assumed to be 1/2 inch thick, longitudinally stiffened near the deck by angles with 6 inch webs and 4 inch flanges, also 1/2 inch thick. The vertical spacing was chosen to be 36 inches and the transverse web spacing was assumed to be 12 feet. Under the action of the internal pressure, p, the flange stress would be 6240p, tension. If the seaway stress is assumed to be 10,000 psi and the thermal stress is chosen at 20,000 psi, then a stress of only 10,000 psi is available to bring the total to yield for a 40,000psi steel. Therefore, the surge pressure cannot exceed 1.6 psi before tension yielding will occur at the flange. According to Figure 45 this means a required effective vent area of 74 sq. ft. to meet the bottom of the range shown on the figure and 110 sq. ft. at the top of the range.

CONCLUSIONS

Temperatures

1. The determination of temperatures due to thermal shock in a ship hold may be performed to engineering accuracy ($\pm$ 10 percent precision) using 2-dimensional heat transfer analysis in vertical and athwartship coordinates only. The heat flow fore and aft does not appear to exert a significantly large influence on the temperatures at the transverse centerplane of the ship where the peaks would be.

2. The prediction of peak temperatures can be made to engineering accuracy using the quasistatic procedure described in this report. Some additional effort may be required to resolve details of convective heat transfer at corners and at boundary changes (the air-water interface, for example).

3. The quasistatic procedure assumes convective and radiative heat transfer properties which are constant along the length of the heat transfer path and independent of the shape and size of the wing tank. Greater prediction accuracy may be achieved and some of the large discrepancies between theory and experiment may be identified, if path-length-dependent properties are used and if the influence of tank shape and size are considered.

4. The calculation procedures are applicable with engineering accuracy to any heat transfer problem in a ship including transients.

5. Convection will dominate the heat transfer process over large regions of a ship. Radiation will be approximately one order of magnitude less and conduction will be two orders of magnitude less.

Stresses

6. The calculation of the peak thermal stress in a ship subjected to the thermal shock in a hold may be performed to satisfactory engineering accuracy by use of

$$\sigma = \alpha ET(A_2/A_1)/(1 + A_2/A_1) \qquad (48)$$

or

$$\sigma = \alpha ET/(1 + A_2/A_1) \qquad (49)$$

7. If the hypothetical limit, $\sigma_o = \alpha ET_o$ were to be used to calculate the peak stress, the result would be conservative by a factor as large as 4. If the ultimate attainable stress from Figure 7 were to be used in an attempt to consider the influence of surface heat transfer, the result also would be conservative, but of the order of 17 percent to approximately a factor of 2.

8. Out-of-plane bending of the tank hold walls apparently is not a problem for a ship with the proportions of the thermoelastic model. However, it might be significant in an actual ship.

Other Ship Problems

9. If the fluid boils after being poured from a ruptured tank into contact with the hold the resultant pressure surge could lead to destruction of the ship. A large venting area must be available to avoid a large pressure surge.

10. In the case of a leak, instead of a catastrophic tank failure, the chilled zone of the hold could be small in which case A_2/A_1 would be large and the thermal stress in the chilled zone would approach αET_o if the fluid boils on contact with the steel of the hold. The influence of pressure surging may modify this effect by rapidly enlarging the leak in which case the time of the thermal transient will control the stress level.

RECOMMENDATIONS

1. Further studies should be performed on convective heat transfer in ship-detail configurations to increase the accuracy of prediction procedures of this report and to help find reliable modeling laws for this mode of heat transfer.

2. Analyses, experiments and design studies should be conducted on the problem of pressure surge. These should include measurements of the convective heat transfer coefficients of various liquid natural gases.

3. Local thermal shock problems should be investigated experimentally and the data should be compared to theoretical predictions (such as Eqs. (48) and (49)).

4. An examination should be made of the effect of ship motion on convective cell stability and the relationship to the heat transfer process.

5. One problem which in the past has received considerable attention with little in the way of a satisfactory conclusion is the behavior of a structure when mechanical stresses are applied in conjunction with thermal stresses. The range of current practice extends from algebraic addition of the two stresses in some cases to complete neglect of the thermal stresses in others. From the standpoint of stress analysis, the stresses should be added if superposition holds. Otherwise the addition process must be modified. From the standpoint of failure of the ship structure the proper procedure probably would lie between the two extremes mentioned here. It is suggested that an exploratory study be made to determine the proper approach for ship design.

Acknowledgements

The authors wish to express appreciation to Messrs. Richard Goldman, John Pozerycki and Roger Milligan for work which they did in the thermoelastic phase of this project on model design and instrumentation, conduct of the experiments and reduction of the data.

APPENDIX I

EXPERIMENTAL TEMPERATURE DATA

The following pages contain the temperatures for all model experiments.

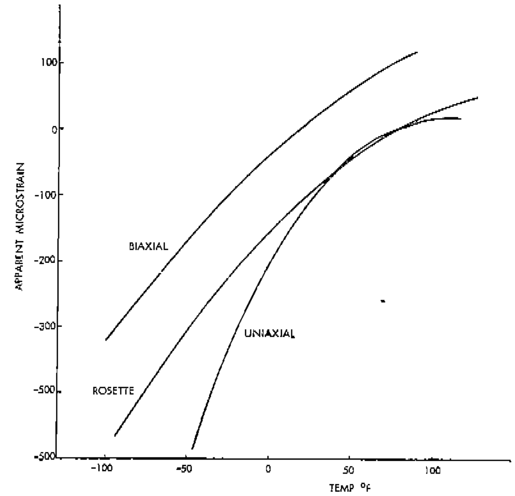

FIGURE A-1 - Correction Curve for Effect of Temperature on Strain Gage Signal.

TABLE A-I - Basic Calculation Data for Temperature Models

Model	2T8	2T4	2T2	3T12	3T6	3T3
L (ft)	1	2/3	1/2	1.5	1.0	0.75
At 40° ΔT, h_1(BTU/hr-ft-°F)	0.4	0.4	0.4	0.4	0.4	0.4
At 90° ΔT, h_2(BTU/hr-ft-°F)	0.54	0.54	0.54	0.54	0.54	0.54
k(BTU/hr-ft-°F)	25	25	25	25	25	25
t (ft)	0.010	0.010	0.010	0.00267	0.00267	0.00267
$2h_1/kt$ (ft^{-2})	3.2	3.2	3.2	12.1	12.1	12.1
$2h_2/kt$ (ft^{-2})	4.32	4.32	4.32	16.2	16.2	16.2
$(Q_r/Q_c)_1$	0.3	0.3	0.3	0.3	0.3	0.3
$(Q_r/Q_c)_2$	1.2	1.2	1.2	1.2	1.2	1.2
g_1 (ft^{-1})	2.12	2.12	2.12	3.96	3.96	3.96
g_2 (ft^{-1})	3.08	3.08	3.08	5.97	5.97	5.97
g_1L	2.12	1.42	1.06	5.95	3.96	2.97
g_2L	3.08	2.06	1.54	8.96	5.97	4.47

TABLE A-II - Temperature Data for Theoretical Profiles, °F

Run	g_L	T_F	T_A	T_W	$\frac{T_F + T_W}{2}$	$\frac{T_W - T_F}{2}$	T_1 [1]	$\frac{T_1 + T_A}{2}$	$\bar{T}$	$\frac{\bar{T}}{T_W - T_F}$
2T8-1	3.08	-43	78	70.5	13.8	56.8	20.3	49.1	35.3	0.311
2T8-2	3.08	-27	74	71	22	49	26.8	50.4	28.4	0.292
2T8B-1	3.08	-38	80	73	17.5	55.5	23.8	51.9	34.4	0.314
2T8B-2	3.08	-38	81	71.5	16.8	54.8	24.6	52.8	36.0	0.329
2T4-1	1.42	37	74	67	52	15	53.5	63.8	11.8	0.393
2T4-2	1.42	42	74	75	58.5	16.5	58.3	66.2	7.7	0.233
2T4B-1	2.06	-21	74.5	68	23.5	44.5	24.9	49.7	26.2	0.285
2T4B-2	1.42	38.8	72.5	67	53	14.1	54.1	63.3	10.3	0.365
2T2-1	1.06	43	76	74	58.5	15.5	57.9	67.0	8.5	0.274
2T2-2	1.06	43	75	72	57.5	14.5	57.1	66.1	8.6	0.297
2T2B-1	1.06	38.8	75	74	56.4	17.6	55.5	65.2	8.8	0.250
2T2B-2	1.06	38.8	72	72	55.4	16.6	54.3	63.2	7.8	0.235
3T12-1	5.95	39	74	75	57	18	58.2	66.1	9.1	0.253
3T12-2	5.95	36	72	72	54	18	55.5	63.8	9.8	0.272
3T12B-1	5.95	38.8	74	70	54.4	15.6	56.7	65.4	11.0	0.353
3T12B-2	5.95	38.8	73	70	54.4	15.6	56.5	64.8	10.4	0.334
3T6-1	3.96	39	73.5	73.5	56.3	17.3	56.3	64.9	8.6	0.249
3T6-2	3.96	35	70	71	53	18	52.8	61.4	8.4	0.233
3T6-3	3.96	35	70	69	52	17	52.2	61.1	9.1	0.268
3T6B-1	3.96	38.8	71.0	68.5	53.7	14.9	54.2	62.6	8.9	0.299
3T6B-2	3.96	38.8	73.0	68	53.4	14.6	54.6	63.8	10.4	0.359
3T3-1	2.97	34	77.5	78	56	22	54.4	66.0	10.0	0.227
3T3-2	2.97	36	75	75	55.5	19.5	54.2	64.6	9.6	0.246
3T3B-1	2.97	38.8	75.5	71.5	55.2	16.4	54.9	65.2	10.0	0.305
3T3B-2	2.97	38.8	75	72	55.4	16.6	54.9	65.0	9.6	0.289

[1] Weighted average of metal temperatures assuming linear variation between chilling fluid and water.

TABLE A-V - Temperature References for Thermoelastic Model

Location	Model Initial Temp.	Fluid Initial Temp.	T

TABLE A-III - Experimental Temperature Summary, θ = 1800 Sec
All Temperatures ^{O}F

Run	T_C 1	2	3	4	5	6	7	8
2T8-1	60	54	39	10	-16	-4	34	40
2T8-2	67	56	44	18	-11	1	39	46
2T8B-1	52	41	26	-6	-31	-16	27	43

APPENDIX II

EXPERIMENTAL STRESS DATA

The following pages contain the stresses for the thermoelastic model experiments. The strains were computed after the appropriate corrections had been made to the gage readings according to the curves in Figure A1. The stress components were derived from the strains and the mechanical properties of T-1 steel utilizing the appropriate equations shown in the previous section. The principal normal stresses and maximum shears were then calculated.

All data were normalized for assessment of uniformity. Some of the results are plotted in the section discussing the steel model. The results are copies of the printout of the computer program used to convert the raw data. The minimized stresses employed σ_O as the reference. The three coefficients C1, C2 and C3 are the normalized principal normal stresses and the normalized maximum shear. No significance should be attached to the relation between the magnitudes of the normalized principal normals and the subscripts 1 and 2. The directions and magnitudes of the maximum values were identified through logic and not through a sign convention.

TABLE A-IV - $J = (T - T_F)/(T_W - T_F)$

Run	Thermocouple									$\frac{\bar{T}}{T_W - T_F}$
	gL	1	2	3	4	5	6	7	8	
2T8-1	3.08	0.907	0.855	0.722	0.467	0.238	0.344	0.678	0.731	0.311
2T8-2	3.08	0.959	0.847	0.724	0.459	0.163	0.256	0.673	0.745	0.292
2T8B-1	3.08	0.811	0.712	0.577	0.288	0.063	0.198	0.586	0.730	0.314
2T8B-2	3.08	0.858	0.776	0.621	0.311	0.119	0.256	0.621	0.730	0.329
2T4-1	1.42	0.833	0.533	0.333	0	0.200	0.500	0.667	0.667	0.393
2T4-2	1.42	0.788	0.515	0.333	0.091	0.091	0.333	0.545	0.758	0.233
2T4B-1	2.06	-	0.528	0.315	0.067	0.056	0.180	0.652	0.371	0.285
2T4B-2	1.42	0.823	0.433	0.291	0.007	0.007	0.326	0.574	0.539	0.365
2T2-1	1.06	0.613	0.323	0.129	-0.194	0	0.290	0.452	0.452	0.274
2T2-2	1.06	0.759	0.414	0.241	0.138	0.103	0.345	0.552	0.586	0.297
2T2B-1	1.06	0.915	0.659	0.489	0.233	0.006	0.119	0.432	0.403	0.250
2T2B-2	1.06	0.789	0.337	0.187	0.036	0.006	0.157	0.428	0.488	0.235
3T12-1	5.95	0.750	0.722	0.528	-0.056	-0.056	0.167	0.611	0.528	0.253
3T12-2	5.95	0.861	0.778	0.694	0.083	0.083	0.333	0.694	0.583	0.272
3T12B-1	5.[illegible]	0.872	0.744	0.712	0.295	0.038	0.103	0.551	0.551	0.353
3T12B-2	5.95	0.840	0.744	0.583	0.038	0.006	0.167	0.583	0.615	0.334
3T6-1	3.96	0.899	0.667	0.464	-0.145	-0.087	0.232	0.580	0.609	0.249
3T6-2	3.96	0.833	0.667	0.472	0.028	0	0.333	0.611	0.611	0.233
3T6-3	3.96	0.882	0.765	0.559	0.059	0.029	0.324	0.618	0.618	0.268
3T6B-1	3.96	0.882	0.680	0.478	0.040	0.040	0.108	0.512	0.613	0.299
3T6B-2	3.96	0.829	0.658	0.452	0.007	-0.062	0.075	0.452	0.452	0.357
3T3-1	2.97	0.841	0.568	0.159	0.205	0.091	0.341	0.591	0.614	0.227
3T3-2	2.97	0.846	0.538	0.333	0.128	0.051	0.333	0.590	0.615	0.246
3T3B-1	2.97	0.862	0.557	0.434	0.251	0.037	0.190	0.495	0.557	0.305
3T3B-2	2.97	0.849	0.488	0.247	0.127	0.036	0.157	0.488	0.519	0.289

TABLE A-V - Temperature References for Thermoelastic Model

Location	Model Initial Temp.		Fluid Initial Temp.		T_o	
	°C	°F	°C	°F	°C	°F
A	+23.0	+73.4	-39.0	-38.2	62.0	111.6
1	+23.0	+73.4	-30.0	-22.0	53.0	95.4
2	+23.0	+73.4	-23.5	-10.3	46.5	83.7
3	+23.0	+73.4	-39.0	-38.2	62.0	111.6
4	+23.0	+73.4	-39.0	-38.2	62.0	111.6
5	+23.0	+73.4	-23.5	-10.3	46.5	83.7
6	+23.0	+73.4	-24.5	-12.1	47.5	85.5
7	+23.0	+73.4	-30.0	-22.0	53.0	95.4
8	+24.0	+75.2	-32.5	-26.5	56.5	101.7
9	+23.0	+73.4	-24.5	-12.1	47.5	85.5
10	+24.0	+75.2	-32.5	-26.5	56.5	101.7
11	+24.0	+75.2	-32.5	-26.5	56.5	101.7

TABLE A-VI - Normalized Temperatures for Thermoelastic Model

Time Sec.	A Model Temp.	A T/T_o	1 Model Temp.	1 T/T_o	2 Model Temp.	2 T/T_o	3 Model Temp.	3 T/T_o	4 Model Temp.	4 T/T_o	5 Model Temp.	5 T/T_o
0	23	0	23	0	23	0	23	0	23	0	23	0
5	17	0.097	23	0	23	0	23	0	23	0	23	0
10	12	.177	23	0	23	0	23	0	23	0	23	0
15	9	.226	23	0	23	0	23	0	23	0	23	0
20	8	.242	23	0	23	0	22	.008	22	.003	22.5	.011
40	3.5	.315	23	0	23	0	21	.024	21.5	.024	21.5	.032
60	0.5	.363	23	0	23	0	20	.048	20	.048	20.5	.054
80	-2	.411	23	0	23	0	19	.065	19	.065	20	.065
100	-4	.444	22.5	.009	23	0	18	.081	18	.081	19.5	.075
120	-5.5	.460	22.5	.009	23	1	17	.089	17	.097	18.5	.097
140	-6.5	.476	22	.019	23	0	16.5	.105	15.5	.121	18	.108
160	7.5	.492	22	.019	22.5	.011	15.5	.121	15	.129	17.5	.118
180	-8	.500	21.5	.028	22	.022	15	.129	14	.145	17	.129
200	-8.5	.508	21.5	.028	22	.022	14	.145	13	.161	16	.151
220	-9	.516	21	.038	21.5	.032	14	.145	12.5	.169	15	.172
240	-9	.516	21	.038	21	.043	13	.161	12	.177	15	.172
260	-9	.516	20.5	047	21	.043	13	.161	11.5	.185	15	.172
280	-9.5	.524	20	.057	21	.043	12.5	.169	10.5	.202	14	.194
300	-9.5	.524	20	.057	21	.043	12	.177	10	.210	13.5	.204
320	-9.5	.524	19.5	.066	20.5	.054	12	.177	10	.210	13.5	.204
340	-9.5	.524	19.5	.066	20	.065	11	.185	9	.218	13	.215
360			19	.075	20	.065					12.5	.226
380			18.5	.085	19.5	.075					12	.237
400			18	.084	19.5	.075					12	.237

TABLE A-VI (Cont'd) - Normalized Temperatures for Thermoelastic Model

Time Sec.	6 Model Temp.	6 T/T_o	7 Model Temp.	7 T/T_o	8 Model Temp.	8 T/T_o	9 Model Temp.	9 T/T_o	10 Model Temp.	10 T/T_o	11 Model Temp.	11 T/T_o
0	23.0	0	23	0	24.0	0	23	0	24.0	0	24.0	0
5	23	0	23	0	24	0	23	0	21.5	.044	24.0	0
10	23	0	23	0	24	0	22.5	.011	21	.053	23.0	.018
15	23	0	23	0	24	0	21.5	.032	19.5	.080	21	.053
20	23	0	23	0	24	0	20	.063	17	.124	19	.088
40	22	.021	21.5	.028	23	.018	16	.147	11	.230	14	.177
60	21	.042	20	.057	22	.035	13	.202	7	.301	10	.248
80	20	.063	18.5	.085	20	.071	10	.274	4	.354	7.5	.292
100	19.5	.074	17	.113	18.5	.097	8.5	.305	1.5	.398	5	.336
120	18.5	.095	15.5	.142	17	.124	7.0	.337	0	.425	3	.372
140	18	.105	14	.170	16	.142	5.5	.368	-1.5	.451	2	.389
160	17	.126	13	.189	15	.159	5.0	.379	-3.0	.478	.5	.416
180	16.5	.137	11.5	.217	13	.195	4.0	.400	-4.0	.496	-.5	.434
200	16	.147	10.5	.236	12	.212	3	.421	-4.5	.504	-1.0	.442
220	15	.168	9.	.264	11	.230	2.5	.432	-5.0	.513	-2.	.460
240	14.5	.179	8.5	.274	10	.248	2	.442	-5.5	.522	-2.5	460
260	14	.189	7.5	.292	9	.265	1.5	.453	-6.0	.531	-3	.478
280	13.5	.200	7.	.302	8.5	.274	1.5	.453	-6.5	.540	-3	.478
300	13	.211	6	.321	8	.283	1.0	.463	-6.5	.540	-3.5	.487
320	12.5	.221	5	.340	7	.301	1.0	.463	-7.0	.549	-4	496
340	12	.232	4.5	.349	6.5	.310	1.0	.463	-7.0	.549	-4	496
360	11.5	.242	4	.358	6	.319	1.0	463	-7.5	.558	-4	496
380	11	.253	3.5	.370	5	.336	5	474	-7.5	.558	-4	496
400	11	.253	3	.377	5	.336	0	.484	-7.5	.558	-4.5	504

APPENDIX II

EXPERIMENTAL STRESS DATA

The following pages contain the stresses for the thermoelastic model experiments. The strains were computed after the appropriate corrections had been made to the gage readings according to the curves in Figure A1. The stress components were derived from the strains and the mechanical properties of T-1 steel utilizing the appropriate equations shown in the previous section. The principal normal stresses and maximum shears were then calculated.

All data were normalized for assessment of uniformity. Some of the results are plotted in the section discussing the steel model. The results are copies of the printout of the computer program used to convert the raw data. The minimized stresses employed σ_o as the reference. The three coefficients C1, C2 and C3 are the normalized principal normal stresses and the normalized maximum shear. No significance should be attached to the relation between the magnitudes of the normalized principal normals and the subscripts 1 and 2. The directions and magnitudes of the maximum values were identified through logic and not through a sign convention.

TABLE A-VII - Thermoelastic Model Stresses (PSI)

LOCATION No. 1 $\sigma_o = 18603$

TIME	STRAINS: X	Y	45	OUTPUT: STRESSES TENSILE X	Y	SHEAR	MAX	MAX NORM	MIN NORM	ANGLE (DEG)	C1	C2	C3
5	-47	0	0	-1499	-435	0	531	-435	-14YS	0	-.0234	-.0806	0
10	-57	0	0	-1818	-527	0	645	-527	-1818	0	-.0284	-.0977	0
15	-66	0	0	-2105	-611	0	746	-611	-2105	0	-.0329	-.1132	0
20	-66	0	0	-2105	-611	0	746	-611	-2105	0	-.0329	-.1132	0
40	-85	0	0	-2710	-786	0	962	-786	-2710	0	-.0423	-.1457	0
60	-94	0	0	-2997	-870	0	1063	-870	-2997	0	-.0468	-.1611	0
80	-94	0	0	-2997	-8W0	0	1063	-870	-2997	0	-.0468	-.1611	0
100	-113	0	0	-3603	-1045	0	1278	-1045	-3603	0	-.0562	-.1937	0
120	-123	0	0	-3922	-1138	0	1392	-1138	-3922	0	-.0612	-.2108	0
140	-118	5	0	-3716	-932	0	1392	-932	-3716	0	-.0501	-.1998	0
160	-127	5	0	-4P03	-1015	0	1493	-1015	-4003	0	-.0546	-.2152	0
180	-136	5	0	-4290	-1098	0	1595	-1098	-4290	0	-.0591	-.230V	0
200	-13V	5	0	-4290	-1098	0	1595	-109X	-4290	0	-.0591	-.2306	0
220	-136	5	0	-4290	-1098	0	1595	-1098	-4290	0	-.0591	-.2306	0
240	-146	5	0	-4609	-1191	0	1708	-1191	-4609	0	-.064	-.2478	0
260	-143	8	0	-4486	-1068	0	1708	-1068	-4468	0	-.0574	-.2411	0
280	-150	10	0	-4690	-1069	0	1810	-1069	-4690	0	-.0575	-.2521	0
300	-150	10	0	-4690	-1069	0	1810	-1069	-4690	0	-.0575	-.2521	0
320	-150	10	0	-4690	-1069	0	1810	-1069	-4690	0	-.0575	-.2521	0
340	-150	10	0	-4690	-1069	0	181P	-1069	-4690	0	-.0575	-.2521	0
360	-155	15	0	-4803	-955	0	1924	-955	-4803	0	-.0514	-.2582	0
380	-155	15	0	-4803	-955	0	1924	-955	-4803	0	-.0514	-.2582	0
400	-155	15	0	-4803	-955	0	1924	-955	-4803	0	-.0514	-.2582	0

LOCATION No. 2 $\sigma_o = 16322$

TIME	STRAINS: X	Y	45	OUTPUT: STRESSES TENSILE X	Y	SHEAR	MAX	MAX NORM	MIN NORM	ANGLE (DEG)	C1	C2	C3
5	-6	-6	-6	-247	-247	45	45	-202	-293	45.	-.0124	-.0179	.0027
10	-6	-16	-18	-540	-566	158	194	-258	-648	27.23	-.0158	-.0397	.00Y7
15	-6	-25	-18	-423	-853	56	222	-416	-860	7.37	-.0255	-.0527	.0034
20	-6	-25	-18	-423	-853	56	222	-446	-860	7.37	-.0255	-.0527	.0034
40	-16	-25	-18	-742	-945	-57	116	-727	-960	-14.53	-.0446	-.0588	-.0035
60	-16	-35	-16	-834	-1264	-170	273	-775	-1323	-19.15	-.0475	-.0811	-.0105
80	-25	-35	-29	-1121	-1347	-23	115	-1119	-1350	-5.66	-.0666	-.0827	-.0014
100	-25	-35	-29	-1121	-1347	-23	115	-1119	-1350	-5.66	-.0666	-.0827	-.0014
120	-25	-35	-29	-1121	-1347	-23	115	-1119	-1350	-5.66	-.068V	-.0827	-.0014
140	-35	-35	-29	-1440	-1440	-136	135	-1304	-1570	-45.0	-.0799	-.0966	-.0084
160	-35	-35	-39	-1440	-1440	90	90	-1349	-1530	40.	-.0827	-.0938	.0055
180	-42	-33	-37	-1645	-1441	-12	102	-1440	-1645	3.17	-.0883	-.1006	-.0007
200	-42	-33	-37	-1645	-1441	-12	102	-1440	-1645	3.17	-.0883	-.1006	-.0007
220	-50	-32	-36	-1850	-1463	-114	233	-1454	-1920	14.52	-.0691	-.1176	-.007
240	-49	-31	-35	-1849	-1442	-114	233	-1413	-1879	14.52	-.0666	-.1151	-.007
260	-49	-31	-35	-1849	-1442	-11T	233	-1413	-1879	14.52	-.06V6	-.1151	-.007
280	-49	-40	-46	-1933	-1729	33	107	-1723	-1938	-9.22	-.1056	-.1186	.002
300	-49	-40	-46	-1933	-1729	33	107	-1723	-1938	-9.22	-.1056	-.1166	.002
320	-47	-38	-44	-1850	-1647	33	107	-1641	-1856	-9.22	-.1006	-.1137	.002
340	-45	-36	-42	-1766	-1564	33	107	-1559	-1774	-9.22	-.0955	-.1087	.002
360	-55	-36	-42	-20X7	-1657	-80	229	-1643	-2101	10.11	-.1007	-.1287	-.0049
380	-4Y	-30	-3V	-1840	-1410	-80	229	-139V	-1854	10.11	-.0855	-.1136	-.00T9
400	-49	-30	-36	-1840	-1410	-80	229	-1396	-1854	10.11	-.0855	-.1136	-.0049

LOCATION No. 3 $\sigma_o = 21762$

TIME	STRAINS: X	Y	45	OUTPUT: STRESSES TENSILE X	Y	SHEAR	MAX	MAX NORM	MIN NORM	ANGLE (DEG)	C1	C2	C3
5	8.5	-8	-17	197	-177	390	432	443	-423	32.22	.0203	-.0195	.0179
10	25	-25	-42	565	-566	950	1106	1106	-1107	29.61	.0008	-.0509	.0436
15	25	-33	-59	491	-821	124T	1407	1242	-1572	31.09	.0571	-.0W23	.0572
20	25	-4P	-68	427	-1045	1369	1054	1246	-1863	30.87	.0572	-.0857	.0629
40	30	-43	-71	558	-1P94	1T60	1677	1410	-1945	30.24	.0648	-.0894	.067
60	35	-38	-92	764	-888	2048	220X	2147	-2271	34N01	.0986	-.1044	.0941
80	40	-33	-104	97P	-683	2433	2569	2713	-2426	35.62	.1246	-.1115	.1118
100	37	-28	-107	920	-551	2523	2628	2813	-24T4	36.67	.1293	-.1123	.1159
120	37	-28	-115	920	-551	2704	2803	2988	-2619	37.39	.1375	-.1204	.1242
14P	29	-36	-124	591	-880	2727	2825	2681	-2970	37.45	.1232	-.1365	.1253
160	34	-40	-119	714	-961	2625	2756	2632	-2880	36.15	.120Y	-.1324	.1206
180	34	-48	-119	640	-1216	2535	2699	2411	-2988	34.94	.1106	-.1373	.1164
200	30	-43	-105	556	-1094	2229	2377	2110	-2646	34.83	.09V9	-.1216	.1024
220	21	-43	-89	271	-1177	1765	1908	1455	-2361	33.84	.0669	-.1085	.0811
240	21	-43	-89	271	-1177	1765	1908	1455	-2361	33.84	.0669	-.1085	.0811
260	15	-50	-87	15	-1456	1573	1736	1016	-2457	32.46	.0467	-.1129	.0722
280	15	-50	-87	15	-1456	1573	1736	1016	-2457	32.46	.0467	-.1129	.0722
300	18	-47	-84	139	-1332	1573	1736	1140	-2334	32.46	.0524	-.1073	.0722
320	18	-47	-84	139	-1332	1573	1736	1140	-2334	32.46	.0524	-.1073	.0722
340	18	-47	-84	139	-135R	1573	1736	1140	-23S4	32.46	.0524	-.1073	.07R2

TABLE A-VII (Cont'd) - Thermoelastic Model Stresses (PSI)

LOCATION No. 4 $\sigma_o = 21762$

OUTPUTZ STRESSES

TIME	STRAINS: X	Y	45	TENSILE X	Y	SHEAR	MAX	MAX NORM.	MIN NORM.	ANGLE (DEG)	C1	C2	C3
5	18	-18	9	407	-408	-204	455	455	-456	-13.29	.0209	-.021	-.0094
10	27	-36	0	527	-899	-102	720	535	-906	-4.07	.0245	-.0417	-.0047
15	36	-45	0	731	-1102	-102	922	737	-1108	-3.18	.0336	-.0509	-.0047
20	36	-55	0	639	-1421	-216	1052	661	-1443	-5.9	.0303	-.0664	-.0099
40	41	-59	14	761	-1502	-521	1245	875	-1616	-12.3V	.0402	-.0743	-.024
60	55	-63	19	1170	-1501	-521	1433	1268	-1598	-10.65	.0583	-.0735	-.024
80	56	-62	29	1212	-1459	-725	1519	1395	-1643	-14.24	.0641	-.0755	-.0333
100	65	-62	29	1499	-1376	-623	1566	1626	-1505	-11.71	.0748	-.0692	-.0287
120	65	-62	29	1499	-1376	-623	1566	1626	-1505	-11.71	.0748	-.0692	-.0287
140	61	-57	34	1417	-1254	-725	1519	1601	-1438	-14.24	.0735	-.0661	-.0333
160	61	-57	34	1417	-1254	-725	1519	1601	-1438	-14.24	.0735	-.0661	-.0333
180	66	-61	39	1540	-1335	-827	1657	1760	-1556	-14.95	.0809	-.0715	-.038
200	68	-59	32	1622	-1253	-623	1566	1751	-1382	-11.71	.0804	-.0635	-.0287
220	87	-59	32	2228	-1077	-408	1701	2277	-1127	-6.93	.1046	-.0518	-.0186
240	90	-56	35	2351	-954	-408	1701	2401	-1003	-6.93	.1103	-.0461	-.0188
260	90	-56	35	2351	-954	-408	1701	2401	-1003	-6.93	.1103	-.0461	-.0186
280	95	-51	31	2557	-748	-204	1664	2569	-761	-3.52	.118	-.035	-.0094
300	95	-51	31	2557	-748	-204	1664	2569	-761	-3.52	.118	-.055	-.0094
320	95	-60	31	2473	-1035	-306	1780	2500	-1061	-4.95	.1148	-.0488	-.0141
340	100	-55	36	2679	-829	-306	1780	2706	-856	-4.95	.1243	-.0394	-.0141

LOCATION No. 5 $\sigma_o = 16322$

OUTPUT: STRESSES

TIME	STRAINS: X	Y	45	TENSILE X	Y	SHEAR	MAX	MAX NORM.	MIN NORM.	ANGLE (DEG)	C1	C2	C3
5	28	-15	52	753	-220	-1030	1139	1406	-872	-32.36	.0861	-.0535	-.0632
10	28	-15	71	753	-220	-1460	1538	1606	-1272	-35.79	.1106	-.078	-.0895
15	28	-15	71	753	-220	-1460	1538	1806	-1272	-35.79	.1106	-.078	-.0895
20	28	-15	71	753	-220	-1460	1538	1806	-1272	-35.79	.1106	-.078	-.0895
4P	22	-30	73	424	-754	-1743	1639	1675	-2005	-35.68	.1026	-.1228	-.1068
60	10	-43	59	-79	-1279	-1709	1811	1132	-2490	-35.33	.0693	-.1526	-.1048
80	18	-51	49	102	-1460	-1483	1675	997	-2355	-31.12	.061	-.1443	-.0909
100	13	-57	42	-113	-1698	-1449	1651	746	-2556	-30.67	.0457	-.1566	-.0888
120	15	-55	35	-31	-1615	-1245	1475	653	-2299	-26.77	.04	-.1409	-.0763
140	9	-62	27	-267	-1894	-1212	1453	363	-2544	-28.22	.0222	-.1559	-.0742
160	9	-62	27	-267	-1894	-1212	1453	363	-2544	-28.22	.0222	-.1559	-.0742
160	2	-69	19	-575	-2182	-1189	1434	56	-2613	-27.97	.0034	-.1724	-.0729
200	5	-75	22	-535	-2345	-1291	1576	136	-3016	-27.46	.0083	-.1846	-.0791
220	0	-80	15	-740	-2551	-1245	1535	-106	-3185	-26.99	-.0065	-.1952	-.0763
240	0	-89	15	-823	-2836	-1347	1681	-149	-3512	-26.61	-.0091	-.2152	-.0826
260	0	-89	5	-823	-2636	-1121	1506	-324	-3337	-24.03	-.0199	-.2045	-.068W
280	5	-84	20	-618	-2632	-1347	1681	57	-3307	-26.61	.0035	-.2026	-.0826
300	-12	-84	-9	-1160	-2789	-883	1201	-773	-3176	-23.65	-.0474	-.1946	-.0541
320	-10	-82	-7	-1077	-2707	-883	1201	-691	-3094	-23.65	-.0424	-.1896	-.0541
340	-9	-90	-6	-1120	-2953	-985	1345	-651	-3382	-23.53	-.0424	-.2072	-.0604
360	-9	-90	-6	-1120	-2953	-985	1345	-651	-3382	-23.53	-.0424	-.2072	-.0604
380	-7	-97	-14	-1120	-3156	-861	1333	-806	-34W2	-20.09	-.0494	-.2128	-.0527
400	-7	-97	-14	-1120	-3158	-861	1333	-806	-3472	-20.09	-.0494	-.2128	-.0527

LOCATION No. 6 $\sigma_o = 16673$

OUTPUT: STRESSES

TIME	STRAINS: X	Y	45	TENSILE X	Y	SHEAR	MAX	MAX NORM	MIN NORM	ANGLE (DEG)	C1	C2	C3
5	-56	9	0	-1703	-231	0	735	-231	-1703	0	-.0139	-.1021	0
10	-85	18	0	-2544	-213	0	1165	-213	-25I4	0	-.0128	-.1526	0
15	-85	18	0	-2544	-213	0	1165	-213	-2544	0	-.0128	-.1526	0
20	-85	18	0	-2544	-213	0	1165	-213	-2544	0	-.0128	-.1526	0
40	-90	22	0	-2666	-131	0	1267	-131	-2666	0	-.0079	-.1599	0
60	-98	23	0	-2912	-173	0	1369	-173	-2912	0	-.0104	-.1747	0
80	-93	28	0	-2707	32	0	1369	32	-2707	0	.0019	-.1624	0
100	-103	28	0	-3025	-60	0	1482	-60	-3025	0	-.0036	-.1815	0
120	-108	32	0	-3148	21	0	1584	21	-31T8	0	.0013	-.188X	0
140	-107	24	0	-3190	-225	0	1482	-225	-3190	0	-.0135	-.1913	0
160	-106	25	0	-3149	-183	0	1482	-183	-3149	0	-.011	-.1889	0
180	-112	29	0	-3303	-111	0	1595	-111	-3303	0	-.0067	-.198W	0
200	-121	29	0	-3590	-195	0	1697	-195	-3590	0	-.011W	-.2153	0
220	-117	24	0	-3509	-317	0	1595	-317	-3509	0	-.019	-.2105	0
240	-116	25	0	-3468	-276	0	1595	-276	-3468	0	-.0166	-.208	0
260	-114	27	0	-3385	-194	0	1595	-194	-3385	0	-.0116	-.2031	0
280	-119	29	0	-3526	-176	0	1675	-176	-3526	0	-.0106	-.2115	0
300	-120	30	0	-3549	-154	0	1697	-154	-3549	0	-.0092	-.2129	0
320	-120	21	0	-3632	-440	0	1595	-440	-3632	0	-.0264	-.2179	0
340	-119	22	0	-3591	-399	0	1595	-399	-3591	0	-.024	-.2154	0
360	-127	24	0	-3828	-410	0	1708	-41P	-3828	0	-.0246	-.2296	0
380	-125	26	0	-3745	-327	0	1708	-327	-3745	0	-.0196	-.2247	0
400	-125	26	0	-3745	-327	0	1708	-327	-3745	0	-.0196	-.2247	0

TABLE A-VII (Cont'd) - Thermoelastic Model Stresses (PSI)

LOCATION No. 7 $\sigma_o = 16673$

	STRAINS:			OUTPUT: STRESSES TENSILE		SHEAR		MAX	MIN	ANGLE			
TIME	X	Y	45	X	Y		MAX	NORM	NORM	(DEG)	C1	C2	C3
5	-71	0	0	-2264	-657	0	603	-657	-2264	0	-.0394	-.1308	0
10	-81	0	0	-2563	-749	0	916	-749	-2585	0	-.045	-.154Y	0
15	-91	0	0	-2902	-842	0	1029	-842	-2902	0	-.0505	-.1741	0
20	-91	0	0	-2902	-842	0	1029	-842	-2902	0	-.0005	-.1741	0
40	-97	5	0	-3047	-738	0	1154	-738	-3047	0	-.0443	-.1828	0
60	-102	-2	0	-3271	-1007	0	1131	-10P7	-3271	0	-.0604	-.1962	0
80	-97	-8	0	-3167	-1152	0	1007	-1152	-3167	0	-.0691	-.19	0
100	-95	-6	0	-30X5	-1070	0	1007	-1070	-3085	0	-.0642	-.185	0
120	-102	-15	0	-3391	-14R2	0	984	-1422	-3391	0	-.0853	-.2034	0
140	-97	-21	0	-3287	-1567	0	860	-1567	-3287	0	-.094	-.1972	0
160	-92	-16	0	-3082	-1361	0	860	-1361	-3082	0	-.0817	-.1848	0
180	-89	-13	0	-2958	-1238	0	860	-1238	-2958	0	-.0743	-.1774	0
200	-86	-22	0	-2946	-1497	0	724	-1497	-2946	0	-.089X	-.1767	0
220	-82	-18	0	-2781	-1332	0	724	-1332	-2781	0	-.0799	-.1668	0
240	-79	-20	0	-2704	-1369	0	667	-1369	-2704	0	-.0821	-.1622	0
260	-77	-24	0	-2677	-1478	0	595	-1478	-2677	0	-.0886	-.1606	0
280	-75	-22	0	-2595	-1395	0	599	-1390	-2595	0	-.0837	-.1557	0
300	-72	-31	0	-2583	-1654	0	464	-1654	-2583	0	-.0993	-.1549	0
320	-67	-26	0	-2377	-1449	0	464	-1449	-2377	0	-.0869	-.1426	0
340	-66	-25	0	-2336	-1408	0	464	-14P8	-2336	0	-.0845	-.14P1	0
360	-62	-26	0	-2218	-1403	0	407	-1403	-2218	0	-.0841	-.133	0
380	-62	-32	0	-2273	-1594	0	339	-1594	-2273	0	-.0956	-.1363	0
400	-59	-23	0	-2094	-1279	0	407	-1279	-2094	0	-.0767	-.1256	0

LOCATION No. 8 $\sigma_o = 19832$

	STRAINS:			OUTPUT: STRESSES TENSILE		SHEAR		MAX	MIN	ANGLE			
TIME	X	Y	45	X	Y		MAX	NORM	NORM	(DEG)	C1	C2	C3
5	-25	9	0	-714	55	0	384	55	-714	0	.002R	-.036	0
10	-33	9	0	-969	-19	0	475	-19	-969	0	-.001	-.0489	0
15	-33	9	0	-969	-19	0	475	-19	-969	0	-.001	-.0489	0
20	-42	9	0	-1256	-102	0	577	-102	-1256	0	-.0052	-.0634	0
40	-51	9	0	-1543	-185	0	679	-185	-1543	0	-.0094	-.0778	0
60	-51	9	0	-1543	-185	0	679	-185	-1543	0	-.0094	-.0778	0
80	-59	9	0	-1798	-259	0	769	-259	-1798	0	-.0131	-.0907	0
100	-59	9	0	-1798	-259	0	769	-259	-1798	0	-.0131	-.0907	0
120	-63	14	0	-1880	-137	0	871	-137	-1880	0	-.0069	-.0948	0
140	-63	14	0	-1880	-137	0	871	-137	-1880	0	-.0069	-.0948	0
160	-63	14	0	-1880	-137	0	871	-137	-1880	0	-.0069	-.0948	0
180	-63	14	0	-1880	-137	0	871	-137	-1880	0	-.0069	-.0948	0
200	-63	14	0	-1880	-137	0	871	-137	-1880	0	-.0069	-.0948	0
220	-63	5	0	-1963	-424	0	769	-424	-1963	0	-.0214	-.099	0
240	-63	5	0	-1963	-424	0	769	-424	-1963	0	-.0214	-.099	0
260	-63	5	0	-1963	-424	0	769	-424	-1963	0	-.0214	-.099	0
280	-60	8	0	-1839	-300	0	769	-300	-1839	0	-.0152	-.0928	0
300	-69	-1	0	-2210	-670	0	769	-670	-2210	0	-.0338	-.1114	0
320	-68	-1	0	-2178	-661	0	758	-661	-2178	0	-.0334	-.1098	0
340	-58	1	0	-1840	-505	0	667	-505	-1840	0	-.0255	-.0928	0
360	-58	1	0	-1840	-505	0	667	-505	-1840	0	-.0255	-.0928	0
380	-58	1	0	-1840	-505	0	667	-505	-1840	0	-.0255	-.0928	0
400	-58	1	0	-1840	-505	0	667	-505	-1840	0	-.0255	-.0928	0

LOCATION No. 9 $\sigma_o = 16673$

	STRAINS:			OUTPUT: STRESSES TENSILE		SHEAR		MAX	MIN	ANGLE			
TIME	X	Y	45	X	Y		MAX	NORM	NORM	(DEG)	C1	C2	C3
5	0	0	0	0	0	0	0	0	0	-45.01	0	0	0
10	0	0	0	0	0	0	0	0	0	-45.01	0	0	0
15	0	0	0	0	0	0	0	0	0	-45.01	0	0	0
20	0	0	0	0	0	0	0	0	0	-45.01	0	0	0
40	-11	0	0	-322	0	0	160	-1	-322		-.0001	-.0193	0
60	-11	0	0	-322	0	0	160	-1	-322	0	-.0001	-.0193	0
80	-17	0	0	-497	0	0	248	-1	-497	0	-.0001	-.0298	0
100	-17	0	0	-497	0	0	248	-1	-497	0	-.0001	-.0298	0
120	-17	0	0	-497	0	0	248	-1	-497	0	-.0001	-.0298	0
140	-17	0	0	-497	0	0	248	-1	-497	0	-.0001	-.0298	0
160	-17	0	0	-497	0	0	248	-1	-497	0	-.0001	-.0298	0
18P	-17	0	0	-497	0	0	248	-1	-497	0	-.0001	-.0R98	0
200	-23	0	0	-672	0	0	335	-1	-672	0	-.0001	-.0403	0
220	-23	0	0	-672	0	0	335	-1	-672	0	-.0001	-.0403	0
24P	-23	0	0	-672	0	0	335	-1	-672	0	-.0P01	-.0403	0
260	-23	0	0	-672	0	0	335	-1	-672	0	-.0001	-.0403	0
280	-23	0	0	-672	0	0	335	-1	-672	0	-.0001	-.0403	0
300	-23	0	0	-672	0	0	335	-1	-672	0	-.0001	-.0403	0
320	-23	0	0	-672	0	0	335	-1	-672	0	-.0001	-.0403	0
340	-23	0	0	-672	0	0	335	-1	-672	0	-.0001	-.04P3	0
360	-23	0	0	-6W2	0	0	335	-1	-672	0	-.0001	-.0403	0
380	-23	0	0	-672	0	0	335	-1	-672	0	-.0001	-.0403	0
400	-23	0	0	-672	0	0	335	-1	-672	0	-.0001	-.0403	0

TABLE A-VII (Cont'd) - Thermoelastic Model Stresses (PSI)

LOCATION No. 10 $\sigma_o = 19832$

TIME	STRAINS: X	Y	45	OUTPUT: STRESSES TENSILE X	Y	SHEAR	MAX	MAX NORM	MIN NORM	ANGLE (DEG)	C1	C2	C3
5	0	0	0	0	0	0	0	0	0	-45.01	0	0	0
10	0	0	0	0	0	0	0	0	0	-45.01	0	0	0
15	0	0	0	0	0	0	0	0	0	-45.01	0	0	0
20	0	0	0	0	0	0	0	0	0	-45.01	0	0	0
40	0	0	0	0	0	0	0	0	0	-45.01	0	0	0
60	0	0	0	0	0	0	0	0	0	-45.01	0	0	0
80	0	0	0	0	0	0	0	0	0	-45.01	0	0	0
100	0	0	0	0	0	0	0	0	0	-45.01	0	0	0
120	0	0	0	0	0	0	0	0	0	-45.01	0	0	0
140	-13	0	0	-380	0	0	189	-1	-380	0	-.0001	-.0192	0
160	-13	0	0	-380	0	0	189	-1	-380	0	-.0001	-.0192	0
180	-13	0	0	-380	0	0	189	-1	-380	0	-.0001	-.0192	0
200	-13	0	0	-380	0	0	189	-1	-380	0	-.0001	-.0192	0
220	-13	0	0	-380	0	0	189	-1	-380	0	-.0001	-.0192	0
240	-13	0	0	-380	0	0	189	-1	-380	0	-.0001	-.0192	0
260	-13	0	0	-380	0	0	189	-1	-380	0	-.0001	-.0192	0
280	-13	0	0	-380	0	0	189	-1	-380	0	-.0001	-.0192	0
300	-13	0	0	-380	0	0	189	-1	-380	0	-.0001	-.0192	0
320	-13	0	0	-380	0	0	189	-1	-380	0	-.0001	-.0192	0
340	-13	0	0	-380	0	0	189	-1	-380	0	-.0001	-.0192	0
360	-13	0	0	-380	0	0	189	-1	-380	0	-.0001	-.0192	0
380	-25	0	0	-730	0	0	365	0	-730	0	0	-.0369	0
400	-25	0	0	-730	0	0	365	0	-730	0	0	-.0369	0

LOCATION No. 11 $\sigma_o = 19832$

TIME	STRAINS: X	Y	45	OUTPUT: STRESSES TENSILE X	Y	SHEAR	MAX	MAX NORM	MIN NORM	ANGLE (DEG)	C1	C2	C3
5	-9	0	0	-263	0	0	131	-1	-263	0	-.0001	-.0133	0
10	5	0	0	145	0	0	72	145	0	0	.0073	0	0
15	17	0	0	496	0	0	248	496	0	0	.025	0	0
20	32	0	0	934	0	0	467	934	0	0	.0471	0	0
40	72	0	0	2102	0	0	1051	2102	0	0	.106	0	0
60	91	0	0	2657	0	0	1328	2657	0	0	.1339	0	0
80	109	0	0	3182	0	0	1591	3182	0	0	.1604	0	0
100	124	0	0	3620	0	0	1810	3620	0	0	.1825	0	0
120	143	0	0	4175	0	0	2087	4175	0	0	.2105	0	0
140	145	0	0	4233	0	0	2116	4233	0	0	.2134	0	0
160	153	0	0	4T67	0	0	2233	4467	0	0	.2252	0	0
180	158	0	0	4613	0	0	2306	4613	0	0	.2326	0	0
200	163	0	0	4759	0	0	2379	4759	0	0	.2399	0	0
220	159	0	0	4642	0	0	2321	4642	0	0	.2341	0	0
240	164	0	0	4788	0	0	2394	4788	0	0	.2414	0	0
260	156	0	0	4555	0	0	2277	4555	0	0	.2296	0	0
280	156	0	0	4555	0	0	2277	4555	0	0	.2296	0	0
300	161	0	0	4701	0	0	2350	4701	0	0	.237	0	0
320	152	0	0	4438	0	0	2219	4438	0	0	.2237	0	0
340	144	0	0	4204	0	0	2102	4204	0	0	.212	0	0
360	144	0	0	4204	0	0	2102	4204	0	0	.212	0	0
380	144	0	0	4204	0	0	2102	4204	0	0	.212	0	0
400	149	0	0	4S50	0	0	2175	4350	0	0	.2193	0	0

Faulty Teleprinter Translation

N = .	U = 5
P = 0	V = 6
Q = 1	W = 7
R = 2	X = 8
S = 3	Y = 9
T = 4	

REFERENCES

1. "Heat Transmission", McGraw-Hill, 1954 (McAdams, W. H.)

2. "Numerical Analysis of Heat Flow", McGraw-Hill, 1949 (Dusinberre, G.M.)

3. "Waermespannungen," Springer - Verlag, 1953 (Melan, E. and Parkus, H.)

4. "An Exploratory Study of Stress Concentrations in Thermal Shock Fields," Trans, ASME, Journal of Engineering for Industry, Vol.84, Series B, No. 3, pp. 343-350, August 1962 (Becker, H.)

5. "Temperature-Induced Stresses in Beams and Ships," Naval Ship Research and Development Center Report - DTMB No. 937, June 1955 (Jasper, Norman H.)

6. "Service Stresses and Motions of the ESSO Asheville, A T-2 Tanker, Including a Statistical Analysis of Experimental Data," Naval Ship Research and Development Center Report - DTMB No. 960, September 1955. (Jasper, Norman H.)

7. "Thermal Stresses in Ships," Ship Structure Committee Report SSC-95, October 30, 1956 (Hechtman, R. A.)

8. "Temperature Distribution and Thermal Stresses," Ship Structure Committee Report No. SSC-152, June 1964. (Lyman, P. T. and Meriam, J. L.)

9. "Stress Concentration Design Factors," John Wiley, 1963 (Peterson, R. E.)

10. "Photothermoelastic Investigation of Thermal Stresses in Flat Plates," Trans. ASME, Journal of Basic Engineering, Vol. 85, Series D, No. 4, pp. 566-568, December 1963. (Becker, H. and Colao, A.)

11. "Thermoelastic Stress Concentrations", American Institute of Aeronautics and Astronautics Meeting, January 1966 (Becker, H.and Bird, F.)

12. "Thermal Stress Concentration Caused by Structural Discontinuities," Experimental Mechanics, Vol. 9, No. 12, pp. 558-564, December 1969. (Emery, A.F., Williams, J. A., and Avery, J.)

13. "Thermo-Structural Analysis Manual", WADD-TR-60-517, Vol. 1 (AD 286908), August 1962. (Switzky, A., Forray, M.J. and Newman, M.)

14. "A Treatise on Photoelasticity," Cambridge University Press, 1931 (Coker, E. G. and Filon, L.N.G.)

15. "Photoelasticity," John Wiley, 1941 (Frocht, M. M.)

16. "An Exploratory Study of Three-Dimensional Photothermo-elasticity," Journal of Applied Mechanics, Vol. 28, No. 1, pp. 35-40, March 1961. (Tramposch, H. and Gerard, G.)

17. "Physical Properties of Plastics for Photothermoelastic Investigations," Journal of Applied Mechanics, Vol. 25, No. 4, pp. 525-528, December 1958. (Trans. ASME, Vol. 80, pp. 525-528, 1958 (Tramposch, H., and Gerard, G.)

18. "Photothermoelastic Investigation of Transient Thermal Stresses in a Multiweb Wing Structure," Journal of the Aero/Space Sciences, Vol. 26, No. 12, pp. 783-786, December 1959 (Gerard, G., and Tramposch, H.)

19. "Photothermoelastic Investigation of a Trimetallic Strip," Part II New York University Report SM 60-4, July 1960. (Becker, H. and Colão, A.)

20. "A Nomographic Solution to the Strain Rosette Equations," Proc. of the Soc. for Exper. Stress Analysis, Vol. 4, No. 1, 1946, pp. 9-26 (Hewson, T. A.)

21. "Temperature Response Charts", Wiley 1963 (Schneider, P.J.)

Security Classification

DOCUMENT CONTROL DATA - R & D

(Security classification of title, body of abstract and indexing annotation must be entered when the overall report is classified)

1. ORIGINATING ACTIVITY *(Corporate author)* Sanders Associates, Inc. Nashua, New Hampshire	2a. REPORT SECURITY CLASSIFICATION Unclassified 2b. GROUP

3. REPORT TITLE

THERMOELASTIC MODEL STUDIES OF CRYOGENIC TANKER STRUCTURES

4. DESCRIPTIVE NOTES *(Type of report and inclusive dates)*

FINAL

5. AUTHOR(S) *(First name, middle initial, last name)*

H. BECKER
A. COLAO

6. REPORT DATE August, 1973	7a. TOTAL NO. OF PAGES 74	7b. NO. OF REFS 21
8a. CONTRACT OR GRANT NO. N00024-70-C-5119 b. PROJECT NO. c. d.	9a. ORIGINATOR'S REPORT NUMBER(S) SSC-241 9b. OTHER REPORT NO(S) *(Any other numbers that may be assigned this report)*	

10. DISTRIBUTION STATEMENT

DISTRIBUTION UNLIMITED

11. SUPPLEMENTARY NOTES	12. SPONSORING MILITARY ACTIVITY Naval Ship Systems Command

13. ABSTRACT

Theoretical calculations and experimental model studies were conducted on the problem of temperature and stress determination in a cryogenic tanker when a hold is suddenly exposed to the chilling action of the cold fluid. The initiation of the action is presumed to be the sudden and complete rupture of the fluid tank.

Model studies of temperatures and stresses were performed on instrumented steel versions of a ship with center holds and wing tanks. Supplementary studies also were conducted on plastic models using photothermoelasticity (PTE) to reveal the stresses. Temperatures and stresses were computed using conventional procedures for comparison with the experimentally determined data. Simple calculation procedures were developed for temperature prediction and for stress determination.

The highly simplified theoretical predictions of temperature were in fair agreement with the experimental data in the transient stage and after long intervals. The temperatures and stresses reached peak values in every case tested and maintained the peaks for several minutes during which time the behavior was quasistatic. The experimental temperatures were in good agreement with predictions for the thin models representative of ship construction.

Evidence was found for the importance of convective heat transfer in establishing the temperatures in a ship. In some cases this may be the primary process by which a thermal shock would be attenuated in a cryogenic tanker. It also would influence thermal model scaling.

An important result of the project was the good agreement of the maximum experimental stresses with theoretical predictions which were made from the simple calculations. This agreement indicates the possibility of developing a general design procedure which could involve only a few minutes of calculation time to obtain the peak stress values.

SHIP RESEARCH COMMITTEE
Maritime Transportation Research Board
National Academy of Sciences-National Research Council

The Ship Research Committee has technical cognizance of the interagency Ship Structure Committee's research program:

PROF. J. E. GOLDBERG, Chairman, *School of Civil Engineering, Purdue University*

DR. H. N. ABRAMSON, *Tech. Vice President, Dept. of Mech. Sciences, S. W. Res. Institute*

PROF. R. W. CLOUGH, *Prof. of Civil Engineering, University of California*

PROF. W. J. HALL, *Prof. of Civil Engineering, University of Illinois*

DR. S. R. HELLER, JR., *C'man, Civil & Mech. Eng. Dept., The Catholic Univ. of America*

MR. G. E. KAMPSCHAEFER, JR., *Manager, Technical Services, ARMCO Steel Corporation*

MR. R. C. STRASSER, *Director of Research, Newport News Shipbuilding & Dry Dock Company*

MR. H. S. TOWNSEND, *Vice President, U. S. Salvage Association, Inc.*

DR. S. YUKAWA, *Consulting Engineer, General Electric Company*

Advisory Group II, "Ship Structural Design Procedures and Analysis", prepared the project prospectus and evaluated the proposals for this project:

Dr. S. R. HELLER, Jr., Chairman, *Civ. & Mech. Eng. Dept., The Catholic Univ. of America*

MR. C. M. COX, *Asst. Naval Architect, Newport News Shipbuilding & Dry Dock Company*

MR. C. R. CUSHING, *President, C. R. Cushing & Company*

PROF. J. KEMPNER, *Dept. of Aerospace Engrg. & Applied Mech., Polytechnic Inst. of B'lyn*

PROF. J. R. PAULLING, JR., *Dept. of Naval Architecture, University of California*

MR. D. P. ROSEMAN, *Chief Naval Architect, Hydronautics, Inc.*

The SR-191 Project Advisory Committee provided the liaison technical guidance, and reviewed the project reports with the investigator:

CAPT. R. M. WHITE, USCG, Chairman, *Chief, Applied Engrg. Sect., U.S. Coast Guard Acad.*

MR. D. P. COURTSAL, *Chief Marine Engineer, DRAVO Corporation*

MR. M. L. SELLERS, *Naval Architect, Newport News Shipbuilding & Dry Dock Company*

SHIP STRUCTURE COMMITTEE PUBLICATIONS

These documents are distributed by the National Technical Information Service, Springfield, Va. 22151. These documents have been announced in the Clearinghouse Journal U.S. Government Research & Development Reports (USGRDR) under the indicated AD numbers.

SSC-229, *Evaluation and Verification of Computer Calculations of Wave-Induced Ship Structural Loads* by P. Kaplan and A. I. Raff. 1972. AD 753220

SSC-230, *Program SCORES - Ship Structural Response in Waves* by A. I. Raff, 1972. AD 752468

SSC-231, *Further Studies of Computer Simulation of Slamming and Other Wave-Induced Vibratory Structural Loadings on Ships in Waves* by P. Kaplan and T. P. Sargent. 1972. AD 752479

SSC-232, *Study of the Factors Which Affect the Adequacy of High-Strength, Low Alloy Steel Weldments for Cargo Ship Hulls* by E. B. Norris, A. G. Pickett, and R. D. Wylie. 1972. AD 752480

SSC-233, *Correlation of Model and Full-Scale Results in Predicting Wave Bending Moment Trends* by D. Hoffman, J. Williamson, and E. V. Lewis. 1972. AD 753223

SSC-234, *Evaluation of Methods for Extrapolation of Ship Bending Stress Data* by D. Hoffman, R. van Hooff, and E. V. Lewis. 1972. AD 753224

SSC-235, *Effect of Temperature and Strain Upon Ship Steels* by R. L. Rothman and R. E. Monroe. 1973.

SSC-236, *A Method for Digitizing, Preparing and Using Library Tapes of Ship Stress and Environment Data* by A. E. Johnson, Jr., J. A. Flaherty, and I. J. Walters. 1973.

SSC-237, *Computer Programs for the Digitizing and Using of Library Tapes of Ship Stress and Environment Data* by A. E. Johnson, Jr., J. A. Flaherty, and I. J. Walters. 1973.

SSC-238, *Design and Installation of a Ship Response Instrumentation System Aboard the SL-7 Class Containership S.S. SEA-LAND McLEAN* by R. A. Fain. 1973.

SSC-239, *Wave Loads in a Model of the SL-7 Containership Running at Oblique Headings in Regular Waves* by J. F. Dalzell and M. J. Chiocco. 1973.

SSC-240, *Load Criteria for Ship Structural Design* by E. V. Lewis, R. van Hooff, D. Hoffman, R. B. Zubaly, and W. M. Maclean. 1973.